Winter 1997

Analysis of cured-in-place pipes (CIPP) installed in circular and oval deteriorated host pipes

Abdel-Aziz Mabrouk Omara

INFORMATION TO USERS

This manuscript has been reproduced from the microfilm master. UMI films the text directly from the original or copy submitted. Thus, some thesis and dissertation copies are in typewriter face, while others may be from any type of computer printer.

The quality of this reproduction is dependent upon the quality of the copy submitted. Broken or indistinct print, colored or poor quality illustrations and photographs, print bleedthrough, substandard margins, and improper alignment can adversely affect reproduction.

In the unlikely event that the author did not send UMI a complete manuscript and there are missing pages, these will be noted. Also, if unauthorized copyright material had to be removed, a note will indicate the deletion.

Oversize materials (e.g., maps, drawings, charts) are reproduced by sectioning the original, beginning at the upper left-hand corner and continuing from left to right in equal sections with small overlaps. Each original is also photographed in one exposure and is included in reduced form at the back of the book.

Photographs included in the original manuscript have been reproduced xerographically in this copy. Higher quality 6" x 9" black and white photographic prints are available for any photographs or illustrations appearing in this copy for an additional charge. Contact UMI directly to order.

UMI

A Bell & Howell Information Company
300 North Zeeb Road, Ann Arbor MI 48106-1346 USA
313/761-4700 800/521-0600

ANALYSIS OF CURED-IN-PLACE PIPES (CIPP) INSTALLED IN CIRCULAR AND OVAL DETERIORATED HOST PIPES

by

Abdel-Aziz M. Omara, B.Sc. M.Sc.

A Dissertation Presented in Partial Fulfillment
of the Requirements for the Degree
Doctor of Engineering

COLLEGE OF ENGINEERING
LOUISIANA TECH UNIVERSITY

February 1997

LOUISIANA TECH UNIVERSITY

THE GRADUATE SCHOOL

February 13, 1997
Date

We hereby recommend that the thesis prepared under our supervision by Abdel-Aziz M. Omara entitled Analysis of Cured-in-Place Pipes Installed in Circular and Oval Deteriorated Host Pipes be accepted in partial fulfillment of the requirements for the Degree of Doctor of Engineering

Supervisor of Thesis Research

Head of Department

Civil Engineering
Department

Recommendation concurred in:

Advisory Committee

Approved:
Director of Graduate Studies

Dean of the College

Approved:
Dean of Graduate School

GS Form 13
8/96

ABSTRACT

This dissertation presents new analytical models for the structural analysis of Cured-In-Place Pipes (CIPP) used in the rehabilitation process of deteriorated pipelines. Both cases of partially and fully deteriorated pipelines are considered. Specifically, analytical models for the stability of CIPP encased in either circular or oval partially deteriorated host pipes are presented. The proposed models for the case of partially deteriorated host pipes were compared with the results of experimental works. Results of the experimental work, which was done during the course of this research, were used in the comparison. Other, previously done, related experimental work were also added to the experimental results database used in validating those models. Another analytical model for the static analysis of CIPP encased in fully deteriorated host pipe was also developed and compared with the results of finite element analyses. The research concludes that the proposed models in this dissertation compare favorably with either the experimental or the finite element results.

To my Son, Daughter, and Wife
Kareem, Sherouk, and Eman

.....With Love

TABLE OF CONTENTS

PART II

DESIGN OF CIPP ENCASED IN FULLY DETERIORATED HOST PIPES

LIST OF TABLES

LIST OF FIGURES

ACKNOWLEDGMENTS

I would like to express my gratitude and sincere appreciation to Dr. Leslie K. Guice and Dr. Fred Akl for their encouragement, guidance, support, and continuous advice which made this dissertation possible. Thanks for their extended office hours, patience, and their effort in correcting the manuscript of this dissertation. Also, I would like to thank Mr. Lynn Osborn and Insituform Technologies, Inc., for providing the required materials and installations for conducting the experimental work involved in this research. Sincere appreciation is also extended to Dr. Tom Straughan, Dr. Raja Nassar, and Dr. Randall Barron for their support, encouragement, and service on my advisory committee. This acknowledgment could not be complete without thanking Mrs. Johnie Owens for her great love and support during my study for this dissertation.

Most of all, thanks to my wife, whose understanding, patience, support, and love made this work real. For their support, encouragement, prayer, and love, thanks to my parents, and finally thanks to mighty GOD for continuous grace and gifts.

CHAPTER 1

INTRODUCTION AND RESEARCH OBJECTIVES

1.1 Introduction

Infrastructure decay, which is caused by many years of neglect, has been recognized for centuries and more emphatically over the past ten to twenty years. Until recently, the most common construction method to repair deteriorated sewer and water pipelines was the open-trench method which includes excavation of the ground, removal of the deteriorated pipelines, and replacement with new ones. Since many existing pipelines are located principally in congested areas, open-trench construction causes significant disruption of service, destroys public property, and presents unsafe trenches to pedestrians and construction workers.

In recent years, trenchless methods which either replace or repair existing pipelines without the need to excavate the ground have become recognized as viable alternatives. Most of the problems associated with open-trench construction can be eliminated by using trenchless technology methods, and, in many cases, the job can be performed at the same or lower cost than with conventional open-trench operations.

1.2 CIPP Technique

The Cured-In-Place Pipe (CIPP) technique for rehabilitating deteriorated pipelines was first introduced in the United States in 1977 (Li, 1994). CIPP enables deteriorated pipelines to be repaired and restores integrity from within by the insertion of a lining material through existing manholes. The liner is a resin-impregnated tube. The tube is fabricated to a size that, when installed, will fit tightly against the internal pipe wall. The tube is installed either by inversion using a hydraulic head, or it may be winched in place. When the resin cures, by circulating hot water, it hardens into a continuous, snug-fitting tube inside the original host pipe.

CIPP is used to rehabilitate and to reconstruct existing pipelines to achieve the following purposes:

1. To seal joints and cracks and restore the pipeline integrity:
    a. to reduce the infiltration of groundwater into a waste-water sewer and thereby reduce treatment plant operation costs and the possible elimination of unnecessary capital expenditures for more capacity;
    b. to prevent soil infiltration into the waste-water and storm drain sewers, thereby avoiding collapse of soil voids and damage to surface improvements;
    c. to prevent the exfiltration of conveyed pollutant fluids which may contaminate the soil and groundwater;

d. to smooth irregularities at joints, breaks, and cracks, and to provide a smooth inside pipe surface with a low roughness coefficient which improves flow characteristics.

2. To increase or restore the strength of an existing soil-pipe system or to span limited-sized holes in the wall or joints of existing pipes.
3. To provide improved corrosion resistance for the inner surface of the pipeline.

1.3 Problem Defined

The CIPP technique is fairly new, and many questions still need to be answered regarding the performance of CIPP. Specifically, the structural design methodologies for these systems are still in their infancy when compared to those for components in bridges, buildings, and other structures. Yet, design approaches for these older structural systems are continuously evolving and improving as more research is conducted and more experience is gained. The pipeline rehabilitation design process is also evolving as new research results are obtained, and it is expected that enhancements in the design process will lead to more cost-effective and durable designs.

Finding the appropriate design equations for CIPP which could produce safe and economical designs has been recognized as the most demanding problem faced by industry. Without adequate and economical design procedures, CIPP techniques may never achieve their true and full potential because of the reluctance of engineers to consider CIPP as a valuable alternative to traditional construction techniques.

The status of the original host pipe as partially or fully deteriorated pipe controls the design methodology for the CIPP. In partially deteriorated pipe, the external host pipe and the internal liner work together to carry the applied external loads. In this integrated structure, the host pipe plays the role of defending the structure against the surrounding soil pressure while the liner, because of the leaking of the host pipe, carries the groundwater hydrostatic pressure.

In the case of a fully deteriorated pipe, the host pipe is not structurally sound; therefore, it is disregarded in the design. In this case, the CIPP is designed as a buried pipe which interacts with the surrounding soil to carry the applied loads. The applied loads are the soil pressure above the buried pipe and the groundwater hydrostatic pressure, if any. The amount of support the soil can provide and the loads it can exert on the pipe depend on the relative stiffness between the CIPP and the surrounding soil. The liner under the effect of loads may behave as a flexible or a rigid pipe. Flexible pipes exhibit more deformation under the first sign of loads than rigid pipes. Only flexible pipes are considered in this research.

The current formulae for the design of CIPP in both partially and fully deteriorated host pipes are either empirical in nature, with limited scope and range of applications, or analytical solutions with limited practical value. For instance, the available analytical design equation for the case of partially deteriorated pipe depends on an expression derived primarily for the case of unconstrained pipe under the effect of hydrostatic pressure. This configuration does not resemble the actual situation of

CIPP encased in a partially deteriorated host pipe. The expression was modified based on experimental results to account for the existence of the host pipe as a rigid constraint around the CIPP. However, this enhancement does not guarantee a satisfactory design since it is based on limited test results, and a new design equation is needed.

In most cases, pipelines are out-of-round (oval) as a result of their construction or deterioration. Pipeline ovality has been recognized as the cause for the considerable reduction in the strength of installed CIPP. Current design equations suggests a remarkable reduction in the strength of CIPP when it is installed in oval host pipes. The proposed reduction factor, however, is not built upon the principles of engineering mechanics; rather it has been developed based on geometrical considerations. For that reason, many people in industry believe that providing a design expression, based on solid principles of mechanics, for the case of CIPP encased in oval host pipes is as important, if not more important, than considering the case of a circular liner.

1.4 Objectives

The main objective of this dissertation is to formulate comprehensive and practical equations for the design of CIPP. It is proposed to develop new equations with more sound theoretical bases than the ones currently in use and to lay the theoretical groundwork for further development of design methodologies. Specifically, it is proposed to introduce new formulae for the buckling pressure for the cases of CIPP encased in circular and oval partially deteriorated host pipes. Also, a new approach for

the static analysis of buried flexible pipes based on Vlasov's soil model, which is applicable to the case of a fully deteriorated pipe, is presented.

The problem of designing a CIPP encased in a partially deteriorated host pipe requires a totally different analytical approach than the one in which the CIPP is designed for fully deteriorated host pipe. Therefore, this dissertation is divided into two main parts. Part I includes Chapters 2 through 4, and it provides an overview of the relevant literature and the derivation of the proposed analytical models. It also presents the experimental work which has been done for CIPP encased in partially deteriorated oval pipes. Chapter 5 presents conclusions and recommendations for further studies covering Part I of the dissertation. Part II encompasses Chapters 6 and 7, including a literature review and a new analytical model for buried flexible pipes. This model is applicable to the case of fully deteriorated host pipes. Chapter 8 includes conclusions and recommendations for further studies for Part II.

PART I

DESIGN OF CIPP ENCASED IN PARTIALLY DETERIORATED HOST PIPES

CHAPTER 2

BUCKLING THEORIES OF CIPP

2.1 Related Research

This chapter presents the literature review and current practice in the design of CIPP installed in partially deteriorated circular and oval host pipes. The literature review and current practice in the design of CIPP in fully deteriorated host pipes will be discussed in detail in Part II of this dissertation.

2.1.1 Basic Buckling Theory of a Free Ring

The research on cylindrical tubes under external pressure dates back to the middle of the nineteenth century (Fairbairn, 1858). In his experimental work, Fairbairn concluded that the pipe length and the ratio of diameter-to-wall thickness are important parameters in determining buckling pressure. Bresse (1866), using small deflection theory, studied the stability of a thin free-standing (no outside constraint) circular ring under external hydrostatic pressure (see Fig. 2.1) and arrived at the following expression:

$$P_{cr} = \frac{3EI}{R^3} \qquad \ldots (2.1)$$

where P_{cr} = critical buckling pressure;

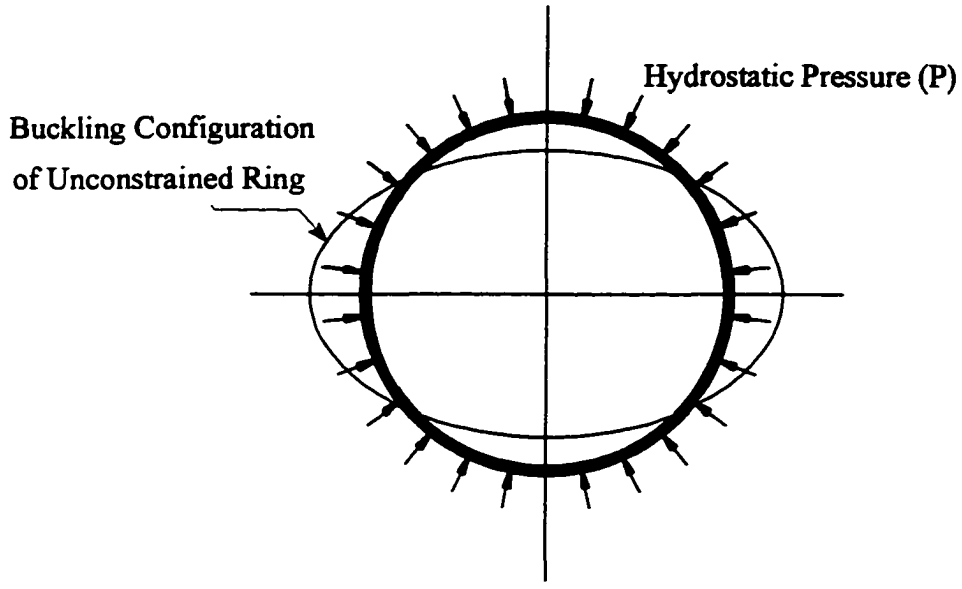

Fig. 2.1 Buckling of Unconstrained Circular Ring
Loaded By a Hydrostatic Pressure

E = modulus of elasticity;

I = moment of inertia of the ring's cross-section;

R = mean radius of the ring.

G.H. Bryan (1888) used the minimum potential energy criterion of stability to formulate a similar expression to Equation (2.1) for the case of an infinitely long free-standing pipe under hydrostatic external pressure. His equation differs from Equation (2.1) in the term E which has been replaced by $E/(1-\nu^2)$ to account for the plane strain condition of the infinitely long pipe. Considering this modification and substituting for $I=bt^3/12$, where b is the width and in this case is unity, the resulting equation is

$$P_{cr} = \frac{2E}{1-\nu^2}\left(\frac{t}{D}\right)^3 \quad \ldots (2.2)$$

where D = mean diameter of pipe;

t = mean pipe wall thickness;

ν = Poisson's ratio.

This equation can be written in the following form:

$$P_{cr} = \frac{2E}{1-\nu^2}\,\frac{1}{(SDR-1)^3} \quad \ldots (2.3)$$

where SDR = Standard Dimension Ratio, outside pipe diameter/mean pipe wall thickness.

Equation (2.3) is frequently credited to Timoshenko because of the summary of ring stability presented in his classical text (Timoshenko and Gere, 1961).

Timoshenko's equation has served for many years as the basis for designing CIPP liner systems. Timoshenko's equation is derived for an unconstrained circular pipe loaded by an external hydrostatic pressure. This configuration neglects the existence of the host pipe as rigid constraints confining the liner.

2.1.2 Current Practice in the Design of CIPP

The current practice in the design of CIPP installed in partially deteriorated host pipes uses ASTM F1216-93, Equation X1.1. This equation is a modification of Timoshenko's equation, Equation (2.3). These modifications are the addition of an enhancement factor, safety factor, ovality reduction factor, and the substitution of the long-term modulus of elasticity for the short-term modulus to allow for the creep of plastics. The equation requires that the CIPP be capable of supporting only the external hydrostatic groundwater pressure as follows:

$$P_w = \frac{2KE_L}{(1-\nu^2)} \frac{1}{(SDR-1)^3} \frac{C}{N} \quad \ldots (2.4)$$

where P_w = groundwater pressure;

K = enhancement factor;

E_L = long-term modulus of elasticity;

N = overall safety factor; and,

C = ovality factor.

The enhancement factor, K, can be attributed to the increase in the buckling resistance of a CIPP liner caused by support from the confining host pipe. The

minimum value recommended by ASTM F1216-93 is 7. An analysis of experimental results conducted at Louisiana Tech University (Guice, et al., 1994) has shown that K varies significantly from one product to another.

The long-term flexural modulus, E_L, of a specific CIPP system is determined by multiplying the short-term flexural modulus, E, by the creep modulus factor. The choice of the creep factor depends on the estimated duration of the application of the load, P_w, in relation to the design life of the structure. ASTM F1216-93 suggests a reduction of 50% in the short-term flexural modulus to account for the creep of the liner over a design life of 50 years. However, this reduction may vary from one product and manufacturer to another.

The ovality reduction factor, C, is proposed in ASTM F1216-93 to account for the reduction in the CIPP carrying capacity because of the host pipe initial imperfection or ovalization. This factor is calculated using the average measured maximum or minimum diameter of the existing oval pipe as follows:

$$C = \left[\frac{(1-q)}{(1+q)^2}\right]^3 \qquad \ldots (2.5)$$

where

$$q = \frac{\text{maximum diameter - mean diameter}}{\text{mean diameter}} \quad \text{or} \quad \frac{\text{mean diameter - minimum diameter}}{\text{mean daimeter}} \qquad \ldots (2.6)$$

The objective of any CIPP design is to determine the liner thickness. ASTM F1216-93 specifies three requirements for the resulting thickness. These requirements are (1) the design thickness should be able to bear the applied groundwater water pressure, P_w, as stated in Equation (2.4), (2) the design thickness should satisfy a minimum requirement of SDR in case no groundwater pressure exists, and (3) the design thickness of an ovalized CIPP should be capable of carrying the excess stress caused by this ovalization. These requirements are presented in the following equations:

$$t_1 = \frac{D}{\left[\frac{2KE_LC}{P_wN(1-\nu^2)}\right]^{\frac{1}{3}} + 1} \quad \ldots (2.7)$$

$$t_2 = \frac{D}{100} \quad \ldots (2.8)$$

$$t_3 = \frac{3qD}{0.5 + \sqrt{0.25 + \left[6q\left(\frac{\sigma_{BL}}{P_wN_b(1+q)}\right)\right]}} \quad \ldots (2.9)$$

where σ_{BL} the long-term allowable flexural strength for the CIPP material. It should be noted that Equation (2.7) is another form of Equation (2.4) presenting the liner thickness as the unknown. A value of 1.5 is often suggested for the overall safety factor, N, and the bending stress safety factor, N_b.

Despite this effort to modify Timoshenko's equation, its suitability for CIPP design purposes has been questioned. Different models which closely resemble the

problem of CIPP encased in rigid host pipe, may be found in the literature. Some of these models are discussed in detail in the following sections.

2.1.3 Buckling of a Thin Ring Encased in a Rigid Circular Host Pipe

Several approaches to the analysis of the failure of a thin ring encased in a rigid cavity of constant size can be found in the literature. In his study of steel tunnel linings, Amstutz (1969) presented a theory based on the assumption that failure occurs in the first mode when the yield stress in an outer fiber is first reached. Amstutz stated that under actual conditions, the plastic behavior of steel will cause the lining to yield at lower load than needed to cause elastic snap-through buckling. However, for thin pipes, the primary mode of structural failure is buckling, which relates to the geometry of a structure and its stiffness, rather than to the strength of the material.

The prevention of buckling of the CIPP under external hydrostatic pressure is one of the primary criteria typically used in the design of these liners. Leaky host pipes allow the groundwater to fill the gap between the liner and the host pipe and exert a hydrostatic pressure on the liner while the host pipe still carries the soil loads.

Research on the buckling phenomenon of a thin ring within a rigid cavity began with the analysis of a confined ring subjected to a thermal expansion. This problem was analyzed by Lo, et al. (1962). They solved the large-deflection equilibrium equation for the curved beam and defined the critical circumferential load. Zagustin and Herrmann (1967) investigated a thin elastic ring constrained in a rigid circular

surface under a uniformly distributed parallel loading. An analytical solution for the relation between the load and the associated deformed shape of the ring was found.

While this work contributes to the understanding of constrained pipe behavior, the resulting models are not particularly applicable to the current problem. Other constrained models which are more relevant are summarized below.

2.1.3.1 Chicurel's Model

Chicurel (1968) considered the shrink buckling of a thin elastic circular ring which is compressed by being inserted into a circular opening of smaller diameter than the outside diameter of the free ring. The shrink buckling phenomenon is not the same as the buckling phenomenon of CIPP liners because shrink buckling is caused only by hoop compression, while the buckling of CIPP liners is due to external uniform pressure. For shrink buckling, the hoop compressive force is relieved immediately after buckling occurs. For a pipe under hydrostatic pressure, the load is sustained after buckling is initiated, and the energy associated with the sustained pressure must be considered. Nevertheless, the approaches for shrink buckling and external uniform pressure are comparable with each other up until the point where buckling is initiated.

Figure (2.2) illustrates the deformed geometry, presented by Chicurel, for the buckled portion of the ring. Viewing the buckled portion as an axially compressed curved beam, Chicurel used the solution introduced by Timoshenko for a similar problem to describe the buckled geometry of deformation. Combining the geometry of deformationand the boundary conditions, Chicurel introduced equations for the

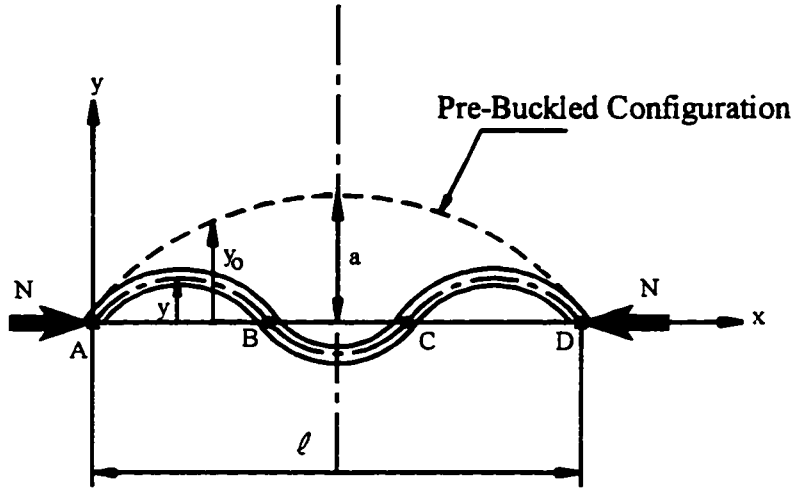

Fig. 2.2 Chicurel's Geometry of Deformation

prebuckling hoop compression force N_o which causes the thin ring to buckle for the extreme cases of no-slip and no-friction as follows:

$$N_0 = 2.487 \frac{E}{R} \sqrt{A I} \quad \ldots \quad (2.10)$$

$$N_0 = 2.67 A E \left(\frac{I}{A R^2} \right)^{\frac{3}{5}} \quad \ldots \quad (2.11)$$

where A = cross-sectional area of ring;

R = mean radius of the ring;

E = modulus of elasticity;

I = moment of inertia of the ring's cross-section; and,

N_0 = prebuckling compression force in buckled arc.

Similar results can be developed for the critical pressure of a thin ring under external uniform pressure. If a thin ring is compressed by an external uniform pressure P, the relation between the hoop compression N_o and the uniform external pressure could be related by $P = N_o/R$ (Li, 1994). Considering this modification, the equivalent critical hydrostatic pressure of CIPP encased in rigid host pipe for the cases of no-slip and no-friction are

$$P_{cr} = \frac{2.76E}{1-\nu^2} \left(\frac{t}{D} \right)^{\frac{11}{5}} \quad \ldots \quad (2.12)$$

$$P_{cr} = \frac{2.87 E}{1 - \nu^2} \left(\frac{t}{D} \right)^2 \quad \ldots \quad (2.13)$$

Obviously, the actual situation of buckling of the liner does not match completely either the no-slip or no-friction cases. The case of no-slip, Equation (2.12), provides a lower bound for the buckling pressure. It should be noted again that Equations (2.12) and (2.13) were derived from the shrink buckling of a thin ring which neglects the effect of the applied pressure occurring over the arc after buckling is initiated. Also, the critical pressure P_{cr} was equivalently transformed from the prebuckling hoop compression force N_o.

2.1.3.2 Cheney's Model

Cheney (1971) used the linear small-deflections theory to study stability of a circular ring encased in rigid boundaries under the effect of external uniform pressure. The ring is envisioned, after buckling occurred, to consist of two parts: an upper part that buckles inward, and a lower part that bears tightly against the outer rigid wall (Fig. 2.3). In the upper part of the ring, the ring is free to take any shape compatible with the differential equation and the boundary conditions at $\theta = \pm\phi$. The lower part, however, can have deflection only in the circumferential direction; radial deflections are not admitted. He further assumed that the walls of the cavity move inward with the ring resisting outward movement but not inward movement.

The governing equations of equilibrium were derived using the principle of minimum potential energy. The energy expression is obtained by summing the internal strain energies caused by extension and bending of the centroid axis minus the work done by the external pressure and boundary forces and moments (Fig. 2.3):

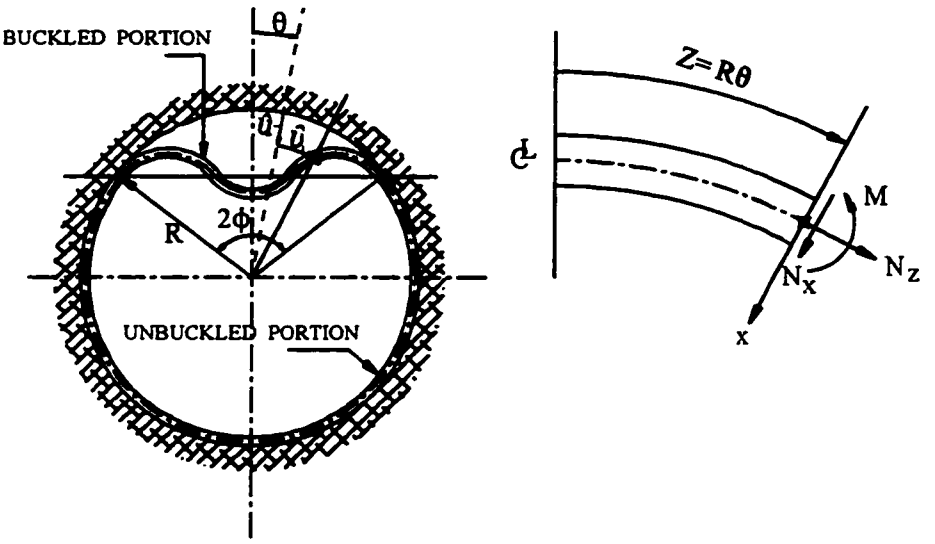

Fig. 2.3 Cheney's Model of Buckling of a Thin Ring Loaded by a Uniform External Pressure.

$$\Pi = \frac{1}{2}\int_{-\phi}^{+\phi}\left\{EA\,\hat{\epsilon}_{\theta\theta}^2 + EI\,\hat{\kappa}^2 - \frac{P}{R}\left[(\hat{u}')^2 - \hat{u}^2\right]\right\} R\,d\theta - \left[N_z\hat{v} + N_x\hat{u} + \frac{M}{R}(\hat{v}+\hat{u}')\right]_{-\phi}^{+\phi} \quad \ldots (2.14)$$

where Π = total potential energy;

P = external uniform pressure;

N_z = hoop stress resultant;

N_x = shear stress resultant;

$\hat{u}$ = radial displacement of the ring at center-line;

$\hat{v}$ = circumferential displacement of the ring at center-line;

θ = circumferential coordinate along z axis, $\theta = z/R$;

M = bending moment in cross-section;

$\pm\phi$ = values of θ at the buckled portion boundaries;

$\hat{\kappa}$ = $(\hat{u}'' + \hat{u})/R^2$ change in curvature of the ring center-line;

$\hat{\epsilon}_{\theta\theta}$ = $(\hat{v}' - \hat{u})/R$, and, $(\,)' \equiv \frac{d}{d\theta}(\,)$.

Having the lower part of the ring bearing against the cavity wall during buckling gives rise to an additional uniform pressure around this part of the ring. The shear resultant forces, N_x, at the boundaries, $\theta = \pm\phi$, are required to balance the additional pressure and to maintain the equilibrium of the lower part.

By minimizing the total potential energy and successively integrating by parts, Cheney derived the following differential equations governing the buckling of the ring:

$$\frac{EA}{R^2}(\hat{v}'-\hat{u}) = Ck^2\frac{EI}{R^4} \quad \text{. . (2.15)}$$

$$\hat{u}'^{v} + (1+k^2)\hat{u}'' + k^2\hat{u} = Ck^2 \quad \text{. . (2.16)}$$

where C is an arbitrary constant and k is defined as follows:

$$k^2 = \frac{PR^3}{EI} + 1 \quad \text{. . (2.17)}$$

If the boundaries of the buckling portion are confined at $\theta = \pm\phi$ and the appropriate boundary conditions are applied to the differential equations, the value of k can be determined by solving the following two equations in k and ϕ simultaneously:

$$k = \frac{R}{i}\left(\frac{1-\phi\cot\phi}{\pi\cot\phi}\right)^{\frac{1}{2}} \quad \text{. . (2.18)}$$

$$\phi\cot\phi = k\phi\cot k\phi \quad \text{. . (2.19)}$$

where i = radius of gyration $= (I/A)^{1/2} = (t^2/12)^{1/2}$

Examining Equations (2.18) and (2.19) graphically shows that values of k are not case sensitive for values of ϕ. This is true when $R/i \to \infty$, which is the case for thin rings. Therefore, for the purpose of simplifying the solution, the case of $\phi=0$ is considered. As the critical arc angle ϕ goes to zero, the solution for Equations (2.18) and (2.19) is

$$k_{cr} = 1.57\left(\frac{R}{i}\right)^{\frac{2}{5}} \quad \text{. . (2.20)}$$

The critical pressure P_{cr} of the rigidly encased thin ring is determined by rewriting Equation (2.17):

$$P_{cr} = \frac{(k_{cr}^2 - 1)\, EI}{R^3} \quad \ldots \quad (2.21)$$

For relatively thin pipes (e.g., $SDR > 30$), $k^2\text{-}1 \approx k^2$. Substituting Equation (2.20) into Equation (2.21) and considering an infinitely long pipe, then

$$P_{cr} = \frac{2.55\, E}{1 - \nu^2} \left(\frac{t}{D}\right)^{\frac{11}{5}} \quad \ldots \quad (2.22)$$

2.1.3.3 Glock's Approach

Glock (1977) analyzed the stability problem of a circular thin ring encased in rigid boundaries under the effect of external hydrostatic pressure as well as thermal load. Glock's model assumes that there is no friction between the ring and the rigid cavity, but unlike Cheney's model, Glock's model does not require the cavity wall to move inward with the ring. Glock used the nonlinear-deformation theory to develop his model. However, the derivation of Glock's model is not fully documented, and the theoretical bases upon which he built his model are not cited. For the benefit of future research, the complete derivation of this model is presented in Chapter 3.

2.1.4 Buckling of a Thin Ring Encased in a Rigid Oval Host Pipe

The significance of studying a problem such as the buckling of a thin liner encased in a rigid oval host pipe arises from its importance to industry. In the design

process of CIPP, the design engineer must continuously evaluate the effects of manufacturing tolerances, cross-sectional imperfections, and the existing ovalization of the original pipeline on the structural performance of the liner. In most cases, deteriorated pipelines are out-of-round, and special considerations should be taken in the design to include the effect of this ovalization.

ASTM F1216-93 has incorporated the effect of the host pipe ovalization on its requirement of CIPP strength by adopting the ovality reduction factor, C, as presented in Equation (2.5). In the following sections, other models which been found in the literature and could be applicable to the case of CIPP encased in a rigid oval host pipe are presented.

The static behavior of the cylindrical shell of arbitrary cross-sections have been analyzed by many authors. Novozhilov (1959) presented a method to analyze the behavior of a cylindrical short-shell with an elliptical cross-section and loaded by a uniform normal external pressure.

Romano and Kempner (1962) conducted a series of studies on the static analysis of an oval cylindrical shell whose curvature can be described by the following expression:

$$\frac{1}{r} = \frac{1}{r_o}\left(1 + \xi \cos\frac{4\pi s}{L_o}\right) \qquad \ldots (2.23)$$

where r = local radius of curvature, and it is a function of the circumferential coordinates;

r_o = radius of a circle whose circumference is equal to that of the oval;

ξ = eccentricity constant of the oval;

L_o = circumference of oval pipe = $2\pi r_o$; and,

s = circumference coordinate.

Equation (2.23) represents a group of oval shapes which are slightly different than the corresponding ellipses having the same semiaxes.

Slocum (1909) estimated the collapse uniform external pressure of long, unconstrained elliptical tubes from the collapse pressure of an "equivalent" circular cylinder. The diameter of this equivalent circular cylinder was taken as the maximum diameter of the ellipse. The additional stiffness of the ellipse was not considered in the analysis. Therefore, the collapse pressure of an elliptical tube is related to the original round tube by the relationship

$$P_{oval} = P_o \alpha^9 \quad \ldots \quad (2.24)$$

where P_{oval} = collapse pressure of elliptical pipe;

P_o = collapse pressure of originally round pipe;

α = minor axis ellipse coordinate/original pipe diameter.

This research predicts significant reductions in collapse pressure for elliptical cross-sections. For example, the collapse pressures for elliptical cross-sections with 5% and 10% ovality (α = 0.95 and 0.90, respectively) are only 63% and 39%,

respectively, of the collapse pressures predicted for the original circular cross-sections. These values are close to the reduction values suggested by ASTM F1216-93 of 64% for the case of 5% ovality and 41% for 10% ovality.

Soong and Choi (1985) solved the problem of a thin elastic ring compressed by being inserted into a rigid elliptic boundary whose circumference is smaller than the unstressed length of the ring. This problem is similar to the shrink buckling problem introduced by Chicurel (1968) for the case of a circular ring. They presented the governing differential equations, boundary conditions, and step-by-step solution procedures for three different buckling cases. These cases were the snap-through buckle, the two-buckle case with no friction, and two-buckle with no-slip.

Li and Guice (1995) studied the stability of CIPP encased in rigid elliptical host pipe and loaded by external hydrostatic pressure. Following a similar analysis for the shrink buckling presented by Chicurel (1968), they reached the following formula for the ovality reduction factor 'C':

$$C = \frac{1}{(1+q)^{\frac{8}{5}}\,(1-q)^{\frac{1}{5}}} \qquad \ldots (2.25)$$

A comparison between their suggested value for 'C' and the proposed value by ASTM F1216-93 was also presented. This comparison has shown that the reduction factor presented in ASTM F1216-93 gives conservative values compared to Equation (2.25). However, no experimental work was presented to support this conclusion.

Kurt and Mark (1981) developed an approach to predict the short-term collapse pressure of oval buried flexible thermoplastic pipelines. The soil radial support has been linearized in the solution and presented in terms of the modulus of subsurface reaction. Expressing the oval pipes in terms of the curvature function shown in Equation (2.23), the solution reduces to two infinite recurrence formulas. The short-term collapse pressure was calculated by solving these infinite recurrence formulas numerically. Parametric studies were conducted to evaluate the effects of cross-sectional ovality versus the supporting soil stiffness on the predicted short-term collapse pressure. These studies have shown that the cross-sectional ovality does not have a significant impact on predicted collapse pressure compared to this significant influence of the surrounding soil stiffness on the collapse pressure. Another conclusion drawn from these parametric studies is that the use of an equivalent circle whose radius is equal to the maximum radius of the non-circular cross-section has greatly magnified the influence of ovality when predicting short-term collapse pressure.

2.2 Research Need

In a recent study on the stability of CIPP encased in rigid circular host pipes, different theoretical models were compared with experimental results (Li, 1994). Models under study include ASTM F1216-Equation X1.1, Chicurel's model (1968), Cheney's model (1971), and Glock's model (1977). The study shows that ASTM F1216- Equation X1.1 gives a remarkable marginal error in comparison with experimental results. It also concludes that the model proposed by Glock (1977) gives

the most appropriate values for the instantaneous buckling pressure among other models. The documented distinction of Glock's model (1977) among other stability models makes it the best candidate to replace the current design equation. However, the derivation of Glock's model (1977) in his paper is not fully documented, and the theoretical bases upon which he built his model are not cited. Therefore, and for the benefit of future research in CIPP design methodology, it is imperative to reproduce Glock's equations and to validate this model experimentally. Also, because of the importance of studying the effect of pipeline ovalization on the capacity of the installed CIPP, it is desirable to investigate such a problem. A similar model to Glock's approach (1977) and which is applicable to the case of CIPP encased in oval host pipes is needed.

Chapter 3 presents a complete derivation for Glock's model. It also provides a comparison study between Glock's model and the results of three sets of experimental work. Chapter 4 includes a derivation of a new model for the stability of CIPP encased in oval host pipes. The new model is validated with experimental work which was done during the course of this research.

CHAPTER 3

GLOCK's MODEL FOR THE INSTABILITY OF CIPP

3.1 Glock's Approach

Consider the system of polar coordinates and deformations shown in Fig. (3.1), where u is the radial displacement and v is the circumferential displacement. The following assumptions are used for the case of a thin ring (El-Bayoumy, 1972; Kerr and Soifer, 1969):

$$\sigma_{zz} = 0 \qquad \sigma_{rr} \ll \sigma_{\theta\theta} \qquad \ldots (3.1)$$

$$\varepsilon_{zr} = \varepsilon_{z\theta} = 0 \qquad \ldots (3.2)$$

$$\varepsilon_{r\theta} = 0 \qquad \ldots (3.3)$$

With the above assumptions, the strain energy expression for a thin circular ring reduces to

$$U = \frac{1}{2}\iiint_{V} \varepsilon_{\theta\theta}\,\sigma_{\theta\theta}\,dV \qquad \ldots (3.4)$$

where V is the volume of the ring. Assuming the validity of Hooke's law, the above expression for the strain energy can be rewritten as follows:

$$U = \frac{1}{2}\int_{-\phi}^{+\phi} \left[\iint_{A} E\,\varepsilon_{\theta\theta}^{2}\,dA\right] r\,d\theta \qquad \ldots (3.5)$$

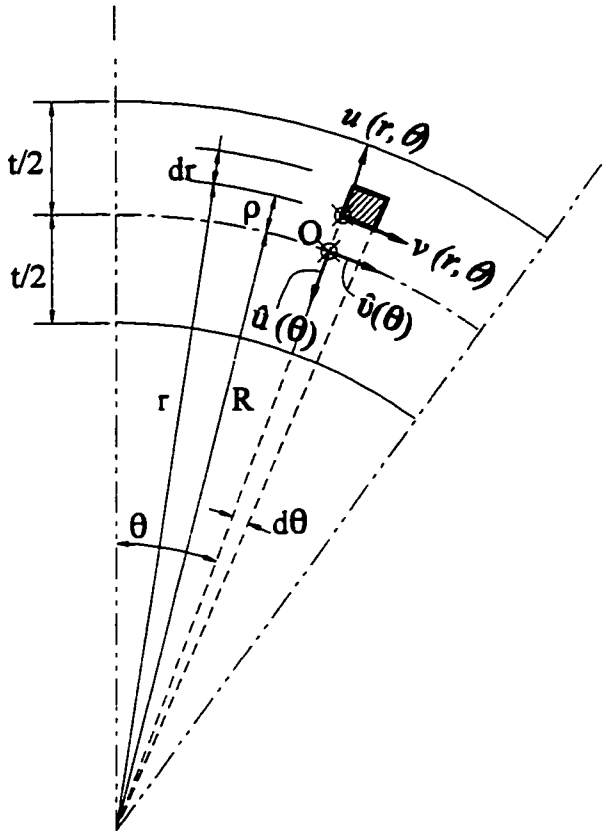

Fig. 3.1 Displacements of a Thin Ring in Polar Coordinates

where r is the radius of the point under consideration as shown in Fig. (3.1). The general expression for the nonlinear circumferential strain is (El-Bayoumy, 1972; Kerr and Soifer, 1969)

$$\varepsilon_{\theta\theta} = \frac{1}{r}\left(\frac{\partial v}{\partial \theta} + u\right) + \frac{1}{2r^2}\left(\frac{\partial u}{\partial \theta} - v\right)^2 + \frac{1}{2r^2}\left(u + \frac{\partial v}{\partial \theta}\right)^2 \quad \ldots (3.6)$$

For thin rings, it is possible to assume that u, v, $v' \ll u'$ (El-Bayoumy, 1972) which reduces expression (3.6) to

$$\varepsilon_{\theta\theta} = \frac{1}{r}(v' + u) + \frac{1}{2r^2}(u')^2 \quad \ldots (3.7)$$

where $(\,)' \equiv \frac{d}{d\theta}(\,)$

Denoting the displacement of the ring axis by $\hat{u}$ and $\hat{v}$, then the displacement components $u(r,\theta)$ and $v(r,\theta)$ may be expressed in terms of the displacement components of the ring axis as follows:

$$u(r,\theta) = -\hat{u}(\theta) \quad \ldots (3.8)$$

$$v(r,\theta) = \hat{v}(\theta) + \rho f(\theta) \quad \ldots (3.9)$$

where ρ is the radial distance from the ring axis to the point under consideration (Fig. 3.1). The unknown function $f(\theta)$ is determined from the linearized form of the condition $\varepsilon_{r\theta}=0$; therefore,

$$f(\theta) = \frac{1}{R}\left(\frac{\partial \hat{u}}{\partial \theta} + \hat{v}\right) \quad \ldots (3.10)$$

where the approximations $\rho \ll R$ and $(1-\rho/R) \approx 1.0$ are used to reach the above expression and R is the ring mean radius. Substituting Equation (3.10) into Equation (3.9), the final forms for $u(r,\theta)$ and $v(r,\theta)$ in terms of $\hat{u}$ and $\hat{v}$ are

$$u(r,\theta) = -\hat{u}(\theta) \quad \ldots \quad (3.11)$$

$$v(r,\theta) = \hat{v} + \frac{\rho}{R}\hat{u}' \quad \ldots \quad (3.12)$$

Using Equations (3.11) and (3.12), the expression for the nonlinear circumferential strain, Equation (3.7) becomes

$$\varepsilon_{\theta\theta} = \hat{\varepsilon}_{\theta\theta} + \rho\hat{\kappa} \quad \ldots \quad (3.13)$$

where

$$\hat{\varepsilon}_{\theta\theta} = \frac{1}{R}(\hat{v}' - \hat{u}) + \frac{1}{2R^2}(\hat{u}')^2 \quad \ldots \quad (3.14)$$

and

$$\hat{\kappa} = \frac{\hat{u}''}{R^2} \quad \ldots \quad (3.15)$$

Equation (3.13) is the general form of the nonlinear circumferential strain of an elastic ring in terms of its central axis displacements. This expression encompasses two parts. The first part, $\hat{\varepsilon}_{\theta\theta}$, represents the axial extension of the ring's centroid axis, and the second part, $\rho\hat{\kappa}$, represents the change of curvature at the point under consideration. Many researchers such as Novozhilov (1953), Kerr and Soifer (1969), and El-Bayoumy

(1972) have used Equation (3.13) to study several problems of circular rings and arches.

In a similar approach to Cheney's model (1971), Glock (1977) envisioned the ring to be made up of two regions: region I and region II as shown in Fig (3.2). Region I includes the buckled part of the ring, where there is no contact between the ring and the external rigid pipe. Region II is the unbuckled portion of the ring, and it is in contact with the rigid host pipe. Region I carries both a hoop force and a bending moment. While in region II, because no change of curvature is induced in this part of the ring, the bending moment vanishes, and only the hoop force needs to be considered.

Substituting Equations (3.14) and (3.15) into Equation(3.5), the strain energy expressions in regions I and II can be written as follows:

$$U_1 = \int_0^{\phi} ER(A\hat{\varepsilon}_{1\theta}^2 + I\hat{\kappa}_1^2)\,d\theta \qquad \ldots (3.16)$$

$$U_2 = \int_{\phi}^{\pi} ER(A\hat{\varepsilon}_{2\theta}^2 + I\hat{\kappa}_2^2)\,d\theta \qquad \ldots (3.17)$$

where

$$\hat{\varepsilon}_{1\theta} = \frac{1}{R}(\hat{v}'_1 - \hat{u}_1) + \frac{1}{2R^2}(\hat{u}'_1)^2 \;; \qquad \hat{\varepsilon}_{2\theta} = \frac{\hat{v}'_2}{R} \qquad \ldots (3.18)$$

$$\hat{\kappa}_1 = \frac{\hat{u}_1''}{R^2} \;; \qquad \hat{\kappa}_2 = 0 \qquad \ldots (3.19)$$

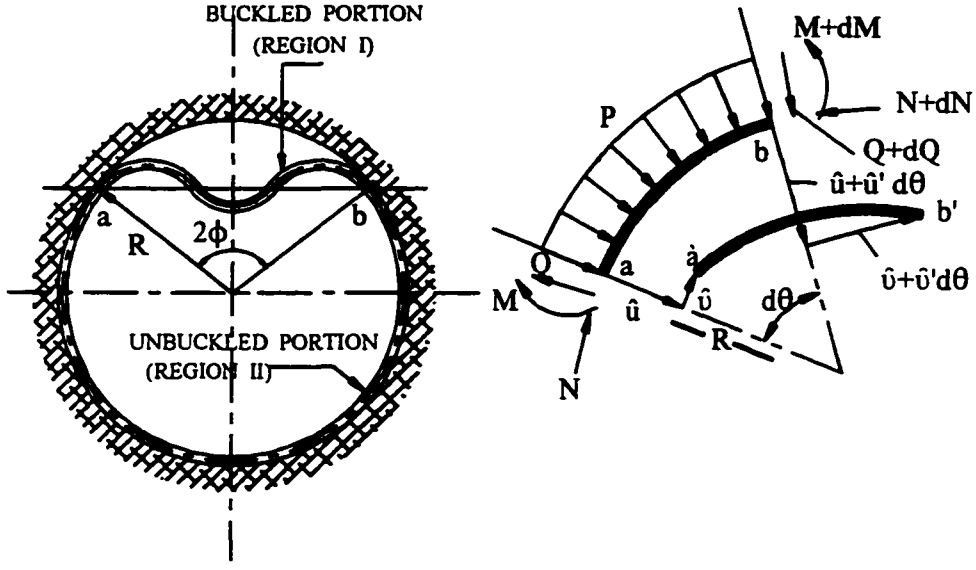

Fig. 3.2 Glock's Buckling Model of a Thin Ring Loaded by a Hydrostatic Pressure

The terms $\hat{u}_1$ and $\hat{u}_2$ denote the radial displacements in region I and II, respectively, and $\hat{v}_1$ and $\hat{v}_2$ are the circumferential displacements. Since Region II is attached to the host pipe, $\hat{u}_2$ and $\hat{\kappa}_2$ are assumed to be zero in the above expression of the strain energy in region II. The total potential energy of the system is

$$\Pi = U_1 + U_2 - W \qquad \text{. . (3.20)}$$

where W is the work potential of the external hydrostatic pressure. Substituting Equations (3.16) and (3.17) into the expression of the total potential energy, Equation (3.20), and collecting similar terms, then

$$\Pi = EI\int_0^{\phi} \hat{\kappa}_1^2 R d\theta + EA\{ \int_0^{\phi} \hat{e}_{1\theta}^2 R d\theta + \int_{\phi}^{\pi} \hat{e}_{2\theta}^2 R d\theta \} - 2\int_0^{\phi} P\hat{u}_1 R d\theta \qquad \text{. . (3.21)}$$

The first term in the above expression represents the potential energy resulting from the change of curvature, and the second term represents the potential energy resulting from the axial strains of the ring center line. Substituting Equations (3.18) and (3.19) into the above expression, the total potential energy in terms of the center line displacements can be stated as

$$\Pi = \frac{EI}{2R^3}\int_0^{\phi} \hat{u}_1'^2 d\theta + EA\{ \int_0^{\phi} [\frac{1}{R}(\hat{v}_1' - \hat{u}_1) + \frac{1}{2R^2}\hat{u}_1'^2]^2 R d\theta + \int_{\phi}^{\pi} [\frac{\hat{v}_2'^2}{R}]^2 R d\theta\} - 2\int_0^{\phi} P_o \hat{u}_1 R d\theta \qquad \text{. . (3.22)}$$

Another simplification for the above expression of the total potential energy was suggested by Glock (1977). This modification entails the assumption of

$$\frac{\partial \hat{v}_1}{\partial \theta} = 0 \quad ; \quad \frac{\partial \hat{v}_2}{\partial \theta} = 0 \qquad \ldots (3.23)$$

which results in the elimination of the term U_2, the strain energy in region II. Of course, this is not the actual situation in that part of the ring. To account for this discrepancy, Glock (1977) averaged the strain energy density caused by the extension strains over the ring's circumference. The reason behind that, as is shown later, is to get the expression of total potential energy, Equation (3.22), in terms of only one unknown displacement, $\hat{u}_1$. Averaging the strain energy caused by hoop force carries the assumption of having a constant hoop force along the entire ring. The average value for this hoop force is calculated by summing the hoop force in region I and dispensing it over the ring circumference as follows:

$$N_{avg} = \frac{EA}{R\pi} \left(\int_0^{\phi} \hat{u}_1'' d\theta - \int_0^{\phi} \frac{\hat{u}_1'^2}{2R} d\theta \right) \qquad \ldots (3.24)$$

By replacing the hoop strain potentials in Equation (3.22) with equivalent terms of the average hoop force, then the total potential energy reduces to

$$\Pi = \frac{EI}{R^3} \int_0^{\phi} \hat{u}_1'^2 \, d\theta + \frac{1}{EA} \int_0^{\pi} N_{avg}^2 \, R d\theta - \int_0^{\pi} P \hat{u}_1 \, R d\theta \qquad \ldots (3.25)$$

Equation (3.25) is the total potential energy form used in Glock's solution (1977). An approximate form for the radial deflection in region I could be assumed as follows:

$$\hat{u}_1 = \hat{u}_o \cos^2\left(\frac{\pi\theta}{2\phi}\right) \qquad 0 \le \theta \le \phi \qquad \ldots (3.26)$$

where $\hat{u}_o$ is the radial deflection at $\theta=0$. Substituting the above approximate form of radial displacements into the expression of N_{avg} and performing the integration results in

$$N_{avg} = \frac{EA\phi}{2R\pi}\left[\hat{u}_o - \frac{\hat{u}_o^2}{8R}\left(\frac{\pi}{\phi}\right)^2\right] \quad \ldots (3.27)$$

It is clear from Equation (3.27) that N_{avg} is a constant value and not a function of θ. Substituting Equation (3.26) into the expression of the total potential energy, Equation (3.25), then

$$\Pi = \frac{EI}{R^3}\int_0^{\phi}\left(-\hat{u}_o\frac{\pi^2}{2\phi^2}\cos\frac{\pi\theta}{2\phi}\right)^2 d\theta + \int_0^{\pi}\frac{N_{avg}^2}{EA}Rd\theta - \int_0^{\pi}P\hat{u}_o\cos^2\left(\frac{\pi\theta}{2\phi}\right)Rd\theta \quad \ldots (3.28)$$

Performing the integration the above expression reduces to

$$\Pi = \frac{EI}{16R^3}\phi\left(\frac{\pi}{\phi}\right)^4\hat{u}_o^2 + \frac{N_{avg}^2}{2}\frac{R\pi}{EA} - \frac{PR}{2}\phi\hat{u}_o \quad \ldots (3.29)$$

Employing the principle of minimum total potential energy, then

$$d\Pi = \frac{\partial\Pi}{\partial\hat{u}_o}d\hat{u}_o + \frac{\partial\Pi}{\partial\phi}d\phi = 0 \quad \ldots (3.30)$$

$$\frac{\partial\Pi}{\partial\hat{u}_o} = 0 \;, \;\&\; \frac{\partial\Pi}{\partial\phi} = 0 \quad \ldots (3.31)$$

Performing the differentiation, the resulting equation will be as follows:

$$\frac{\partial\Pi}{\partial\hat{u}_o} = \frac{EI}{8R^3}\phi\left(\frac{\pi}{\phi}\right)^4\hat{u}_o + N_{avg}\frac{\partial N_{avg}}{\partial\hat{u}_o}\frac{R\pi}{EA} - \frac{PR}{2}\phi = 0 \quad \ldots (3.32)$$

but since

$$\frac{\partial N_{avg}}{\partial \hat{u}_o} = \frac{EA}{R\pi}\frac{\phi}{2}\left[1 - \frac{1}{4}\left(\frac{\pi}{\phi}\right)^2 \frac{\hat{u}_o}{R}\right] \quad \ldots (3.33)$$

then Equation (3.32) becomes

$$\hat{u}_o\left[\frac{EI}{8R^3}\left(\frac{\pi}{\phi}\right)^4 - \frac{N_{avg}}{8R}\left(\frac{\pi}{\phi}\right)^2\right] = \frac{PR}{2} - \frac{N_{avg}}{2} \quad \ldots (3.34)$$

Also,

$$\frac{\partial \Pi}{\partial \phi} = -\frac{3}{16}\frac{EI}{R^3}\left(\frac{\pi}{\phi}\right)^4 \hat{u}_o^2 + N_{avg}\frac{\partial N_{avg}}{\partial \phi}\frac{R\pi}{EA} - \frac{PR}{2}\hat{u}_o = 0 \quad \ldots (3.35)$$

but

$$\frac{\partial N_{avg}}{\partial \phi} = \frac{1}{2}\frac{EA}{R\pi}\left[\hat{u}_o + \frac{1}{8}\frac{\hat{u}_o^2}{R}\left(\frac{\pi}{\phi}\right)^2\right] \quad \ldots (3.36)$$

With the substitution of Equation (3.36) into Equation (3.35), then

$$\hat{u}_o\left[\frac{-3}{16}\frac{EI}{R^3}\left(\frac{\pi}{\phi}\right)^4 + \frac{N_{avg}}{16R}\left(\frac{\pi}{\phi}\right)^2\right] = \frac{PR}{2} - \frac{N_{avg}}{2} \quad \ldots (3.37)$$

Equations (3.34) and (3.37) are two equations with two unknowns, $\hat{u}_o$ and ϕ, and N_{avg} in terms of ϕ could be obtained by subtracting Equation (3.37) from Equation (3.34); then

$$N_{avg} = \frac{5}{3}\frac{EI}{R^2}\left(\frac{\pi}{\phi}\right)^2 \quad \ldots (3.38)$$

Equating Equation (3.38) and Equation (3.24) results in

$$\frac{1}{2}\left(\frac{\phi}{\pi}\right)\hat{u}_o - \frac{1}{16}\left(\frac{\pi}{\phi}\right)\frac{\hat{u}_o^2}{R} - \frac{5}{3}\frac{EI}{EA}\frac{1}{R}\left(\frac{\pi}{\phi}\right)^2 = 0 \qquad \text{. . (3.39)}$$

Equation (3.39) is a quadratic equation in terms of $\hat{u}_o$ with the two roots

$$\hat{u}_o = 4R\left(\frac{\phi}{R}\right)^2 \pm \sqrt{16R^2\left(\frac{\phi}{\pi}\right)^4 - \frac{80}{3}\frac{EI}{EA}\left(\frac{\pi}{\phi}\right)} \qquad \text{. . (3.40)}$$

Also, with the substitution of Equation (3.38) into Equation (3.34), we get

$$-\hat{u}_o = \frac{6PR^4}{EI}\left(\frac{\phi}{\pi}\right)^4 + 10R\left(\frac{\phi}{\pi}\right)^2 \qquad \text{. . (3.41)}$$

Equating Equation (3.40) with Equation (3.41),

$$\frac{PR^3}{EI} = \left(\frac{\pi}{\phi}\right)^2\left[1 \pm \frac{1}{6}\sqrt{16 - \frac{80EI}{3EA}\frac{1}{R^2}\left(\frac{\pi}{\phi}\right)^5}\right] \qquad \text{. . (3.42)}$$

Assuming that

$$\frac{\pi}{\phi} = \gamma \qquad \text{and} \qquad \alpha = \frac{PR^3}{EI}$$

then Equation (3.42) can be simplified to

$$\alpha = \gamma^2\left[1 \pm \frac{1}{6}\sqrt{16 - \frac{80EI}{3EA}\frac{1}{R^2}\gamma^5}\right] \qquad \text{. . (3.43)}$$

and to find the critical pressure P_{cr} then,

$$\frac{\partial P}{\partial \gamma} = 0 \quad \rightarrow \quad \frac{\partial \alpha}{\partial \gamma} = 0 \qquad \text{. . (3.44)}$$

or

$$2\gamma\left[1\pm\frac{1}{6}\sqrt{16-\frac{80}{3}\frac{EI}{EA}\frac{1}{R^2}\gamma^5}\right]\mp\frac{\gamma^2}{12}\frac{\frac{400}{3}\frac{EI}{EA}\frac{\gamma^4}{R^2}}{\sqrt{16-\frac{80}{3}\frac{EI}{EA}\frac{1}{R^2}\gamma^5}}=0 \qquad . . \quad (3.45)$$

with the root

$$\gamma_{cr} = 0.856\left(\frac{EA}{EI}R^2\right)^{1/5} \qquad . . \quad (3.46)$$

Substituting the value of γ_{cr} into Equation (3.43), we get

$$\alpha_{cr} = \begin{bmatrix}0.9690\\0.4964\end{bmatrix}\left(\frac{EA}{EI}R^2\right)^{2/5} \qquad . . \quad (3.47)$$

or

$$\frac{P_{cr}R^3}{EI} = 0.969\left(\frac{EA}{EI}R^2\right)^{2/5} \qquad . . \quad (3.48)$$

Assuming that E is constant for both flexural and axial stiffness and accounting for the plane strain condition of long pipes, the above expression for the critical pressure of thin rings could be reduced to a form similar to the case of thin pipes encased in rigid cavity as follows:

$$P_{cr} = \frac{E}{1-\nu^2}\left(\frac{t}{D}\right)^{2.2} \qquad . . \quad (3.49)$$

3.2 Discussion of Models

The models reviewed in this chapter and Chapter 2 for the case of a thin ring encased in rigid cavity all result in equations for the critical buckling pressure which are similar in form. The basic form of these equations is

$$P_{cr}=\frac{\eta E}{1-\nu^2}\frac{1}{(SDR-1)^{\beta}} \qquad \ldots (3.50)$$

where η = coefficient,

β = exponent.

The resulting coefficients and exponents for each model are summarized in Table (3.1). It should be noted that there are consistencies in the exponents for the different models. Those models which impose a constraint around the surface yield solutions with an exponent of 2.2.

However, the coefficients can vary significantly depending upon the types of assumptions made. Each of the models presented has merits and under certain conditions might be the most appropriate one for consideration. However, each of the models also has limitations, and even for the most complex of the models some factors have not been included.

The stability analysis of a restrained pipe is complicated by nonlinear geometries, various interface and boundary conditions, and nonlinear material behavior. Other factors which must ultimately be considered by a model include visco-elastic

effects, host pipe geometry (such as ovality), and defects as well as other anomalies which may occur.

Table 3.1 Buckling Equation Parameters

Model	Coefficient, η	Exponent, β
Timoshenko unconstrained	2.0	3.0
Chicurel's shrink buckling	2.76	2.2
Cheney's encased ring	2.55	2.2
Glock's encased ring	1.0	2.2

3.3 Evaluation of Buckling Models Through Experimental Results

The application of any analytical model into practice requires validation and calibration through experimental research. Until analytical models have been developed to include the necessary conditions, the resulting equations must be tuned by experiment, and safety factors must be included to address various uncertainties.

The equations derived by the approaches presented above may be evaluated through comparisons with available experimental data. The mathematical tools of linear regression and error analysis may be employed to develop the value of the coefficient and exponent based on the experimental results.

Very little CIPP pipe experimental data exist for evaluating the theoretical models. Some organizations are known to have conducted proprietary experimental work related to this study, but most have not been published in the public domain.

Three sets of data which are used in this evaluation include work done by Aggarwal and Cooper at Coventry Polytechnic in 1984 (unpublished); Lo, Chang, Zhang, and Wright at Utah State University (1993); and Guice and others at Louisiana Tech University (1994).

Aggarwal and Cooper Tests. Aggarwal and Cooper conducted external pressure tests of Insituform liners. In these tests, the liners were inserted in steel pipes. Pressure was applied and increased between the liner and casing in increments of approximately 1/10th of the expected failure pressure, until failure. Internal observation was carried out to determine when bulging occurred. The experimental failure pressure was found to be much larger than the theoretical buckling pressure obtained by Equation (2.3).

An enhancement factor was defined by Aggarwal and Cooper as $K = P_{test}/P_{theory}$. The enhancement factor reflects the difference between the results by experiment and theory. Aggarwal and Cooper indicated that the values of the enhancement factor varied from 6.5 to 25.8 with a range of pipe *SDRs* from approximately 30 to 90. Aggarwal and Cooper indicated that 46 of the 49 tests gave a value of K greater than 7. The term enhancement was used because the buckling resistance of the liners appeared to be significantly enhanced by the constraining effects of the host pipe. For the remaining portion of this chapter, K will simply be referred to as a factor which compensates for the deviation between experimental results and theory.

Aggarwal and Cooper's tests included data for 49 specimens with a relatively large range of standard dimension ratios (SDR from 29.86 to 90.25) and a variety of material properties (modulus of elasticity from 895,700 KPa to 2,521,740 KPa).

Shell Development Company Tests. Shell Development Company conducted an experimental program at Utah State University to evaluate the collapse resistance of CIPP liners made with various epoxy resins (Lo, et al., 1993). The specimens of the tests had a constant outside diameter and different thicknesses. The results of these tests were also analyzed to determine the enhancement factor K. Lo found the values of the factors ranged from 9.66 to 15.1.

Louisiana Tech University Tests. Louisiana Tech University has conducted research on the long-term effects of hydrostatic pressures on CIPP liners under the Corps of Engineers Construction Productivity Advancement Research (CPAR) program (Guice, et al., 1994). Seven different products from five companies were evaluated. Several short-term tests for each product were also conducted. Test specimens were 12 inches in diameter, and SDRs ranged from 30 to 60.

3.3.1 Analysis of Data

If the term P_{test} is defined as the experimental buckling pressure and the factor K is defined as the ratio of P_{test} to P_{cr}, the following equation can be obtained:

$$P_{test} = K \times P_{cr} = \left[\frac{\eta E}{(1-\nu^2)} \frac{1}{(SDR-1)^{\beta}}\right] \times K \qquad . . \quad (3.51)$$

and,

$$Log\left(\frac{P_{test}}{E/(1-\nu^2)}\right) = Log\,\eta - \beta\,Log\,(SDR-1) + Log\,K \qquad . . \quad (3.52)$$

If the subscript of i is used to designate individual test results ($i = 1, 2, 3, \ldots, n$,), where n is the number of the tests in the sample, Equation (3.52) can be expressed in terms of subscript i as follows:

$$Log\left(\frac{P_{test,i}}{E_i/(1-\nu^2)}\right) = Log\,\eta - \beta\,Log\,(SDR_i-1) + Log\,K_i + \varepsilon_i \qquad . . \quad (3.53)$$

The values of η and β may be determined by the particular analytical equation used for the critical pressure P_{cr}. The term $P_{test,i}$ is the test result of i^{th} specimen, while E_i and SDR_i are the corresponding modulus of elasticity and standard dimension ratio. The term K_i reflects the deviation between the theoretical and experimental buckling pressures of a specific test specimen, while ε_i is the associated statistical error. If the results of a series of short-term buckling tests are employed to verify a theoretical equation with corresponding values of constant $Log\ \eta$ and β, a sample $Log\ K_i$ ($i = 1, 2, \ldots n$) can be obtained, and the mean $Log\ K$ and standard deviation s of the test sample can be determined. The factor K is affected by many known and unknown factors of the specimen and the process of testing.

When evaluating different equations, the theoretical formula is first selected, and the error related to the deviation between the theoretical and experimental buckling pressures is determined. On the other hand, it would be interesting to determine the

coefficients and exponents which could best predict the buckling pressures. To do this, best-fitting regression may be employed using the method of least squares.

3.3.2 Results

If the coefficients and exponents presented in Table (3.1) are substituted into Equation (3.53), the data may be analyzed to yield estimates of the mean error $Log\,K$ and the enhancement factor K corresponding to the error for each theoretical equation. The results of this analysis for Timoshenko's unconstrained model and Glock's constrained model are presented in Table (3.2). The results of the best-fitting regression analysis of Aggarwal and Cooper's data are also presented in Table (3.2).

Since the other analytical models presented are similar in form and vary only by a constant with either Timoshenko's or Glock's equations, the results for the other models were not included for comparison in Table (3.2). The average deviations between the theoretical and experimental buckling pressures are smaller for Glock's equation than Timoshenko's equation. Further, a best-fitting regression analysis results in coefficients and exponents very similar to those for Glock's model.

The test results from Shell Development Company and Louisiana Tech University were analyzed for comparison with the Timoshenko and Glock equations. The data were analyzed to determine average values of statistical deviations based upon each of the two models. Those results are summarized in Table (3.3). The smaller deviations between experiment and theory are again noted for Glock's equation.

3.4 Conclusion

The development of several analytical models for the design of CIPP encased in partially deteriorated host pipe were presented and compared with experimental data. The comparison study shows that the coefficient and exponent suggested by Glock's model are the most appropriate values for use in the design of CIPP. Furthermore, it is clear that the enhancement factor, K, of 7 which is in common use in industry to compensate strictly for the deviation between experimental results and the theoretical unconstrained pipe critical pressure is conservative. This factor, of course is not all encompassing as it does not address conditions such as host pipe ovality and stiffness, visco-elastic effects and uncertainties about loading. Other factors must be employed to address these issues in the current design practice.

The conclusion of this study is that Glock's model is the best available model in literature to replace the current design practice. On preliminary basis, it would appear to be possible to accomplish the replacement of the current design equation through the utilization of a coefficient η in Glock's model based on a best-fitting regression analysis of additional test data. Therefore, additional research is required before any new equation can be recommended as a design expression for CIPP.

Table 3.2 Evaluation of Buckling Models With Aggarwal and Cooper Data

Equation	η	β	*LogK*	*K*	s
Timoshenko	2.00	3.00	1.075	11.89	0.139
Glock	1.00	2.20	0.078	1.20	0.107
Best-Fitting Regression	1.07	2.17	0.000	1.00	0.107

Table 3.3 Analysis of Experimental Data

Data	Timoshenko			Glock		
	LogK	*K*	s	*LogK*	*K*	s
Aggarwal and Cooper	1.08	11.89	0.14	0.08	1.20	0.11
Shell Development	1.13	13.38	0.06	0.04	1.10	0.06
Louisiana Tech	0.99	9.81	0.11	-0.05	0.90	0.08

η = coefficient
β = exponent
LogK = mean value (average deviation between theoretical and experiemntal results)
K = the enhancement factor corresponding to the mean value (*LogK*)
s = standard deviation of the error values

CHAPTER 4

INSTABILITY OF CIPP ENCASED IN OVAL HOST PIPES

4.1 Introduction

This chapter presents a new model for predicting the buckling pressure of CIPP encased in rigid oval host pipes. It also encompasses a detailed discussion of the experimental work which has been conducted to verify this new model. The results of the experimental work are compared with the proposed model and other analytical models.

4.2 Analytical Model

Glock's model (1977) for predicting the buckling pressure of CIPP encased in circular host pipes has been presented in Chapter 3. Statistical analyses comparing Glock's model with other buckling models versus three different experimental works have also been presented in this chapter. The results of these analyses showed that Glock's model has the lowest marginal error among other models when it is compared with experimental results. This conclusion reveals the suitability of Glock's assumptions, in general, to study CIPP instability problems. Because of this proven success of Glock's model, a similar model for the case of CIPP encased in oval host

pipes is proposed in this section. The derivation of this new model follows the same basic steps Glock used in the derivation of his model.

Coordinate System. In the analysis of problems which have elliptical boundaries, it is usually preferable to employ a coordinate system which resembles those boundaries. For the problem under study, it is found that employing the system of oval coordinates, as described later, simplifies the problem.

Romano and Kempner (1962) have used this system of coordinates to analyze the deformations and stresses in a short oval cylindrical shell under the effect of external uniform pressure. In their study, they have presented the oval coordinates as shown in Fig. 4.1. In this figure, the term, s, is the circumferential length measured along the oval perimeter, and, r, is the radial coordinate measured as the inner normal to the meridian surface. The terms $\hat{v}$ and $\hat{u}$ are the circumferential and radial displacements of the meridian surface, respectively.

The oval coordinate system (Fig. 4.1) can be characterized implicitly by a governing equation describing its curvature at every point as follows:

$$\frac{1}{R} = \frac{1}{R_o}[1 + \xi\cos(\beta s)] \qquad \ldots (4.1)$$

where R = local radius of curvature as a function of s,

R_o = radius of a circle whose circumference L_o is equal to that of the oval,

$\beta = 4\pi/L_o$, and,

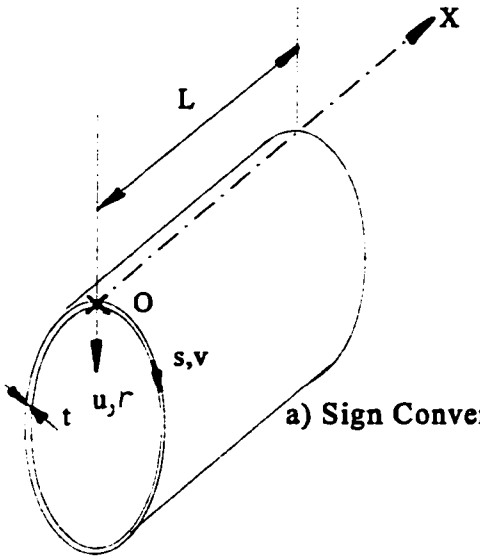

a) Sign Convention For Coordinates and Displacements

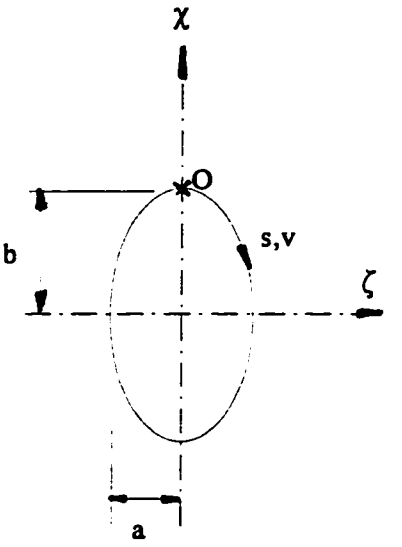

b) Coordinates For Oval

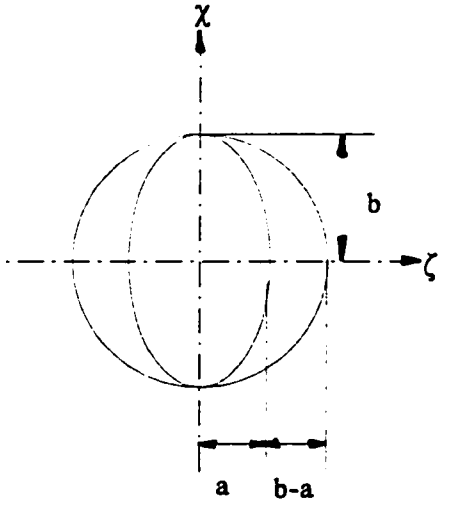

c) Eccentricity of Oval

Fig. 4.1 Sign Convention and Geometrical Properties of Oval Pipe (after Romano and Kempner 1958)

ξ = measure of eccentricity (non-circularity) of the oval and it is a function of the oval semiaxes and obeys the inequality $|\xi| \leq 1$.

The following equation gives ξ in terms of the oval semiaxes:

$$\xi = 3\left[\frac{b-a}{b+a}\right] - \left[\frac{b-a}{b+a}\right]^3 \quad \ldots (4.2)$$

Or,

$$\xi = 3q - q^3 \quad \ldots (4.3)$$

where b = oval major semiaxis,

a = oval minor semiaxis,

q = measure of ovality as stated in ASTM F1216, Equation (2.6).

Figure (4.2) shows the relationship between q and ξ as stated in Equation (4.3). For the purpose of simplifying the problem of stability of CIPP encased in oval host pipe, a slight change in Equation (4.1) is needed. This change is a result of considering a different location for the origin point, as shown in Fig. (4.3). In that case, the governing equation for the radius of curvature is

$$\frac{1}{R} = \frac{1}{R_o}[1 - \xi\cos(\beta s)] \quad \ldots (4.4)$$

The following analysis uses nonlinear small-deflection theory and, in general, it is applicable to the case of homogenous, isotropic, elastic, thin-walled liners.

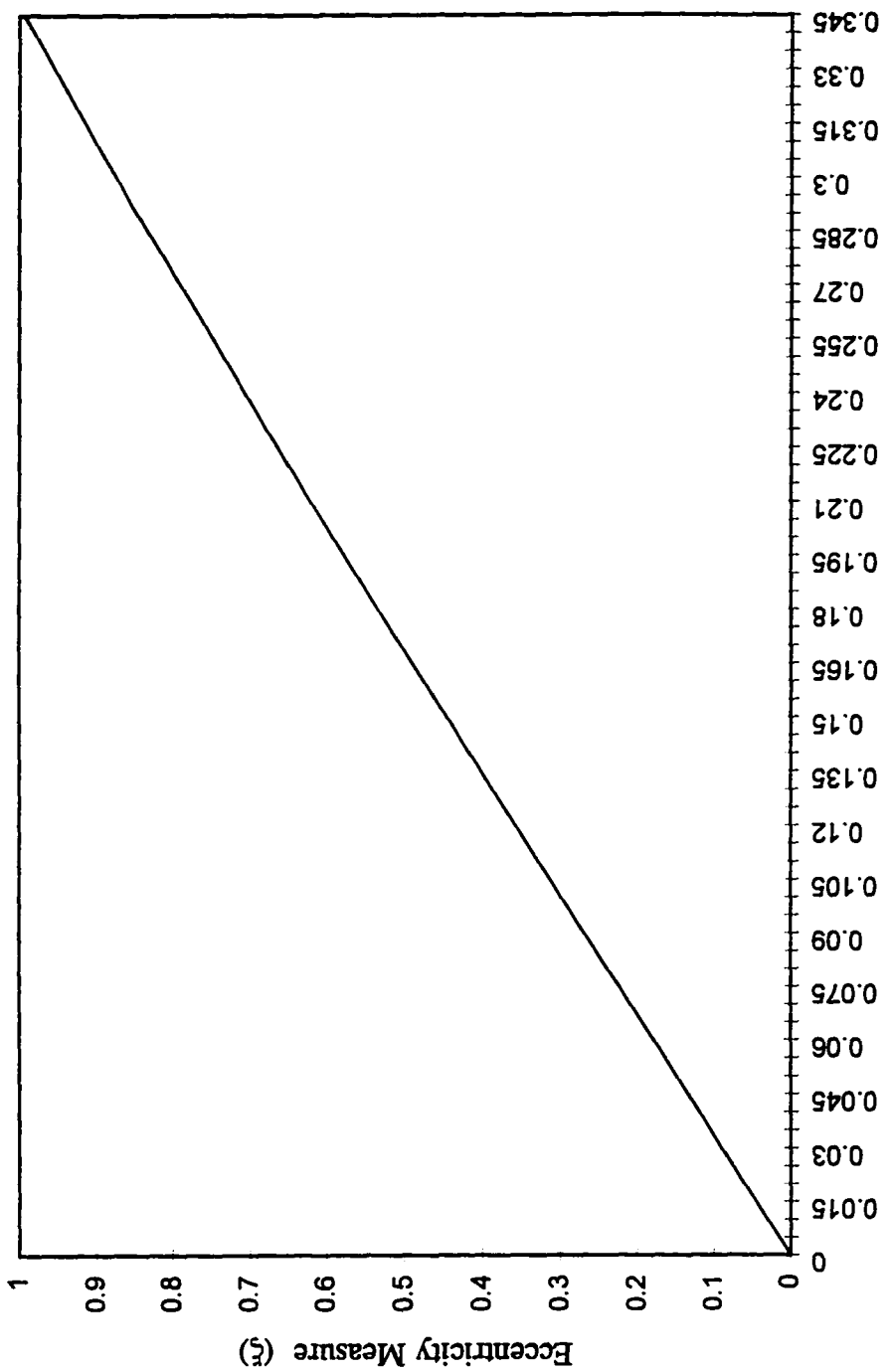

Fig. 4.2 Eccentricity Measure (ξ) versus Degree of Ovality (q)

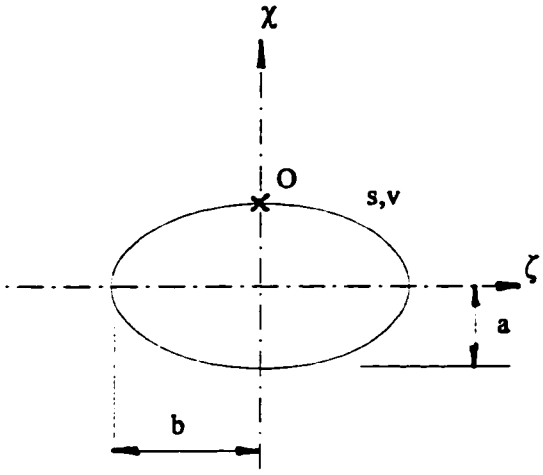

a) Coordinates For Oval (Proposed Model)

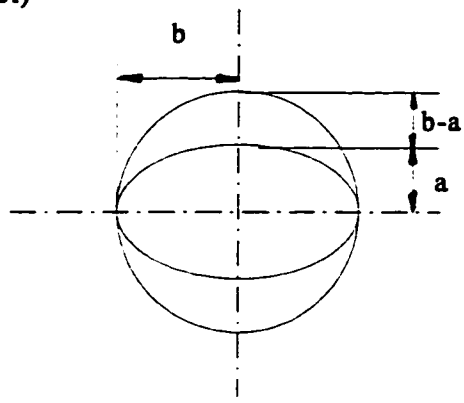

b) Eccentricity of Oval

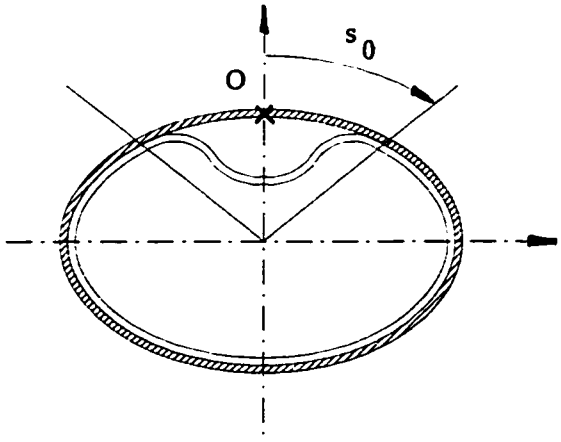

c) Buckling Configuration For the Proposed Model

Fig. 4.3 Coordinates, Eccentricity and Buckling Configuration For Oval Pipes

Therefore, the strain-displacement relationships of the mid-surface of the oval pipe can be presented as follows:

$$\hat{\varepsilon}_s = \left(\frac{\partial \hat{v}}{\partial s} - \frac{\hat{u}}{R}\right) + \frac{1}{2}\left(\frac{\partial \hat{u}}{\partial s}\right)^2 \qquad \ldots (4.5)$$

$$\hat{\kappa}_s = \frac{\partial^2 \hat{u}}{\partial s^2} \qquad \ldots (4.6)$$

where $\hat{\varepsilon}_s$ and $\hat{\kappa}_s$ are the extensional strain and change of curvature of the mid-surface of the oval. When the liner buckles inside the host pipe, it buckles in a small portion of the liner (Fig. 4.3), while the rest of it still bears against the inner walls of the host pipe. In a similar approach to Glock's solution (1977), the radial displacement function, $\hat{u}$, for the buckled portion can be assumed as follows:

$$\hat{u} = \hat{u}_o \cos^2(\gamma s) \qquad \ldots (4.7)$$

where $\hat{u}_o$ = radial deflection at the origin, O,

γ = $\pi/(2s_o)$, and,

s_o = half length of buckled portion.

Averaging the normal force in the liner wall would result in

$$N_{avg} = \frac{EA}{R_o \pi}\int_0^{s_o} \hat{\varepsilon}_s ds = \frac{EA}{R_o \pi}\left[\int_0^{s_o} \frac{\hat{u}}{R} ds - \frac{1}{2}\int_0^{s_o} \left(\frac{\partial \hat{u}}{\partial s}\right)^2 ds\right] \qquad \ldots (4.8)$$

Performing the integrations in Equation (4.8), then

$$N_{avg} = \frac{EA}{4R_o \pi}\frac{1}{\gamma}\left[\frac{\hat{u}_o}{R_o}(\pi - \xi\eta) - \frac{1}{2}\pi \hat{u}^2{}_o \gamma^2\right] \qquad \ldots (4.9)$$

where

$$\eta = \frac{\sin\{(2-\frac{\beta}{\gamma})\gamma s_o\}}{(2-\frac{\beta}{\gamma})} + \frac{\sin\{(2+\frac{\beta}{\gamma})\gamma s_o\}}{(2+\frac{\beta}{\gamma})} + \frac{2\sin\{\beta s_o\}}{\frac{\beta}{\gamma}} \quad \ldots (4.10)$$

Parameter η as stated in Equation (4.10) is dimensionsless. A reasonable value for η and consequently for the buckling load could be obtained by assuming a good approximation for s_o/L_o. This factor is the ratio between half length of the buckled portion to the total perimeter of the ring. Figure (4.4) shows the variation of η versus s_o/L_o. At the limit when $s_o/L_o \to 0$, $\eta \to \pi$. During the course of testing oval pipes under the effect of hydrostatic pressure, it was observed that the value of s_o/L_o increases with the increase in the tested pipe ovality. Only two measurements for this ratio were recorded during testing. The difficulties encountered to access the inside of the pipes and to measure the buckled portion were the reasons for having only two records. Measurements were taken using a regular measuring tape and it was found that s_o/L_o is 0.05 (the internal perimeter is almost 20 times the half-length of the buckled portion of the liner) for the case of 5% ovality and 0.10 for the case of 20% ovality. As a reasonable assumption, it could be stated that this ratio increases linearly with the increase in the degree of ovality, q. Based on this assumption, Fig. (4.5) presents the change in η versus the change in the degree of ovality q.

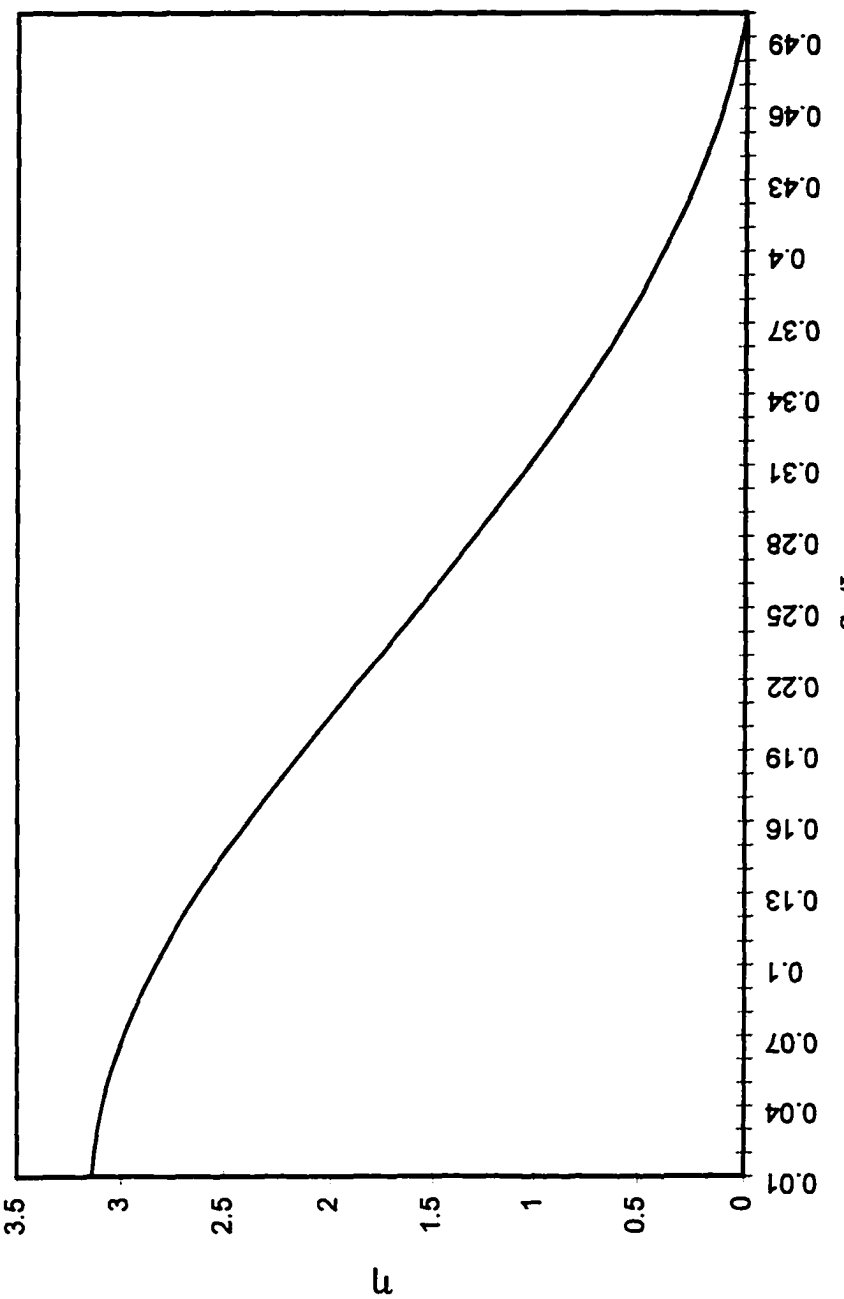

Fig. 4.4 Change in Parameter (η) Versus So/Lo

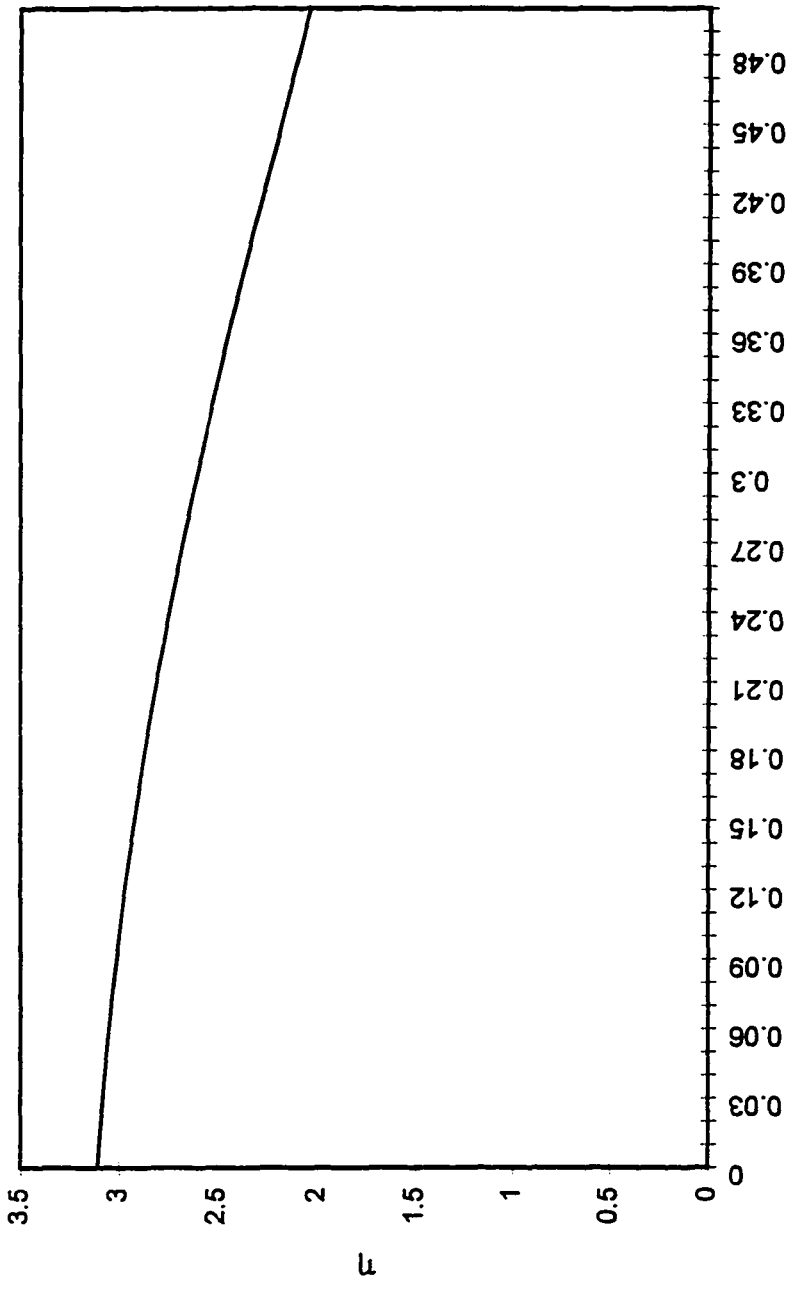

Fig. 4.5 Degree of Ovality (q) versus Parameter (η)

The total potential energy function in terms of the normal force, N_{avg}, the change of curvature, $\hat{\kappa}_s$, and the applied external hydrostatic pressure, P, can be expressed as follows:

$$\Pi = \frac{EI}{2}\int_0^{s_o}(\frac{\partial^2 \hat{u}}{\partial s^2})^2 ds + \int_0^{\frac{L_o}{2}} \frac{N^2}{2EA} ds - \int_0^{s_o} P\hat{u} ds \qquad . . \quad (4.11)$$

Performing the integrations, Equation (4.11) is reduced to

$$\Pi = \frac{EI\pi}{2}(\hat{u}^2{}_o\gamma^3) + N_{avg}{}^2 \frac{R_o\pi}{2EA} - \frac{P\hat{u}_o\pi}{4\gamma} \qquad . . \quad (4.12)$$

Minimizing the total potential energy function, Π, Equation (4.12) requires that

$$d\Pi = \frac{\partial \Pi}{\partial \hat{u}_o} d\hat{u}_o + \frac{\partial \Pi}{\partial \gamma} d\gamma = 0 \qquad . . \quad (4.13)$$

and

$$\frac{\partial \Pi}{\partial \hat{u}_o} = 0 \quad ; \quad \frac{\partial \Pi}{\partial \gamma} = 0 \qquad . . \quad (4.14)$$

where

$$\frac{\partial \Pi}{\partial \hat{u}_o} = EI\pi(\hat{u}_o\gamma^3) + N_{avg}\frac{\partial N_{avg}}{\partial \hat{u}_o}\frac{R_o\pi}{EA} - \frac{P\pi}{4\gamma} = 0 \qquad . . \quad (4.15)$$

$$\frac{\partial \Pi}{\partial \gamma} = \frac{3\pi}{2}EI(\hat{u}_o{}^2\gamma^2) + N_{avg}\frac{\partial N_{avg}}{\partial \gamma}\frac{R_o\pi}{EA} + \frac{P\hat{u}_o\pi}{4\gamma^2} = 0 \qquad . . \quad (4.16)$$

By differentiating Equation (4.9) with respect to $\hat{u}_o$ and γ, respectively, then

$$\frac{\partial N_{avg}}{\partial \hat{u}_o} = \frac{EA}{4\pi R_o}\frac{1}{\gamma}[\frac{(\pi - \xi\eta)}{R_o} - \pi\hat{u}_o\gamma^2] \qquad . . \quad (4.17)$$

$$\frac{\partial N_{avg}}{\partial \gamma} = -\frac{EA}{4\pi R_o}\left[\frac{\hat{u}_o}{R_o}\frac{(\pi - \xi\eta)}{\gamma^2} + \frac{\pi}{2}\hat{u}_o^2\right] \quad \ldots (4.18)$$

Substituting Equations (4.17) and (4.18) into Equations (4.15) and (4.16) results in

$$\hat{u}_o\left[-\pi EI\gamma^4 + \frac{\Pi}{4}N_{avg}\gamma^2\right] = -\frac{P\pi}{4} + \frac{N_{avg}}{4R_o}(\pi - \xi\eta) \quad \ldots (4.19)$$

$$\hat{u}_o\left[\frac{3\pi}{2}EI\gamma^4 - \frac{\Pi}{8}N_{avg}\gamma^2\right] = -\frac{P\pi}{4} + \frac{N_{avg}}{4R_o}(\pi - \xi\eta) \quad \ldots (4.20)$$

Subtracting Equation (4.19) from Equation (4.20), then

$$N_{avg} = \frac{20}{3}EI\gamma^2 \quad \ldots (4.21)$$

Equating Equation (4.21) to Equation (4.9) results in

$$\frac{1}{2R_o}\hat{u}_o^2\gamma^2 - \frac{(1 - \frac{\xi\eta}{\pi})}{R_o^2}\hat{u}_o + \frac{80}{3}\frac{EI}{EA}\gamma^3 = 0 \quad \ldots (4.22)$$

Equation (4.22) is a quadratic equation in $\hat{u}_o$, with the following roots:

$$\hat{u}_o = \frac{(1 - \frac{\xi\eta}{\pi})}{R_o\gamma^2} \pm \sqrt{\frac{(1 - \frac{\xi\eta}{\pi})^2}{R_o^2\gamma^4} - \frac{160}{3}\frac{EI}{EA}R_o\gamma} \quad \ldots (4.23)$$

To find an expression of P in terms of $\hat{u}_o$ and γ, substitute Equation (4.9) with the value of N_{avg} into Equation (4.19):

$$\frac{PR_o}{EI} = \frac{20}{3}\gamma^2(1 - \frac{\xi\eta}{\pi}) - \frac{8R_o\gamma^4}{3}\hat{u}_o \quad \ldots (4.24)$$

Substituting with the value of $\hat{u}_o$, Equation (4.23), into the above expression and simplifying,

$$\frac{PR_o}{EI}=4\gamma^2\left[(1-\frac{\xi\eta}{\pi})\pm\frac{1}{6}\sqrt{16(1-\frac{\xi\eta}{\pi})^2-\frac{2560}{3}\frac{EI}{EA}R_o^3\gamma^5}\right] \quad . . \quad (4.25)$$

To find P_{cr} and γ_{cr}, differentiate Equation (4.25) with respect to γ:

$$\frac{dP}{d\gamma} = 0 \quad . . \quad (4.26)$$

which results in

$$\left[\frac{3}{2}\pm\sqrt{1-\frac{160}{3}\frac{EI}{EA}\frac{R_o^3}{(1-\frac{\xi\eta}{\pi})^2}\gamma_{cr}^5}\right]\mp\frac{\frac{200}{3}\frac{EI}{EA}\frac{R_o^3}{(1-\frac{\xi\eta}{\pi})^2}\gamma_{cr}^5}{\sqrt{1-\frac{160}{3}\frac{EI}{EA}\frac{R_o^3}{(1-\frac{\xi\eta}{\pi})^2}\gamma_{cr}^5}} = 0 \quad . . \quad (4.27)$$

with the root

$$\gamma_{cr} = 0.428\left[\frac{EA}{EI}\frac{(1-\frac{\xi\eta}{\pi})^2}{R_o^3}\right]^{\frac{1}{5}} \quad . . \quad (4.28)$$

Substituting this value of γ_{cr} into Equation (4.25), then

$$P_{cr} = \frac{CE}{(1-\nu^2)}\left(\frac{t}{D}\right)^{2.2} \quad . . \quad (4.29)$$

where

$$C = \left(1-\frac{\xi\eta}{\pi}\right)^{1.8} \quad . . \quad (4.30)$$

Equation (4.29) provides the critical hydrostatic buckling pressure for CIPP encased in oval host pipes. The critical pressure is identified in terms of the liner's mechanical and geometrical properties. Equation (4.29) resembles Glock's equation for the case of perfect circular pipe except for the factor 'C' which reflects the reduction in the liner carrying capacity because of its ovality. The suggested ovality reduction factor, Equation (4.30), is dependent on the pipe degree of ovality, q, and the factor s_o/L_o. Figure (4.6) presents a comparison between different ovality reduction factors 'C' suggested in ASTM F1216, Li and Guice (1995), and the proposed model for different degrees of ovality, q. It shows that there is a close agreement in values between the suggested reduction factor, Equation (4.30), and that presented in ASTM F1216. It also shows that the reduction factor suggested by Li and Guice (1995) gives lower values compared to the other models.

4.3 Experimental Work

4.3.1 Pipe Installation and Specimen Preparation

Eighteen (18) specimens of CIPP encased in oval steel host pipes with three different degrees of ovalities (Fig.4.7) were scheduled for testing. Six (6) pipes were tested for each degree of ovality. The tested degrees of ovality were q = 5%, 10% and 20%, where q is defined in Equation (2.6). These degrees of ovality were chosen based on the recommendations of people working in the CIPP construction industry. They

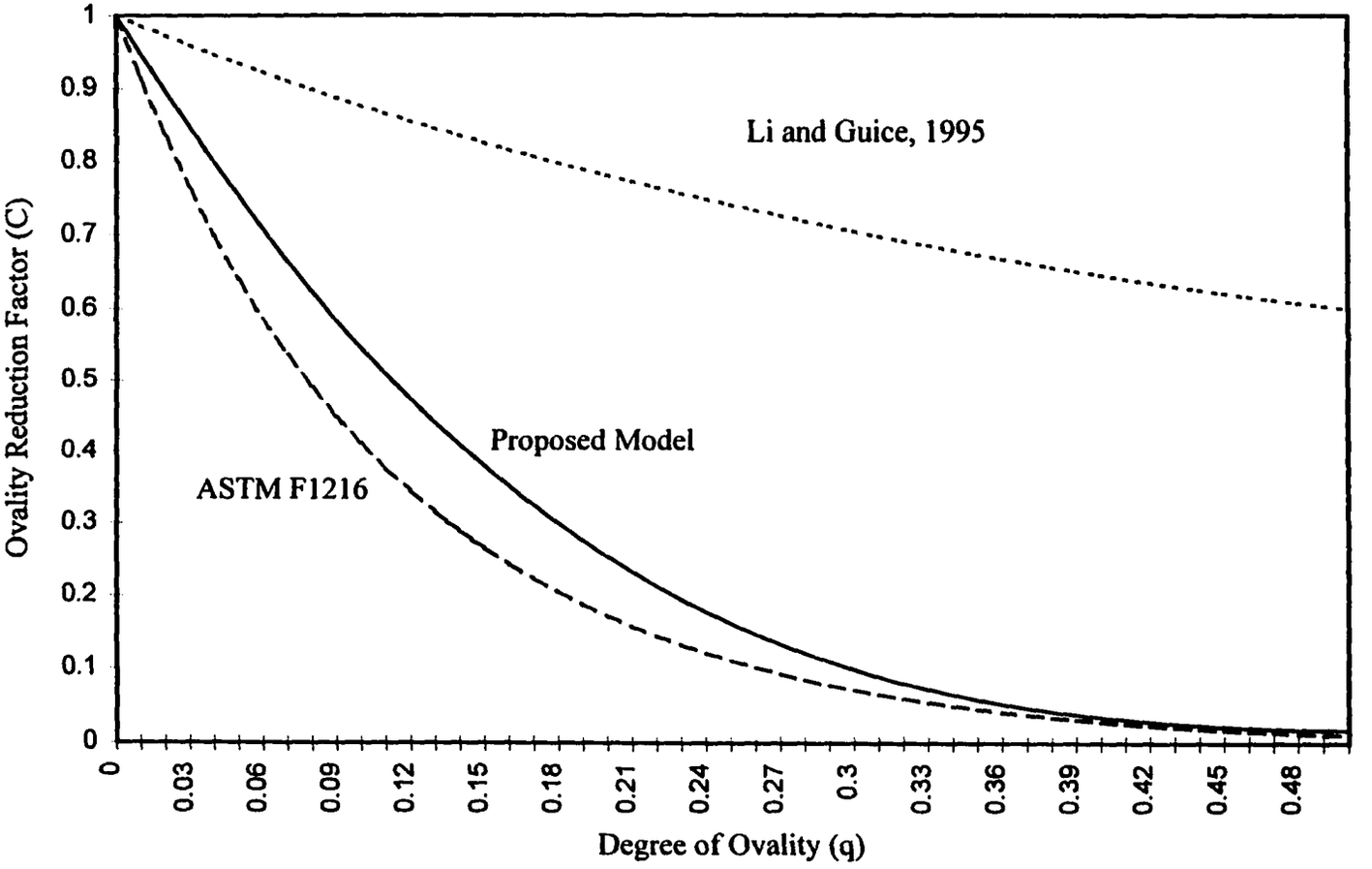

Fig. 4.6 Degree of Ovality (q) versus Ovality Reduction Factor (C)
From ASTM F1216, Li and Guice (1995), and The Proposed Model

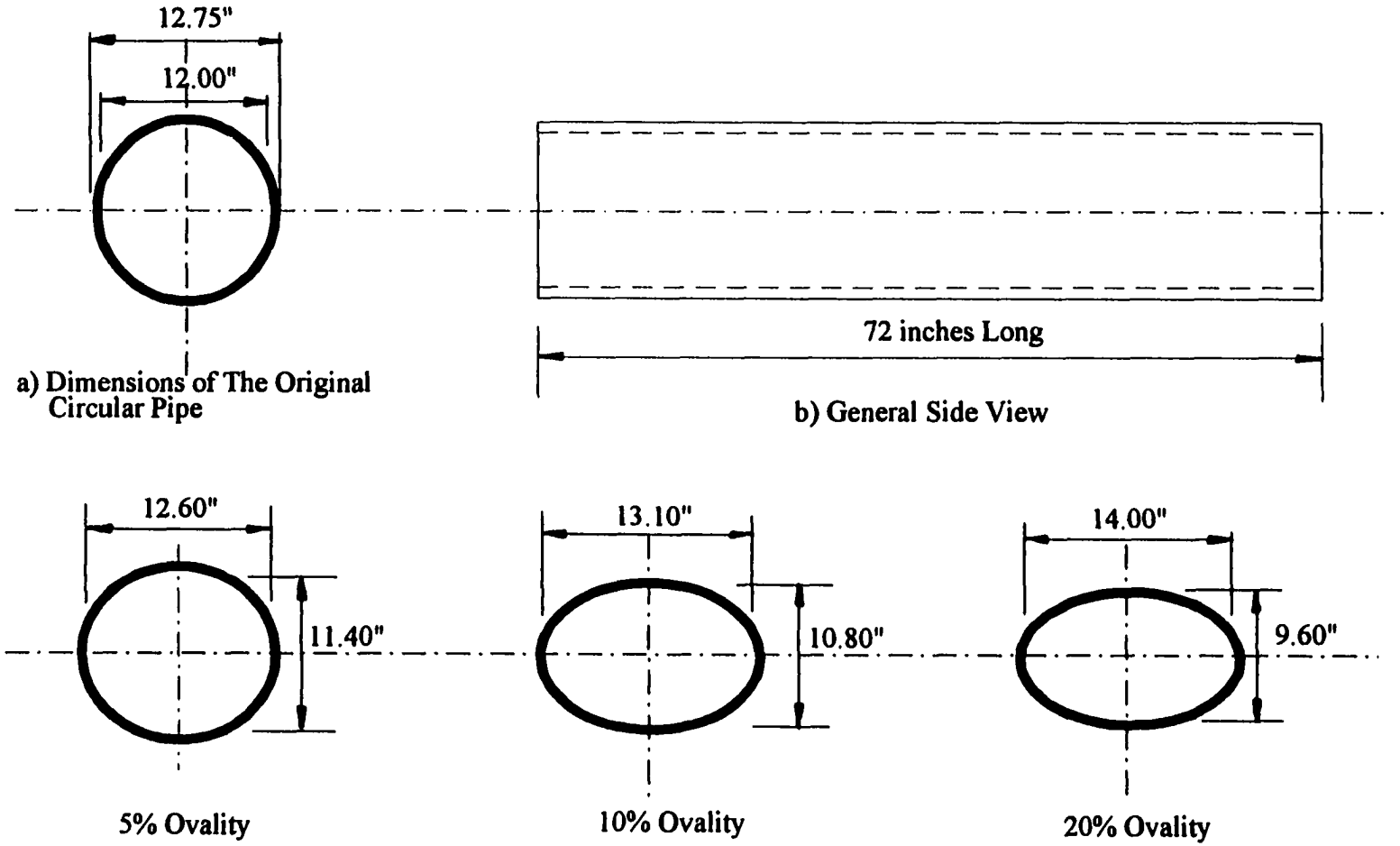

Fig. 4.7 Cross-Sectional Dimensions For Tested Degrees of Ovality

indicated that the most common degree of ovality they face in practice fluctuates around the number q = 10%.

Each test specimen was installed to fit snugly inside a 6-foot-long by 12-inch-initial-ID schedule 40 seamless steel casing (Fig. 4.7). The pipe size was selected to have a length of at least six times the original pipe diameter to minimize the possible effects of edge restraint at the ends. These dimensions were selected based on a preliminary investigation of the effect of the pipe length-to-diameter ratio on the resulting buckling pressure (Guice, et al., 1994).

Pipes were pressed to the required degree of ovality using a 400-ton press which was fitted with special jigs to ensure the roundness of the pipe at points of pressure. To achieve the proposed degree of ovality, each pipe was pressed twice. The first press was provided to bring the pipe's cross-section within the range of the required dimensions. Load was then removed, and the pipe was relinquished to spring up freely. The second press was applied to bring the pipe's cross-section to the required dimensions.

The materials and installations of the CIPP were provided through a contribution from Insituform Technologies, Inc. (ITI), Memphis, Tennessee. Before installation, the steel casing pipes were cleaned using compressed-air sand blasters. Steel casings were then treated with a release agent to minimize the bond between the liner and casing pipes to ensure a uniform water flow around the liner during testing. Then,

they were shipped to Memphis, Tennessee, where the installation process took place at the Insituform facility under the observation of the author.

The individual casing pipes were aligned in continuous rows to allow one continuous installation for each product tested; see Fig.(4.8). Clamshell couplings were installed in between each casing with a distance of about 2 inches left between adjacent clamshells to allow space for cutting the liners and separating the pipes into individual specimens. The plastic liner was then installed in the casing pipes using standard procedures as recommended by ITI (refer to Figs 4.9 to 4.15). During the installation, the liner was forced to pass through two flat plates placed between the pipe sections in order to provide flat specimens for conducting material characterization tests.

After the installation of the liner inside the casing pipe took place, the resin curing was initiated by circulating hot water inside the pipe for a period of time, as specified by the manufacturer, until the resin was cured. During curing, records of the water temperature at different places along the length of the liner and the environmental conditions were recorded.

The liner was cured according to the following curing schedule:

1. Ramped to 140°F and maintained at that temperature for almost 1 hour.
2. Ramped to 180°F and maintained at that temperature for about 4 to 5 hours.
3. Allowed to gradually cool down overnight prior to opening the ends.

After the resin was allowed to cool down to the ambient temperature, the liner was then cut apart and shipped to the testing facility. During transportation to the test

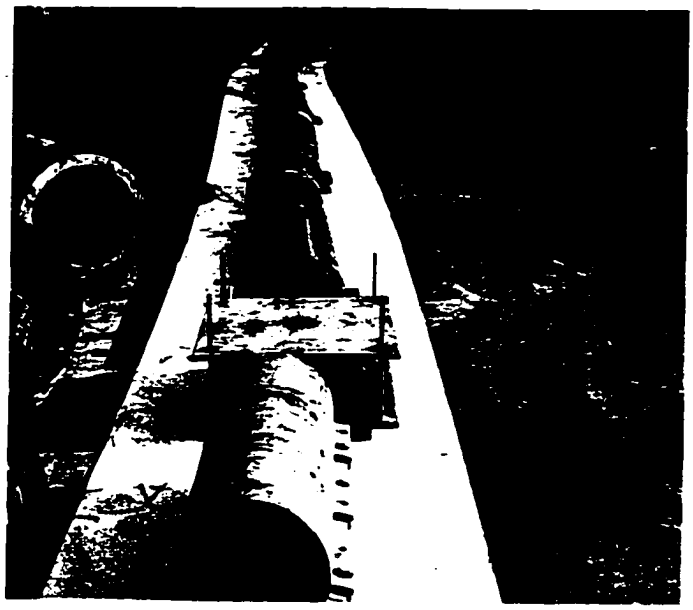

Fig. 4.8 Pipes Were Lined Ready for Installation

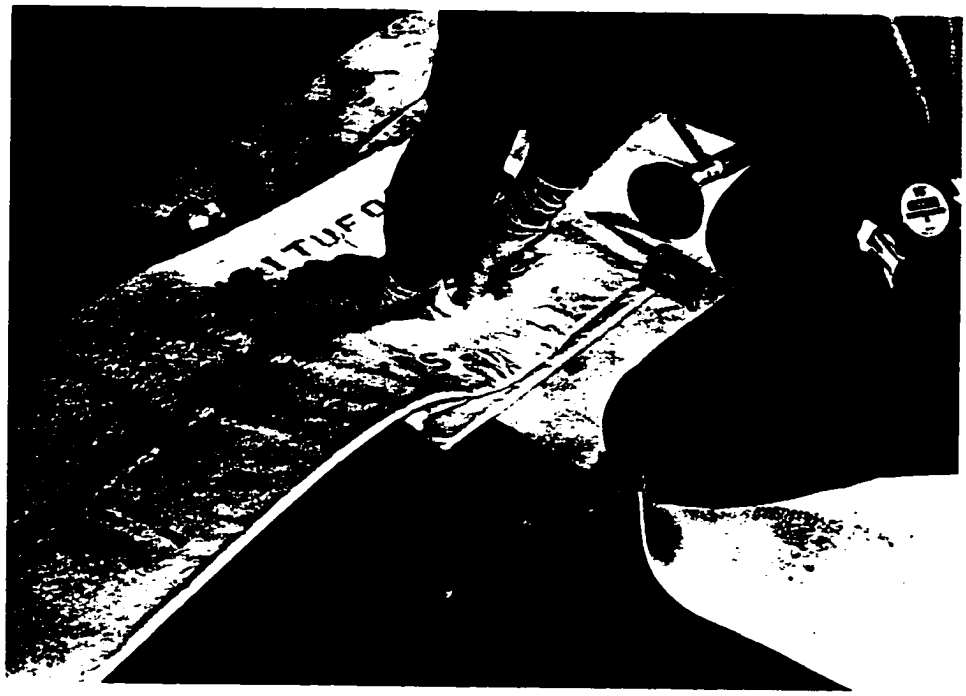

Fig. 4.9 Vacuum Was Used to Impregnate the Tube with Resin

Fig. 4.10 Tube Was Filled with Resin

Fig. 4.11 Tube Was Drawn Through Two Rollers to Ensure a Constant Thickness

Fig. 4.12 After Impregnation with Resin, Tube Was Stored in Cold Water Until Installation

Fig. 4.13 Clamshells Were Placed in Between Pipe Sections

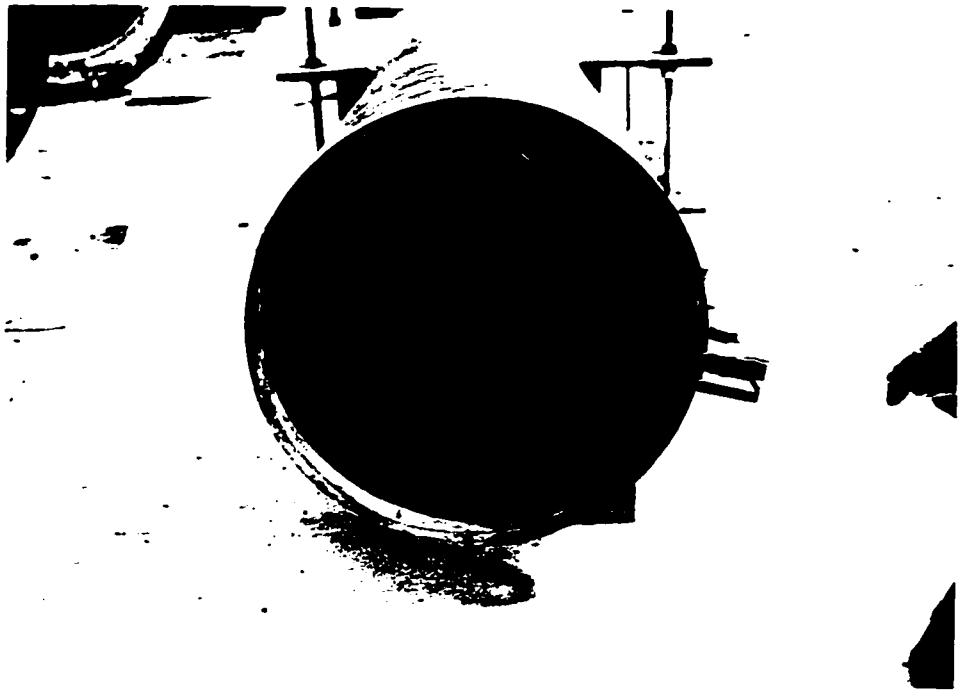

Fig. 4.14 Tube Was Installed by Inversion

Fig. 4.15 After Curing, Pipes Were Cut into Separate Specimens

facility, the clamshells were kept on the ends of the test specimens to serve as a protection for the specimen ends.

Once the specimens were installed and shipped to the testing facility, several steps were required to prepare the specimens for pressure testing. Preparing the specimens for testing involved trimming the ends flush with the clamshells to enable removal of the clamshells. Another 2 to 3 inches were trimmed from each end after the removal of the clamshells to enable the end seals and stiffeners to fit. Any excess resin or dirt was removed, and the ends of the specimens were cleaned and made ready for taking measurements and end sealing.

Measurements were recorded of the liner thickness for at least three different locations on each end of each specimen and averaged to determine the average liner thickness. Measurements of the thickness were made using a micrometer, with an accuracy of 0.001 inch. Table (4.1) provides the recorded measurements of the liner thickness for each tested pipe. All measurements are recorded in inches.

After the completion of taking measurements, specimens were then fitted with the end seals. End seals were provided to close the gap between the liner and the casing pipe at each end. A short piece of steel pipe (stiffener) with diameter smaller than the inner diameter of the CIPP was also fitted into each end of the specimen. These stiffeners were made on a slightly conical shape to facilitate the installation. These stiffeners are provided to support the liner underneath the end seals during testing. These steps were followed for each specimen prior to testing.

Table 4.1 Measurements of Liners Taken Before Short-Term Buckling Tests

Pipe No.	End #1 Thickness Measurements (inch)			End #2 Thickness Measurements (inch)			Avg. Thickness
	#1	#2	#3	#1	#2	#3	(inch)
5-1	0.234	0.231	0.245	0.245	0.228	0.226	0.235
5-2	0.231	0.232	0.221	0.247	0.216	0.238	0.231
5-3	0.256	0.238	0.243	0.223	0.248	0.230	0.240
5-4	0.240	0.236	0.234	0.237	0.238	0.240	0.238
5-5	0.231	0.235	0.236	0.241	0.240	0.224	0.235
5-6	0.239	0.242	0.239	0.225	0.224	0.241	0.235
						Average	*0.236*
						Standard Deviation	*0.003*
10-1	0.224	0.245	0.244	0.237	0.247	0.240	0.240
10-2	0.218	0.230	0.218	0.210	0.235	0.222	0.222
10-3	0.220	0.262	0.220	0.250	0.238	0.258	0.241
10-4	0.234	0.236	0.229	0.226	0.229	0.224	0.230
10-5	0.235	0.226	0.228	0.248	0.240	0.238	0.236
10-6	0.235	0.242	0.231	0.241	0.243	0.244	0.239
						Average	*0.235*
						Standard Deviation	*0.007*
20-1	0.213	0.237	0.252	0.226	0.228	0.230	0.231
20-2	0.212	0.217	0.228	0.268	0.270	0.258	0.242
20-3	0.220	0.217	0.230	0.224	0.246	0.217	0.226
20-4	0.233	0.234	0.235	0.226	0.243	0.237	0.235
20-5	0.241	0.240	0.226	0.239	0.231	0.247	0.237
20-6	0.221	0.254	0.238	0.210	0.230	0.220	0.229
						Average	*0.233*
						Standard Deviation	*0.005*

4.3.2 Testing

After preparing the specimens for testing, an external pressure was applied between the host pipe and the liner from a pressurized water distribution system (Fig. 4.16). This system uses a hydro-pneumatic pressure vessel for its source of pressure. This reservoir has the capacity of almost 300 gallons with a free surface that is held at a constant pressure by an air compressor supplying air through a regulated line. As the liner fails or leaks occur and water is lost from the system, the regulator ensures that the system pressure remains constant. When the water level drops, a level switch is activated which energizes two high-pressure positive displacement pumps connected to the city water system to bring the tank level back to full. As the water level rises, a pressure relief valve is activated to bleed off the excess pressure resulting from compressing the air pocket.

The test specimens were attached to this system through a hose controlled by a regulator to increase the water pressure to the required level. A pressure gauge was attached to this regulator to monitor the change in the water pressure and to provide guidance in controlling the rate of increasing the testing pressure. Two other pressure gauges were ported at both the inlet and the outlet of the tested specimen to define the pressure during testing. The reading of the two gauges was also helpful in controlling the rate of pressure application which was maintained at an approximately constant value. If a significant difference between these gauge readings was observed, the test was stopped and evaluated.

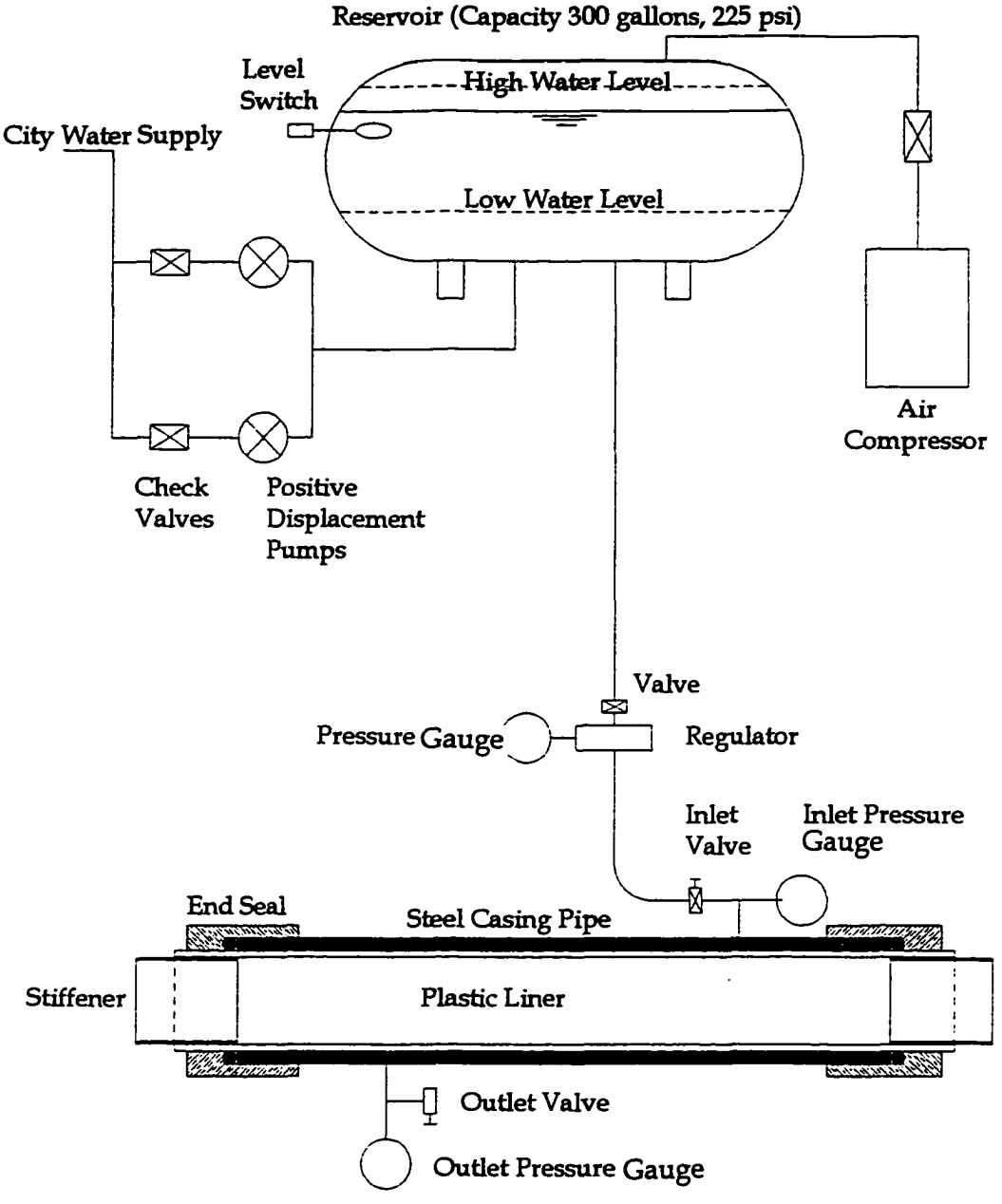

Fig. 4.16 Schematic of the Hydraulic System Used for Testing

Before testing, the annular gap between the liner and the steel casing was bled to remove any air. After attaching the testing supply hose to the pipe inlet as shown in Fig. (4.16), the top gate valve was opened, and water was fed into the bottom of the specimen at very low pressure, usually 5 psi or less. This was continued for about 5 minutes. During this time, if any end seal leaks were observed, the end seals were tightened. Once the water from the top of the casing was free of air bubbles, the steel casing was tapped with a wooden stick to remove any remaining entrapped air.

After bleeding the air, the water pressure was dropped using the regulator, and the outlet gate valve was closed. Initial readings for the three gauges were recorded. However, only the inlet and the outlet gauge readings were included in the averages presented in the results. The regulator was then used to raise the pressure gradually in the specimen. The load rate used for the tests was approximately 0.3 to 0.5 psi/sec. Once the test was started, the rate of load application was held approximately constant until failure of the liner occurred. The rate was adjusted to keep the inlet and outlet pressures close together. During testing, a reading of the three gauges was recorded every 15 seconds until failure. Once the failure occurred, the failure pressure was noted, and the general position of failure and the failure mode, whether buckling or rupture, were recorded.

During the process of conducting the tests, some specimens leaked at the end seals. In those situations and depending on the seriousness of the resulting leaks, the test was stopped. In the case of minor leaking, the test was completed since the

pressure could be maintained between the pipe and the liner despite the leaking. In other specimens where the leaking was major and the pressure was not increasing during testing, the test was stopped until those defects were fixed. Then the tests were restarted at zero pressure.

4.3.3 Test Results

Table (4.2) presents the average measured liner thickness, the failure pressure, and the associated mode of failure for each specimen. Thicknesses are presented in inches while the resulting failure pressure is in psi. The measured failure pressure, P_{test}, is typically representative of an average pressure based upon readings of gauges at both the inlet and the outlet ports of each specimen as shown in Fig. (4.16).

During testing, only the buckling failure mode was observed. The buckling failure mode is due to the instability of the liner under the effect of external pressure. This type of failure was always recognized by the accompanied creaking sounds which indicate the initiation of the buckling failure. The deformation shape in the buckling failure mode always took the bulb shape, as shown in Figures (4.17) and (4.18) for the cases of 5% and 20% ovality, respectively.

Table 4.2 Short-Term Buckling Tests Results

Pipe No.	Avg. Thickness* (inch)	P_{test} psi	Observed Failure Mode
5-1	0.235	57.75	Buckling Failure
5-2	0.231	54.25	Buckling Failure
5-3	0.240	52.50	Buckling Failure
5-4	0.238	49.75	Buckling Failure
5-5	0.235	62.50	Buckling Failure
5-6	0.235	54.50	Buckling Failure
		55.20	*Average*
		4.05	*Standard Deviation*
10-1	0.240	39.25	Buckling Failure
10-2	0.222	37.00	Buckling Failure
10-3	0.241	37.50	Buckling Failure
10-4	0.230	33.00	Buckling Failure
10-5	0.236	35.00	Buckling Failure
10-6	0.239	32.50	Buckling Failure
		35.71	*Average*
		2.43	*Standard Deviation*
20-1	0.231	16.00	Buckling Failure
20-2	0.242	14.30	Buckling Failure
20-3	0.226	23.90	Buckling Failure
20-4	0.235	16.90	Buckling Failure
20-5	0.237	--	pipe was leaking and the test was not completed
20-6	0.229	18.20	Buckling Failure
		17.86	*Average*
		3.28	*Standard Deviation*

* Presented values are tabulated in Table (4.1).

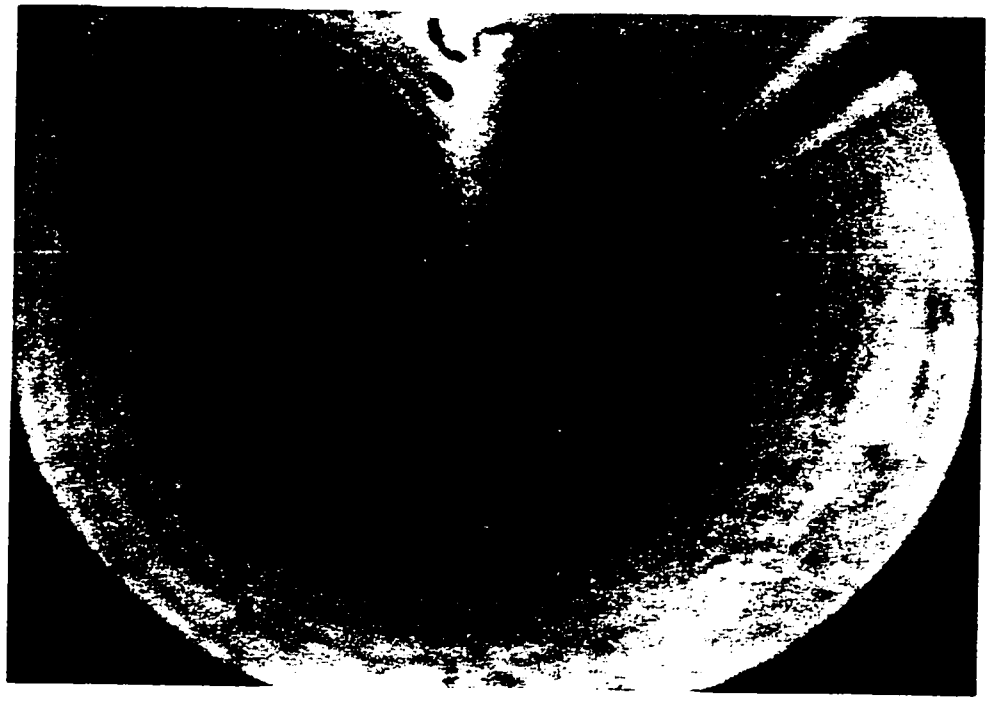

Fig. 4.17 Buckling Mode of Failure (q=5%)

Fig. 4.18 Buckling Mode of Failure (q=20%)

4.4 Material Characterization Tests

Material characterization tests were performed to define the flexural and tensile properties for the CIPP system used in the experimental program. Tests were conducted according to ASTM D790-89 and ASTM D638-89 to determine flexural and tensile properties, respectively. Specimens were taken from those samples installed inside the flat plates placed between the pipe sections during the installation process. Specimens were cut from intermediate sections away from the edges to minimize the effects of the edge curvature on the results. Other than the basic cutting and trimming required for the specimens, no additional machining or surface finish alterations were made. An MTS servo-hydraulic test system was used for conducting tests. The resulting data were recorded automatically with a Keithley Data Acquisition System.

Flexural tests were conducted primarily to determine the flexural modulus of elasticity of the material. Three (3) specimens were tested. Tests were performed using the three-point test method or test method (I) as mentioned in ASTM D790-89. The guidelines mentioned in this specification regarding specimen dimensions were followed strictly. Table (4.3) includes the average measured thickness and width for each specimen before testing. Dimensions in this table are presented in inches.

During testing, the load-deflection data were recorded simultaneously. The load-deflection curve for each specimen was plotted using the recorded data, and the initial slope for each curve was determined and used to calculate the flexural modulus of elasticity. The resulting load-deflection curves for all specimens are provided in

Appendix (A). The calculated flexural modulus of elasticity for each specimen and the average value for all specimens are presented in Table (4.3).

The resulting modulus of elasticity from the tension tests along with the tensile strength at failure, and their averages for four (4) tested specimens are presented in Table (4.4). It is noticed that the average modulus of elasticity resulting from tension tests is higher than the average modulus of elasticity resulting from bending tests by 8.5%.

Table 4.3 Results of Flexural Tests.

Sample No.	Avg. Thickness (inch)	Avg. Width (inch)	Initial Flexural Modulus of Elasticity (psi)
B-1	0.217	0.979	382,287
B-2	0.223	0.990	427,391
B-3	0.221	0.959	362,773
		Average	*390,817*
		Standard Deviation	*27,061*

Table 4.4 Results of Tension Tests.

Sample No.	Avg. Thickness (inch)	Avg. Width (inch)	Tensile Modulus of Elasticity (psi)	Tensile Strength at Break (psi)	Percent of Elongation at Break
T-1	0.223	0.738	459,524	4,152	17.50
T-2	0.228	0.759	368,366	4,174	12.10
T-3	0.223	0.698	352,670	3,806	20.80
T-4	0.225	0.760	528,041	4,148	17.20
		Average	*427,150*	*4,070*	*16.90*
		Standard Deviation	*71,116*	*153*	

4.5 Analysis of Short-Term Buckling Tests

Table (4.5) presents a comparison between the short-term buckling test results versus different analytical models of oval pipes. The analytical models under study include the following:

1. the current design practice (ASTM-F1216-93) with the enhancement factor, K, equal to 7;
2. Glock's model (1977) with the inclusion of the ovality reduction factor, C, as presented in ASTM-F1216, and hereafter will be referred as modified Glock's model;
3. the proposed model presented in this chapter.

The average elastic modulus of elasticity as determined in the flexural tests was used in the analysis. The modulus of elasticity from the flexural test is most commonly used in practice for representing the material stiffness to predict the critical buckling pressure, and that practice is used here as well.

The analysis shows that ASTM-F1216 underestimates the buckling pressure of CIPP encased in oval host pipes for all degrees of ovalities under study. It underestimates the actual buckling pressure by 44% for the case of 5% ovality, 45% for the case of 10% ovality, and 56% for the case of 20% ovality. Since the buckling pressure is underestimated, this analysis is conservative from the design standpoint.

Both the proposed model discussed in this chapter and the modified Glock's model have shown a good agreement with the experimental results. However, the

proposed model showed a better agreement with the experimental results for the case of 5% and 20% ovalities. For the case of 10%, ovality the proposed model overestimates the actual pressure by 20%, while modified Glock's model underestimates it and is closer than the proposed model to the actual value.

The analysis shows also that the proposed model overestimates the critical buckling pressure for all degrees of ovality, while the modified Glock's model underestimates them. That might reveal the unsuitability of both oval and elliptical coordinates used to develop both the proposed model and modified Glock's model, respectively, to study the problem.

Table 4.5 Experimental Results versus Different Analytical Models For Oval Pipes

Degree of Ovality	Experimental Results		ASTM-F1216with K=7.0			Modified Glock's Model			Proposed Model					
	SDR_o (Avg.)	P_{test} (Avg.)	C	P_{cr}	P_{cr} / P_{test}	C	P_{cr}	P_{cr} / P_{test}	ξ	L_o/s_o	η	C	P_{cr}	P_{cr} / P_{test}
5%	50.9	55.2	0.64	31.0	0.56	0.64	50.5	0.91	0.15	20	3.06	0.75	59.4	1.08
10%	51.1	35.7	0.41	19.6	0.55	0.41	32.1	0.90	0.30	15	3.00	0.54	42.7	1.19
20%	51.5	17.9	0.17	7.9	0.44	0.17	13.1	0.73	0.59	10	2.83	0.25	19.5	1.09

E = 390,817 psi
ν = 0.3 (as suggested by ASTM-F1216)
R_o = 6 inches
K = 7 (as suggested by ASTM-F1216)
L_o = $2\pi R_o$

CHAPTER 5

CONCLUSIONS AND RECOMMENDATIONS FOR FURTHER RESEARCH (PART I)

5.1 Conclusions

Analytical models for predicting the critical hydrostatic buckling pressure of CIPP encased in partially deteriorated host pipes were presented. Both cases of circular and oval deteriorated host pipes were considered. The proposed analytical model for the case of circular host pipes was initially developed by Glock (1977). However, the derivation of this model was not complete, and the theoretical bases upon which that model was developed were not cited. For the benefit of future developments in CIPP design methodologies, Glock's equations were reproduced, and the theoretical bases were referenced. The basic steps Glock used to derive his model were then followed to develop a similar analytical model for the case of CIPP encased in oval host pipes. The proposed model resembles Glock's equation for the case of perfect circular pipe except for the factor 'C' which reflects the reduction in the liner carrying capacity because of its ovality. The suggested ovality reduction factor is dependent on the pipe degree of ovality, q, and the factor s_o/L_o.

Both Glock's model and the proposed model for oval pipes were compared with other analytical models versus experimental results. Based on these comparative studies, the following conclusions are obtained:

5.1.1 Case of Circular Host Pipes

1. Glock's model has the lowest marginal error among other analytical models when they are compared with experimental work.
2. The results of best-fitting regression analysis for Aggarwal and Cooper data give coefficient and exponents for the design equation close to Glock's model.
3. ASTM-F1216, Equation X1.1, deviated considerably from the experimental results, and the suggested enhancement factor 'k' was found to vary significantly from product to another.

5.1.2 Case of Oval Host Pipes

1. Only the buckling mode of failure was observed during testing. However, buckling is not the only mode of failure for CIPP. In fact, during a recent experimental study on one of the CIPP systems conducted at Louisiana Tech University, another mode of failure was observed. Failures were identified as splittings in the liner walls. The real cause for this type of failure is yet unknown. Therefore, future research should concentrate on studying other possible modes of failure for CIPP. It is also required to identify the conditions under which those modes of failure are initiated.

2. There is a consistent decrease in the buckling pressure with the increase in the pipe degree of ovality.
3. ASTM-F1216, Equation X.1, underestimates the buckling pressure for all tested degrees of ovality. It deviates from experimental results by 44% for the case of 5% ovality, 45% for the case of 10% ovality, and 56% for the case of 20% ovality.
4. Both the proposed model and the modified Glock's model (see Section 4.5) show good agreement with experimental results and are closer to those results than ASTM-F1216, Equation X.1.
5. The proposed model overestimates the buckling pressure for all degrees of ovality and it deviates from the actual values by 8% to 20% of the test results. Modified Glock's model underestimates all values and it deviates from the test results within the same range as above.

While several models have been investigated and comparisons made but no final recommendation is made because an insufficient amount of research data is available to develop a final design expression at this time.

5.2 Recommendations for Further Research

The analytical models and test results presented in this dissertation should be beneficial to CIPP manufacturers in their quest for continued improvement of their products and designs. However, it should be emphasized that the proposed analytical models were derived under certain assumptions and limitations in theory. Limitations

include the consideration of small-deflections only, linear-elastic materials, no friction on the interface between CIPP and the host pipe, non-linear geometry, and no consideration of the visco-elastic effect (creep).

Further experimental and analytical research is needed to validate the proposed models and to verify the behavior of CIPP systems considering parameters which were not included in this study, such as the following:

1. The effect of addressing other values of SDR and host pipe geometry.
2. The visco-elastic (creep) behavior of the CIPP material over time.
3. The effect of considering other degrees of ovality.
4. The effect of other types of host pipe anomalies, such as a small imperfection over a short length of the host pipe.
5. The effect of the size of the gap between CIPP and confining host pipe.

PART II

DESIGN OF CIPP ENCASED IN FULLY DETERIORATED HOST PIPES

CHAPTER 6

LITERATURE SURVEY

6.1 Introduction

The design of CIPP encased in fully deteriorated host pipe requires a different analytical approach from the case of partially deteriorated host pipe. Fully deteriorated host pipes are not structurally sound to carry external loads or to provide any appreciable support for the encased CIPP. In that case, the host pipe is disregarded in the design, and it is assumed that the CIPP interacts with the surrounding soil to carry the applied loads and the CIPP is designed as a buried pipe.

This part of the dissertation is devoted to studying the problem of CIPP encased in fully deteriorated host pipe. It consists of Chapters 6, 7, and 8. Chapter 6 presents a classification for different buried pipes, sources of supporting strength for each case, and a literature survey for the available analytical methods for those types of structures. Chapter 7 presents a new approach for the design of CIPP encased in fully deteriorated host pipe. This approach utilizes Vlasov's variational method to model the pipe-soil system. Chapter 8 ends Part II by providing conclusions and recommendations for further research.

6.2 Classification of Buried Pipes

Buried pipes are usually classified according to their structural performance as either rigid or flexible. In the design of rigid pipes, the pipe itself is the basic structure which is designed to support the soil loads and the surface loads. In marked contradiction, a very flexible pipe serves as a form to retain the shape of the passageway in soil or as a boundary condition for the soil around the pipe, but the soil itself becomes the basic load-carrying structure. In between these two extreme cases, there are the cases of different relative flexibility between structure and soil (Watkins 1964).

Buried flexible pipes are those buried pipes which by definition exhibit yielding or other noticeable structural deformation immediately at the first sign of load. They continue this yielding or reduction in volume behavior throughout the rising load cycle. A pipe is considered flexible if it experiences at least 2% deflection under the effect of loading, without any structural distress such as rupture or cracking. In contrast, rigid pipes are those pipes which by definition undergo negligible deformation upon loading, almost 2% deflection as the maximum limit without exhibiting any rupture or excessive cracks (Watkins 1964). Most CIPP are manufactured from materials which can endure 2% of deflection or more without expressing any rupture or cracking. Therefore, for most practical purposes, the CIPP encased in fully deteriorated host pipe should be designed as a buried flexible pipe.

6.3 Sources of Supporting Strength of Buried Pipes

In general, buried pipes derive their ability to support the earth above them from two sources: first, the inherent strength of the pipe to resist the external loads and, second, the lateral pressure of the soil at the sides of the pipes. Lateral pressure produces stresses in the pipe ring in opposite directions to those produced by the vertical loads and, thereby, assists the pipe in supporting the vertical loads.

In rigid pipes, the inherent strength of the pipe is the predominant source of supporting strength. The only lateral pressure that can be safely depended upon to augment the load-carrying capacity of the pipes is the active lateral pressure of the soil (Spangler 1973). Rigid pipes deform very little under the vertical loads, and, consequently, the sides do not move outward enough to develop any appreciable passive resistance pressure. In flexible pipes, the pipe itself has relatively little inherent strength, and a large part of its ability to support vertical load is derived from the passive lateral pressure induced as the sides move outward against the soil. The ability of a flexible pipe to deform readily and thus utilize the passive soil pressure on the sides of the pipe is its principle distinguishing structural characteristic and accounts for the fact that these relatively lightweight, low-strength pipes can support earth fills of considerable height without showing evidence of structural distress (Spangler 1973).

6.4 Pipe Design Criteria

Design criteria are usually established by the design engineer based upon required performance and capability of a specified product. When the capability of a product is reached or exceeded, it is said that a design limit has been reached (Moser 1990).

For buried pipes, design limits are the ones at which the buried pipe fails. Failure is directly related to either stress, strain, deflection, or buckling. It is not implied that stress, strain, deflection, and buckling are independent, but only convenient parameters on which to focus one's attention. Failure here refers to collapse rather than merely failure to function satisfactorily under service conditions. Causes of failure of buried pipes are widely varied and dependent upon many factors such as the soil stiffness, pipe stiffness, and loading distribution. According to Luscher and Höeg (1964) and Moser (1990), failure may be initiated due to:

1. wall crushing;
2. excessive deformation leading to caving-in of the crown of the tube;
3. overall elastic buckling of the tube wall under hoop stresses or local instability, for instance, as demonstrated by snap-through buckling caused by local decrease in curvature; and,
4. formation of yield hinges caused by excessive bending or hoop stresses in the tube wall, and collapse occurring when a mechanism develops.

Wall crushing failure is more likely to occur in the case of buried rigid pipe, whereas excessive deformation and/or buckling modes of failure are more likely to occur for buried flexible pipes.

Limiting the pipe deflection under the effect of loads is the design criterion employed in the Iowa formula (Spangler 1941), as discussed later. The ring compression theory (White and Layer 1960) adopted pipe wall crushing or yielding caused by excessive hoop stress as a design criterion. Both the Iowa formula and ring compression theory have a different point of view about which design limit would occur first and cause the pipe to fail. A successful design, however, should consider all possible modes of failure, and the designer should use his or her experience and judgment to predict those possible modes of failure for each particular case. Disregarding any possible mode of failure during the design process might result in unsafe designs.

6.5 Related Research

6.5.1 Semi-Empirical Methods

It is generally recognized that Marston (1913) was the first researcher to bring some engineering insight to the design and analysis of underground conduits (Katona 1993, and Linger 1972). Prior to that time, pipes were installed with limited structural design. Marston was the first researcher to recognize that the loading on an underground structure is dependent on the interaction of the structure and the surrounding soil. His main contribution was to estimate the net vertical soil force

acting on the buried conduit. In 1913, he published the Marston theory on soil drainage pipes (Marston 1913). This theory assumes that the soil load on the underground conduit is due to a prism of soil whose movement relative to the adjacent soil develops and imposes the load on the conduit. This theory clearly takes into account the relative deflection of the pipe and the settlement of the soil.

Despite the effort to consider the soil-structure phenomenon in the design of buried pipes, this effort stopped short at only considering the influence of this phenomenon on applied loads. The design of buried pipes, at that time, was based on comparing vertical loads, calculated using Marston's theory, with the pipe carrying capacity under a three-edge bearing test. Neglecting the interaction between pipe and soil, created as a result of the pipe lateral deflection towards the soil which invokes the soil support for the pipe, made this design methodology applicable only to the design of buried rigid pipes such as clay tile or concrete.

For the design of flexible pipes, the earliest development was based on empirical equations using the results of the American Railway Engineering Association investigation (Linger 1972, AREA, 1926). Design tables were developed for the pipe thickness and diameter for various heights of fill. These tables were based on the assumption that failure occurred when the pipe deflection reached 20% of the diameter. For design purposes, the deflection was limited to 5% of the diameter, thus providing a safety factor of 4. It is interesting to note that no attempt was made to correlate the load-carrying capacity with soil characteristics.

As highway construction increased during the 1930s, the use of larger and more costly drainage structures grew rapidly. The need for a more rational concept for the design of flexible pipes was observed by Spangler, a former student of Marston. Spangler observed that the Marston theory for calculating loads on buried pipes was not adequate for flexible pipe design. Spangler noted that flexible pipes provide little inherent stiffness in comparison to rigid pipes, yet they perform remarkably well when buried in soil (Spangler 1941). This significant ability of flexible pipes to support vertical soil loads is derived from the lateral pressure of the soil at the sides of the pipes, which produces stresses in the pipe ring in opposite directions to those produced by the vertical loads (Spangler 1973, Luscher and Höeg 1964). These considerations, coupled with the idea that the ring deflection may form a basis for flexible pipe design, prompted Spangler to study flexible pipe behavior to determine an adequate design procedure. His research and testing led to the derivation of the Iowa formula published in 1941.

Based on Marston's theory, Spangler estimated the amount of uniformly distributed load at the top of the pipe. He also assumed a uniform pressure over part of the bottom, depending upon the bedding angle. On the sides, he assumed that the horizontal pressure on each side would be proportional to the deflection of the pipe into the soil. The constant of proportionality was called the modulus of passive resistance of the soil. Through analysis, he derived the Iowa formula:

$$\Delta X = \frac{D_L K W_c R^3}{EI + 0.061\ eR^4} \qquad \ldots (6.1)$$

where

ΔX = horizontal deflection or change in diameter, in.;

D_L = deflection lag factor;

K = bedding constant;

W_c = Marston's load per unit length of pipe, lb/in.;

R = mean radius of the pipe, in.;

E = modulus of elasticity of the pipe material, lb/in^2;

I = moment of inertia of the pipe wall per unit length, $in^4/in.$;

e = modulus of passive resistance of the side fill, $lb/(in^2)(in.)$.

Although the Iowa formula, Equation (6.1), was derived mainly to calculate the horizontal deformation of buried pipes, Spangler (1941) assumed that the vertical deflection of buried pipes is equal to the horizontal deformation. However, it is well recognized that the vertical deformation is always greater than the horizontal deformation (Howard 1981). Equation (6.1) can be used to predict deflections of buried pipes if the three semi-empirical constants 'K,' 'D_L,' and 'e' are known. For design purposes, it is recommended that the pipe deflection should not exceed a certain percentage of the nominal pipe diameter. For example, in the case of corrugated steel pipes the calculated deformation should not exceed 5% of the nominal diameter (Moser 1990).

The bedding constant, K, varies with the angle of bedding achieved in the installation. A list of the bedding constants, K, for various values of the bedding angle was determined theoretically by Spangler and published in 1941 (Spangler 1941).

The deflection lag factor, D_L, incorporated in Equation (6.1) was proposed by Spangler to take into consideration the continuous yielding of the soil at the sides of the pipe in response to the horizontal pressures over a considerable period of time. This yielding results in a continuation of the pipe deformation to a value beyond that which is primarily attributable to the vertical load (Spangler 1973). His experience had shown that deflections could increase by as much as 30% over a period of 40 years (Moser 1990). For this reason, Spangler recommended the incorporation of a deflection lag factor in the Iowa formula. The lag factor cannot be less than one, and it depends upon the quality of the soil at the sides of the pipe. A well-graded dense soil will permit very little, if any, residual deflection, and the lag factor can safely be ignored, while a loosely placed soil may induce a relatively large deflection lag. For well-compacted backfill soil, a deflection lag factor of about 1.25 was recommended for design purposes by Spangler (Spangler 1973).

In 1958, Reynold K. Watkins, a graduate student of Spangler, investigated the modulus of passive resistance. The analysis determined that 'e' could not possibly be a true property of the soil in that its units are not those of a true modulus (Watkins and Spangler 1958). As a result of Watkins' effort, another soil parameter was defined.

This was the modulus of soil reaction, $\bar{E} = eR$. Consequently, a new formula called the modified Iowa formula was proposed.

$$\Delta X = \frac{D_L K W_c R^3}{EI + 0.061\ \bar{E}R^3} \quad \ldots (6.2)$$

Several research efforts have attempted to measure the modulus of soil reaction, $\bar{E}$, without success. The most useful method involved the measurement of deflections of a buried pipe for which installation conditions were known, followed by a back-calculation through the Iowa formula to determine the effective value of $\bar{E}$ (Moser 1990). This approach requires assumed values for the load, the bedding factor, and the deflection lag factor. Inconsistent assumptions led to a wide scatter in reported values of $\bar{E}$.

Howard (1981) introduced a new equation to calculate the vertical reaction of flexible pipes. In this equation, referred to as the USBR equation, the percent of vertical deflection is calculated rather than the horizontal deflection since it is of the most concern and the easiest to measure. The USBR equation is strictly an empirical formula based on back-calculated parameters from reported measurements on field installations of flexible pipes. The empirical parameters used in this equation were evaluated assuming a prism load on the pipe and using a pipe stiffness represented by the expression EI/R^3. The equation is written as follows:

$$\Delta Y(\%) = T_f \left[\frac{0.07\gamma h}{EI/R^3 + S_f D_f} C_f \right] + I_f \quad \ldots (6.3)$$

where

ΔY = percent vertical deflection;

T_f = time-lag factor, dimensionless;

0.07 = combination of conversion factors and bedding constant, ft^2/in^2;

γ = back-fill density, lb/ft^3;

h = depth of cover, ft.;

R = pipe radius, ft.;

EI/R^3 = pipe stiffness factor, lb/in^2;

S_f = soil stiffness factor, lb/in^2;

D_f = design factor, dimensionless;

C_f = construction factor, percent vertical factor;

I_f = inspection factor, percent vertical deflection.

Equation (6.3) should be used only when the depth of cover is less than 50 feet and the trench wall support is as good as or better than the pipe bedding (Howard 1981). The various parameters used in Equation (6.3) provide many options as to how the equation may be used. Either the average or the maximum vertical deflection can be predicted. Both the predicted initial and long-term deflections can be calculated.

Both the Iowa formula and the USBR formula use the same design criterion for buried flexible pipes. This criterion assumes that the pipe will fail because of excessive deformations. In 1960, White and Layer proposed the ring compression theory as an alternative criterion for the design of buried flexible pipes. This theory assumes that

the ring deflection of the structure is negligible and that failure occurs by crushing of the pipe walls. It also assumes that the load is distributed uniformly around the pipe, and it neglects the existence of the surrounding soil as an additional support for the pipe.

The major drawback of these traditional methods is that they are not based on the mechanics of pipe-soil interaction. They are rather based on observations and approximations obtained from a large number of laboratory tests on conventional pipes (Katona 1993). Although the Marston/Spangler approach still represents the most popular design method for conventional pipes, it has limitations because of its empirical nature. This limitation restricts its applicability to pipe products whose scale, shape, or materials are outside the parameters of the Marston/Spangler approach. Consequently, the Marston/Spangler approach may not be applicable to new innovations in pipelines installation such as those in trenchless technology.

6.5.2 Elasticity Solution

Burns and Richard (1964) realized the shortcomings in the Marston/Spangler methodology and formulated one of the earliest known closed-form solutions of the problem. Burns and Richard's solution (1964) is suitable for the case of an elastic, very deep cylindrical pipe encased in an isotropic, homogeneous infinite elastic medium with a uniformly distributed pressure acting on a horizontal plane far from the pipe. Two solutions for the soil-pipe interface conditions, bonded and unbonded interfaces, were developed. In the case of bonded interface, it is assumed that the shear stress and the

radial forces are transmitted on the interface between the pipe and the surrounding continuum. For the case of unbonded interface, no shear stress is transmitted on the interface between soil and pipe. Equations for the interaction radial pressure, pipe radial deflection, moment, and thrust for both cases of bonded and unbonded interfaces were developed. Höeg (1968) used an elastic model and formulated a solution similar to that proposed by Burns without imposing a specific value for the soil lateral pressure coefficient.

Two recent studies of pipe-soil interaction (Galili et al. 1978; Shmulevich 1980) compared experimental data with the existing theories. The results show that both the analytical and semi-empirical methods reported above are not applicable for a wide range of pipe-soil stiffness ratios, especially in the intermediate range of semi-flexible pipes. The solutions proposed by Burns and Höeg are not adequate for the following reasons:

1. Solutions are limited to the case of an infinitely distributed surface pressure neglecting other load cases.
2. The effect of soil overburden pressure on the stress values is neglected.
3. They are valid for the case of very deep pipe neglecting the existence of the upper surface as a boundary condition.

Galili and Shmulevich (1981) realized the limitations in the Burns and Höeg solutions and proposed a refined model for the problem which gives good agreement between analytical and experimental work. Their proposed refinement does not depend

on a modification of the theory; instead it depends on proposing more realistic boundary conditions by substituting for the soil lateral pressure coefficient a value gathered from experimental work. This proposed solution gives good agreement with the experimental work; however, its application is limited only to the cases considered in their experimental work.

Both solutions presented by Burns (1964) and Höeg (1968) can be used to design buried flexible pipes using either limiting pipe wall deflections or stress as a design criterion. More rigorous research (Luscher and Höeg, 1964) proved that the excessive deflection or hoop stress are not the only failure patterns of buried pipes, and the buckling failure may take place especially in the case of thin-walled pipes.

6.5.3 Buckling Theories of Buried Pipes

A flexible pipe buckles when compressive force acts to reduce the pipe flexural stiffness so that there is no resistance to lateral movements. In the case of buried flexible pipes, the surrounding soil increases significantly the buckling strength of the pipe. It is not possible to determine the buckling strength of a buried pipe merely by considering only laboratory tests on the unsupported structure. Neither is it feasible to test each structure individually in the field. Theoretical models are therefore needed to quantify the buckling behavior of buried flexible pipes, and these should be verified and calibrated using field and laboratory test data.

Much research has been done to investigate the conditions under which the buried pipe loses its stability. This research is categorized either as unconfined (unsupported) pipe theories or confined pipe theories. Details of each category are presented in the next sections.

6.5.3.1 Unconfined Pipe Buckling Theories

The classical buckling formula of an unconfined ring is presented in Chapter 2 (Equation 2.3). This equation, widely known as Timoshenko's equation, assumes the critical external pressure to be applied hydrostatically and that no support whatsoever exists around the pipe. Allowing the load to be applied hydrostatically neglects the change, during deformation, of the magnitude and direction of the applied pressure on the magnitude of the buckling load. It is well known, however, that small alterations in the character of the applied loads may change the magnitude of the buckling load considerably.

Boresi (1955) has shown that the coefficient in Timoshenko's equation would be 4.5 instead of 3 if the external pressure is assumed to remain directed towards the pipe center during deformation. Bodner (1958) showed that the coefficient would be 4 if the external load maintained a constant direction during deformation.

Armenakas and Herrmann (1963) introduced a more rigorous expression for the critical external pressure which may induce buckling in the ring by considering the ring as a cylindrical shell. A solution for the problem based on their theory of bending of

the cylindrical shell under the influence of a general state of initial stress was presented. The proposed expression for the critical pressure is

$$p_{cr} = k_{c \text{ or } h} \frac{D}{R^3}$$
$$k_c = \frac{n^2}{1+2S}; \text{ and } k_h = n^2 - 1 \quad \ldots (6.4)$$

where k_c and k_h are coefficients related to the constant and hydrostatic loading cases, respectively, and,

R = pipe mean radius;

n = number of circumferential waves and should be an integer;

D = pipe flexural rigidity ($Et^3/12(1-\nu^2)$);

ν = pipe Poisson's ratio;

t = pipe wall thickness;

E = pipe flexural modulus; and,

S = t/2R.

The advantage of Armenakas and Herrmann's equation is that the coefficients k_c and k_h are not fixed values, as is the case in Timoshenko's equation and others; rather, they are functions of the pipe dimensions and the buckling mode. In order to compute these buckling coefficients for a shell with specific dimensions, it is necessary to establish the buckling mode. The authors introduced a set of charts to determine the buckling mode for each case. These charts are an extension to a work done previously by Windenburg and Trilling (1934).

6.5.3.2 Confined Pipe Buckling Theories

The aforementioned buckling models do not address the pipe confining soil as an additional support enhancing the pipe capacity to resist the applied loads. One of the earliest works which addresses the soil existence was developed by Meyerhof and Baikie (1963). Their work is based on the extension of the theory of elastic stability of plates to the problem of curved sheets supported by an elastic medium. Through analysis they proved that

$$N_{cr} = 2\left[\frac{kEI}{(1-\nu^2)}\right]^{\frac{1}{2}} \qquad \ldots (6.5)$$

where N_{cr} = critical hoop force, and,

k = soil coefficient of subgrade reaction.

The other terms were described before. Equation (6.5) is derived for buckling modes higher than the first buckling mode. Meyerhof and Baikie proved that the critical hoop force is practically independent of the radius of the pipe for good compaction of the back-fill.

Luscher (1966) presented a study in which buried flexible pipes were confined by a thick-walled soil cylinder and the system was brought to failure by applying external, uniform, static radial pressure. A theoretical expression for the buckling resistance of the pipe-soil system was derived. Through the analysis, soil is modeled as a series of independent springs resisting the radial deformation of the pipe. The soil modulus of elastic support was presented as a function of the geometrical and

mechanical properties of the confining soil. The critical hoop force in the pipe wall which causes the pipe instability is given by

$$N_{cr} = 2\sqrt{\frac{EIK}{R}} \quad \ldots (6.6)$$

where all parameters are as mentioned before.

Forrestal and Herrmamn (1965) presented the first solution of the stability of buried pipes in which soil was presented as an elastic continuum. The loading on the pipe is assumed to be exerted by the surrounding soil as a uniform external pressure. The critical external pressure for both cases of bonded and unbonded interfaces were presented in the study.

Duns and Butterfield (1971) introduced another solution for the problem considering soil as an elastic continuum surrounding the pipe. The critical hoop force in this case is given by

$$N_{cr} = k(\frac{R}{n})^2 + D(\frac{n}{R})^2 \quad \ldots (6.7)$$

where

$$n^2(n+1)^2 = \frac{12k(1-\nu^2)R^4}{Et^3} \quad \ldots (6.8)$$

Since 'n' must always be a whole number, the critical mode number for a particular pipe geometry will be the nearest integer not greater than the 'n' value satisfying Equation (6.8).

Moore and Booker (1985) presented a solution for the instability of buried flexible pipes. Soil was presented as an elastic medium around the pipe. The uniform hoop force which leads to the pipe instability is given by

$$N_{cr} = (n^2-1)\frac{EI}{R^2} + 2G_sR\left[\frac{2n(1-\nu_s)-(1-2\nu_s)}{n^2(3-4\nu_s)}\right] \quad .. \quad (6.9)$$

where G_s is soil shear modulus and ν_s is the soil Poisson's ratio. Equation (6.9) is valid for the case of rough pipe-soil interface, i.e. no slip along the interface is permitted. For the case of smooth interface, the critical hoop force is given by

$$N_{cr} = (n^2-1)\frac{EI}{R^2} + 2G_sR\left[\frac{1}{2n(1-\nu_s)+(1-2\nu_s)}\right] \quad .. \quad (6.10)$$

6.5.4 Finite Element Methods (FEM)

The finite element analysis (FEA) technique was developed for computer analysis of complex structural systems. The technique was developed to analyze structural responses to different loading conditions. Through the years, the technique has been extended through rigorous mathematical formulation of element behavior. It has proven to be a useful tool in research and in everyday engineering analysis.

One area where the use of FEA has been promoted is in soil-structure interaction mechanics. The finite element analysis for soil-structure interaction problems varies in several ways from finite element analysis of simple linear elastic problems as follows (Moser 1990):

1. The soil properties are strain dependent (nonlinear).

2. For flexible pipes, the structure may be geometrically nonlinear.
3. It may be necessary in some instances to allow movement between the soil and the walls of the pipe.

A number of FE computer programs have been developed to solve the problem of the soil-structure interaction. CANDE (Katona et al. 1976), SPIDA (Selig 1982), and SSTIPN (Moser 1990) are some examples of the available programs. These software packages model the pipe-soil system as a two-dimensional problem. The pipe is represented by either a beam or bar element, and the soil is modeled as a linear or a nonlinear material. These programs could also address the incremental load stages applied during the construction phases.

Despite the similarities between these FE programs they are different in many details:

1. The capability to incorporate some special features in the solution, such as predicting the shear or the tension failure in soil.
2. The capability of meshing the problem and representing different installation and bedding conditions.
3. The capability to incorporate interface elements to allow movement between the soil and the structure.

FEM in soil-structure interaction has many advantages over the closed-form elastic solutions, such as its ability to represent different culvert installations and different types of loads. However, the FEM results are only as good as the ability of

the software to model the behavior of soil structure interaction. The user should have a good knowledge of the FEM and the theory of elasticity, which may be beyond the expertise of many design engineers. Available FEM packages certainly offer the engineer a powerful tool for comprehensive analysis of pipe-soil systems but may not be suitable to meet the needs of the design engineer for a straight-forward, analytical design tool. Therefore an easy, rather accurate, method for determining stress and displacement in the pipe wall under any level or type of loads is needed.

6.5.5 Current Design Practice

The current design practice for CIPP installed in fully deteriorated host pipes is presented in ASTM F1216-93, Equation X1.3. This equation was adopted from ANSI/AWWA C950 by adding the ovality reduction factor, C, as presented in Chapter 2, and using a design safety factor of 1.5, rather than the AWWA safety factor of 1.8. The AWWA equation was a modification of an equation developed by Lusher (1966) to predict the buckling pressure of buried flexible pipes. Therefore, this equation uses the buckling failure as a design criterion. ASTM F1216, Equation X1.3, requires that the CIPP is designed to support hydraulic, soil, and live loads as follows:

$$q_t = \frac{C}{N}[32R_w B' E'_s (\frac{E_L I}{D^3})]^{1/2} \quad \ldots \quad (6.11)$$

where

q_t = total external pressure on pipe, psi (MPa);

R_w = water buoyancy factor (0.67 minimum);

= 1-0.33 (H_w/H);

H_w = height of water above top of pipe, ft(m);

H = height of soil above top of pipe, ft(m);

B = coefficient of elastic support;

= $1/(1+4e^{-0.065H})$ inch-pound units, $1/(1+4e^{-0.213H})$ SI units;

I = $t^3/12$ - moment of inertia of CIPP, $in^4/in.$ (mm^4/mm);

t = thickness of CIPP, in. (mm);

C = ovality reduction factor, as presented in Chapter 2, Equation (2.5);

N = factor of safety;

E_s = modulus of soil reaction, psi (MPa);

E_L = long-term modulus of elasticity for CIPP, psi (MPa); and

D = mean inside diameter of original pipe, in. (mm).

The maximum anticipated groundwater height, H_w, and the soil height, H, should be measured or estimated for design. The value for E_s should be selected on the basis of soil explorations and site engineering judgment. The ASTM further provides in Equation X1.4 that the maximum permissible SDR be determined by a minimum thickness as calculated using the short-term flexural modulus of elasticity, as follows:

$$\frac{EI}{D^3} \cdot \frac{E}{12(SDR)^3} \geq 0.093 \text{ (US Units)} \; ; \geq 0.00064 \text{ (SI Units)} \qquad (6.12)$$

where E = initial modulus of elasticity;

SDR = standard dimension ratio (D/t).

The major shortcomings of ASTM F1216-93 for the design of CIPP installed on fully deteriorated host pipes are

1. There are no guidelines for calculating the external loads, q; rather, it is dependent on the designer's judgment.
2. The solution uses the modulus of subsoil reaction, which is very difficult to obtain accurately, to represent the surrounding soil.
3. The procedure uses the pipe failure by buckling as the only design criterion and neglects other expected failure criteria.
4. In most cases, deteriorated pipes are leaky pipes, which allow for the infiltration of groundwater and fine particles from the soil surrounding the pipe. This immigration of fine particles creates voids and changes mechanical properties in the pipe surrounding area. Therefore, representing soil with one value of subgrade reaction modulus which neglects the change in the mechanical properties in the pipe surrounding soil might lead to unsafe designs. Another method which could take into consideration the difference in mechanical properties between the pipe surrounding soil and the entire soil medium is needed.

6.5 Research Need

Based upon a thorough literature review, it can be concluded that the current methods of analysis of buried flexible pipes are classified into four main groups. The first group includes the conventional solutions of the problem, such as the Iowa formula, the USBR equation, and the ring compression theory. The second group is

the elasticity solutions developed by Burns and Richard (1964) and Höeg (1968). The buckling theories of buried flexible pipe represent the third group of the available solutions for the buried pipes problem while the finite element approach is the fourth group.

It can be concluded that the available analysis methods of buried flexible pipes, excluding the finite element methods, are neither accurate enough for the design purposes nor flexible enough to consider the new innovation in the construction technique for the following reasons:

1. Both the Iowa formula and the USBR equation have been derived based on the results of extensive experimental works; therefore, they are empirical formulae with preliminary analysis involved. The disadvantages of these methods arise from their empirical nature which limits their scope of application inside the range of the pipes' dimensions and properties used in the experimental work (Katona 1993). In addition, they are derived mainly for conventional construction methods, such as the open-cut and embankment construction methods.
2. The ring compression theory developed by White and Layer (1960) neglects the existence of the surrounding soil as a boundary condition. It also assumes that the applied loads are exerted on the pipe uniformly distributed around the pipe peripheral.

3. The elasticity solutions (Burns and Richard, 1964, and Höeg, 1968) suffer from major drawbacks, such as the neglect of the soil's own weight and the pipe burial depth, and their limitation to only one loading case.
4. Both the conventional methods and the buckling theories, including the current design practice ASTM F1216-93 rely on unrealistic parameters, such as the subsoil modulus reaction which has been proved, through years of experience, to be very difficult to obtain accurately and precisely (Vallabhan and Das 1988).
5. The current design practice shortcomings include the failure of providing provisions for calculating the applied loads and considering the other possible failure criteria.
6. All solutions including the current design practice do not reflect the change in the mechanical properties of the pipe surrounding soil. The phenomenon results from the groundwater infiltration into the leaky pipe and washes out the fine particles from the surrounding soil.

A comprehensive solution based on the principles of mechanics of the soil-pipe interaction and which is flexible enough to accommodate field conditions and to eliminate most of the drawbacks of current available methods is needed. In the next chapter, a new approach for the static analysis of buried flexible pipes based on the well-known Vlasov's model will be presented. The suggested solution has the following advantages:

1. it eliminates the use of the subsoil subgrade modulus and replaces it with parameters based on the measurable soil mechanical properties;

2. it considers the effect of the pipe burial depth and treats the soil top surface as boundary condition;
3. it is based on solid principles of mechanics;
4. it addresses the variation on the mechanical properties of the pipe surrounding soil;
5. it can be modified to address different type of loads; and,
6. the solution is developed to study the statics (stress and deflection) of the flexible buried pipes; however, it is possible to modify the solution to address the stability of those structures.

CHAPTER 7

STATICS OF BURIED FLEXIBLE PIPES

7.1 Introduction

In the previous chapter, a literature survey of the analysis of buried flexible pipes was presented. The primary conclusion of Chapter 6 is that the available analytical methods of buried flexible pipes are neither accurate enough for design purposes nor flexible enough to consider the new innovations in construction techniques. A new solution for the problem which could overcome the shortcomings of the available analytical methods is needed.

The purpose of this chapter is to present a new approach for the static analysis of buried flexible pipes. This approach uses Vlasov's soil model (Vlasov and Leont'ev 1966) as a basis to solve for the problem. The presented analysis is valid for the case of an elastic, thin, circular pipe buried in an elastic, homogeneous, isotropic soil and loaded by a concentrated force acting on the soil top surface.

The solution is limited for medium to deep buried pipes with burial depths greater than one pipe diameter measured from the soil surface to the pipe crown. More details regarding this type of limitation are presented through the analysis.

7.2 Vlasov's Soil Model Versus Other Soil Models

The design of buried pipes is considered a soil-structure interaction problem. The field of soil-structure interaction, in general, is constantly advancing to new levels of knowledge and rigor. Many soil-structure interaction models have been developed in the last few decades. None of these models can be said to represent definitely the soil behavior completely and precisely. The degree of precision of each model depends on the assumptions used in the solution.

Winkler (1867) introduced his model to solve for the internal forces of an infinitely long beam resting on soil. His solution carries the assumption that the soil exhibits linear elastic behavior and the pressure on the surface is proportional to the deflection of the soil surface under the load as follows:

$$p = k w \qquad \ldots (7.1)$$

where

p = applied pressure;

k = modulus of subgrade reaction; and,

w = surface deformation of the soil.

In this model, soil is symbolized by a series of vertical springs without any mutual interaction between them. The constant of proportionality, k, of these springs is known as the modulus of subgrade reaction. Winkler's model (1867) is a one-parameter soil model, since it uses one parameter, k, to define the soil capacity of carrying surface loads.

The modulus of subgrade reaction, k, is a dependent on many other factors. Among these factors are the type of load, the loaded area, soil properties, and the depth of soil stratum. It is practically impossible to define a unique value for this modulus for a given type of soil.

Using the concept of unrelated vertical springs to represent the soil has the disadvantage of neglecting the soil shear carrying capacity. Shear stresses are developed in the subsoil if the vertical displacements between adjacent springs vary. Neglecting soil shear-carrying capacity is the major drawback of Winkler's model (1867). This shortcoming has led to non-conservative designs in many practical cases, specifically in the case of uniformly distributed surface loads (Vallabhan and Das, 1988).

Realizing the inconsistency in Winkler's model, many researchers have attempted to account for the shear capacity of soil. Filonenko-Borodich (Kerr 1964) assumed that the top ends of the spring elements are connected to an elastic membrane subjected to a constant tension 'T.' The load-displacement relation in this case is

$$p = kw - T\nabla^2 w \qquad . . \quad (7.2)$$

where ∇^2 is the Laplace operator. The interaction between the spring elements in Filonenko-Borodich's model is characterized by the intensity of the tension field 'T' in the membrane.

Hetenyi (Kerr 1964) in his model accomplished the interaction between the independent spring elements by imbedding an elastic beam or plate in Winkler's model.

It is assumed that the beam or the plate deforms in bending only. The relation between load 'p' and deflection for the three-dimensional case is

$$p = kw + D\,\nabla^2\,\nabla^2 w \qquad \ldots (7.3)$$

where $\nabla^2\ \nabla^2$ is the biharmonic operator. In this case, the interaction of the spring elements is characterized by the flexural rigidity of the plate, D.

Pasternak (Kerr 1964) used a series of compressible vertical elements capable of resisting transverse shear. In this case, the load-displacement relation is

$$p = kw - G\nabla^2 w \qquad \ldots (7.4)$$

The second term on the right-hand side of Equation (7.4) is the effect of the shear interaction of the vertical elements.

Equations (7.2), (7.3), and (7.4) represent the group of two-parameter soil models. These two parameters are the soil modulus of subgrade reaction, k, and the shear modulus which has been represented by the mechanical properties of either a membrane, a beam, or a plate.

Representing soil with two different parameters without any interrelationship between them and the elastic properties of soil is the main shortcoming in this group of soil models.

Vlasov and Leont'ev (1966) introduced a model for analyzing structures on elastic foundations based on the variational principles of mechanics. This model is widely known as Vlasov's soil model. Vlasov and Leont'ev's model is significant in its ability to fine tune the solution according to prior experience or experimental data

describing the phenomenon under consideration. This, of course, can ease the correlation between any experimental work and the analytical solution for most practical purposes.

The general concept of Vlasov's model relies on expending the unknown soil displacements in finite series as follows:

$$u(x,y) = \sum_i U_i(x)\ \psi_i(y) \qquad i=1,2....m \qquad \ldots (7.5)$$

$$v(x,y) = \sum_k V_k(x)\ \phi_k(y) \qquad k=1,2....n \qquad \ldots (7.6)$$

where $u(x,y)$ and $v(x,y)$ represent the displacement at any point within the soil mass in the horizontal and vertical directions, respectively. The functions $U_i\ (x)$ and $V_k\ (x)$ represent the components of displacements at the soil surface, and the functions ψ_i (y) and ϕ_k (y) represent the distribution of the displacements within the soil mass in the vertical direction (Fig. 7.1).

The advantage of using Vlasov's variational method lies in the fact that using a finite series to represent the unknown displacements allows the analyst to have an input in the solution by assuming the shape functions. These functions can be chosen to simulate properly the field conditions based on past experience or field experimental results. It is often convenient to introduce those functions in dimensionless format, and $U_i\ (x)$ and $V_k\ (x)$ will then have the dimension of length.

Assuming the shape function reduces the problem to find a solution for the surface displacement functions U_i (x) and V_k (x). This is equivalent to reducing the problem to a system of a finite number of degrees of freedom in one direction and an

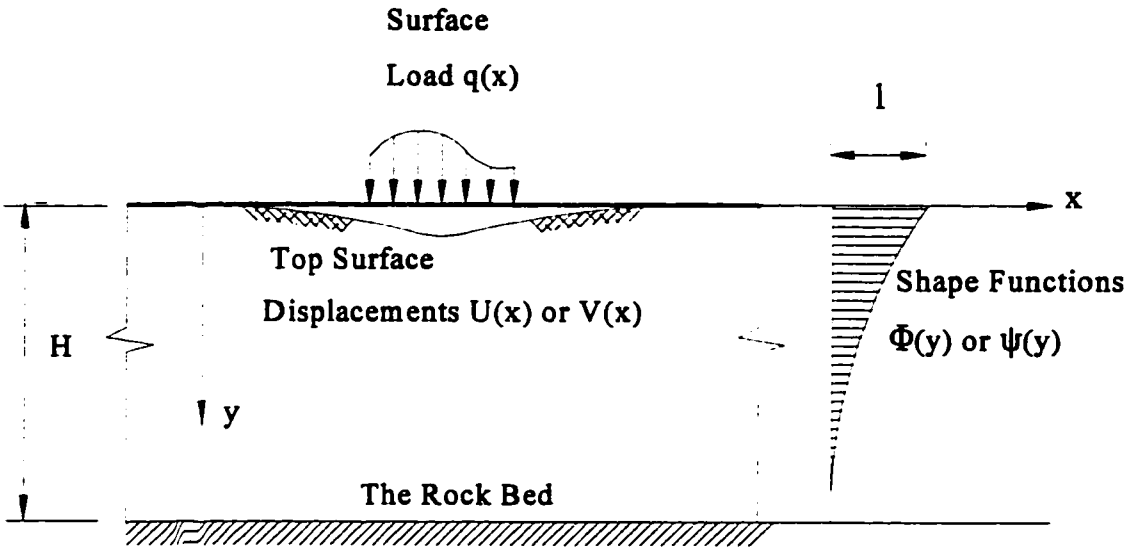

Fig. 7.1 Vlasov's Soil Model

infinite number of degrees of freedom in the other direction. This means that the problem has been transferred from a two-dimensional to a one-dimensional problem.

Using this approach, Vlasov solved a wide range of soil-structure interaction problems. In his solutions, soil properties were described by two generalized elastic parameters. Therefore, this model is considered a two-parameter model. The advantage is that these two parameters are interrelated and dependent on the elastic properties of soil and structure, and the depth of the soil layer.

Increasing the number of terms in Equations (7.5) and (7.6) is, however, undesirable, since an increase in the number of the differential equations would result. The accuracy of the solution could also be increased by a better selection of the shape functions ψ_i (y) and ϕ_k (y) (Vlasov 1966). Therefore, as an approximation, it is always convenient to limit the series to only one term.

7.3 Vlasov's Model Applied to Buried Pipes

7.3.1 Assumptions

Generally, the following assumptions are used throughout the solution:

1. Two-dimensional plane-strain geometry is used.
2. Soil is represented by a linear, elastic, homogeneous, isotropic material.
3. Thin shell theory is used to describe the pipe behavior.
4. Small strain theory is employed.

5. Static plane loading conditions exist with no loads applied in the out-of-plane direction.
6. Full contact between the pipe and the surrounding soil is assumed to exist.

Plane strain implies that the pipe installation is a long, prismatic configuration with no variation in the soil-pipe system or the loading along the longitudinal axis. The inference is that there is no deformation in the longitudinal direction and that every cross-section deforms in the same manner. Consequently, the problem reduces to describing a single representative cross-section.

Soil behaves as a heterogeneous, nonlinear, orthotropic material. It is considered heterogeneous since it can exhibit compressive strains because of the applied forces, but it cannot support any tensile strains. This behavior of soil makes the analysis of buried pipes a difficult problem. The approximation that considering soil behaves as a linear, elastic, homogeneous isotropic material proved its applicability as a good approximation in many soil-structure interaction problems, and it will be used here as well.

Thin shell theory implies that the SDR (Standard Dimension Ratio) of the buried pipe is 20 or more (Ugural, 1981). In most practical applications of CIPP, the SDR exceeds this limit and that justifies the use of thin shell theory. The remainder of the assumptions regarding the loads and the contact between the pipe and the surrounding soil are self-explanatory.

7.3.2 Pipe-Soil Model

Consider an elastic pipe of radius 'a' buried in a homogeneous, isotropic, linearly elastic soil medium at depth 'h' measured from the pipe spring-line up to the top soil surface (Fig.7.2). The total depth of the soil stratum is assumed to be 'H.'

According to St. Venant's principle (Shams and Dym 1985), the disturbance in the original soil state of stress and displacement caused by the existence of the pipe is limited to the vicinity of the pipe. Therefore, the pipe effect on the surrounding soil is assumed to be bounded by an imaginary soil cylinder with radius 'b' (Fig. 7.2). Outside these boundaries, soil returns to its free-field status.

Depending upon the relative stiffness of the pipe and the surrounding medium, radius 'b' may vary roughly between one to two pipe diameters (Burns and Richard 1964). Throughout the proposed solution, radius 'b' is chosen to be one pipe diameter. This choice explains the limitation of the solution discussed in the introduction section of this chapter.

Using the above concept, the pipe-soil model can be visualized as two regions (Fig. 7.2). The first region extends vertically from the top soil surface down to the incompressible layer at depth 'H' and horizontally from $-\infty$ to $+\infty$, excluding the area marked as Region II. The second region outlines a soil cylinder of radius 'b' surrounding the buried pipe.

The division of the buried pipe model into two regions has the advantage of providing the analyst the flexibility to consider any disturbance in the soil properties in

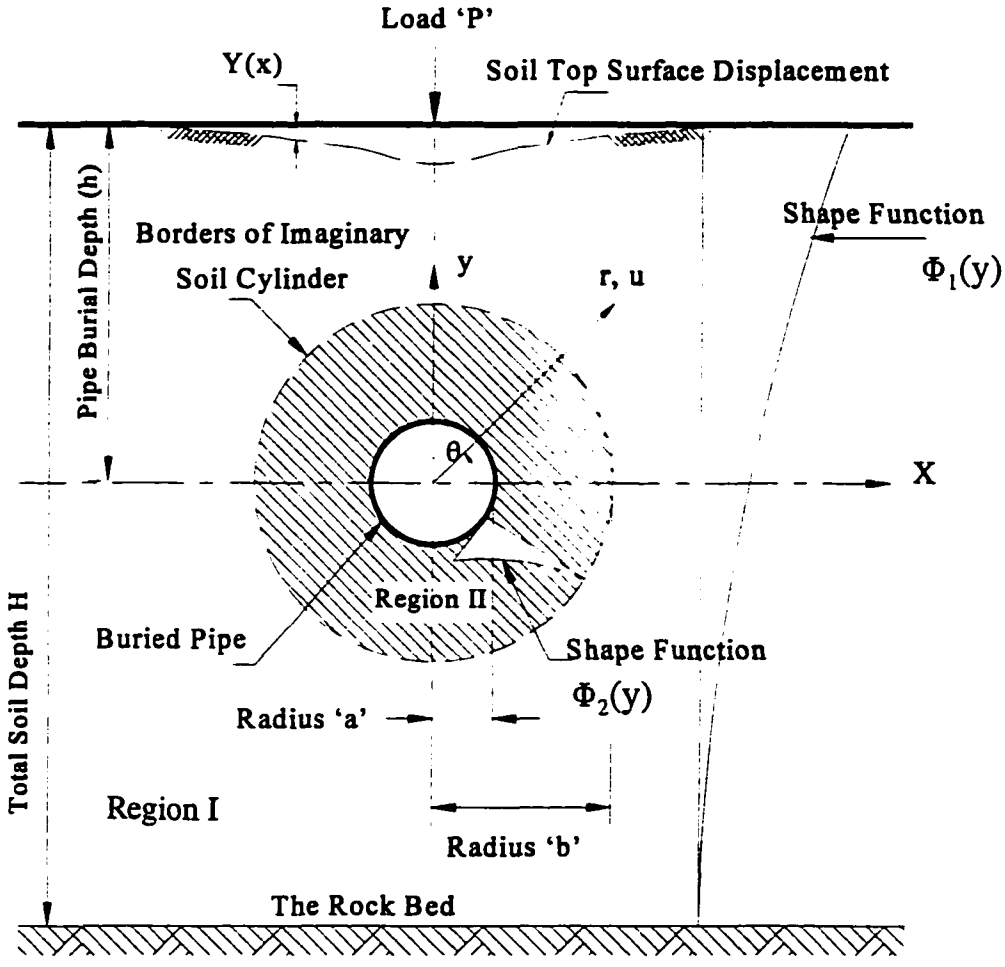

Fig. 7.2 Vlasov's Model Applied to Buried Pipes

the vicinity of the pipe. This disturbance could be a result of either fine particles' migration because of the host pipe leaking or a result of the installation process of a new pipeline using the trenchless techniques. Fine particles' migration creates voids in the soil around the pipe and changes its physical and mechanical properties. While different pipeline installation techniques may result in different types of disturbance in the soil properties. Field and laboratory investigations should play a major role in identifying and quantifying the effect of these disturbances. The focus of this work will be limited to present the new method of analysis.

The division of the pipe-soil model into two regions also allows one to simulate the soil behavior using two sets of shape functions. The first shape function, Φ_1, (Fig. 7.2) was first introduced by Vlasov and Leont'ev (1966). It describes the rate of change of soil surface displacements with depth in Region I. This function is selected based on the soil properties as if no pipe or soil hole exists. A second shape function, Φ_2, is introduced to describe the rate of change of pipe deformations in its vicinity. A description of these two shape functions and the proposed analysis is presented in the following sections.

7.3.3 Displacements Functions

7.3.3.1 Region I

Using the Cartesian coordinate system shown in (Fig. 7.2), the displacement functions in this region can expressed as follows:

$$x_1(x,y) = X(x)\ \psi_1(y) \qquad \ldots (7.7)$$

$$y_1(x,y) = Y(x)\,\phi_1(y) \qquad \ldots (7.8)$$

where $x_1(x,y)$ and $y_1(x,y)$ are the horizontal and vertical displacement components within the soil mass inside Region I, respectively. The functions $X(x)$ and $Y(x)$ represent the soil surface horizontal and vertical displacements, respectively. In most practical applications, the horizontal displacement is negligible in comparison with the value of the vertical displacement (Vlasov,1966). Consequently, the horizontal displacement is neglected in the following analysis. Selecting the shape function $\Phi_1(y)$,

$$\phi_1(y) = \frac{\sinh \gamma\,(H-h+y)}{\sinh \gamma\, H} \qquad \ldots (7.9)$$

where $\Phi_1(h) = 1.0$, $\Phi_1(0) = \sinh\gamma(H-h)/\sinh\gamma H$, $\Phi_1(h-H) = 0$

Equation (7.9) is a modification for the shape function introduced by Vlasov (1966). The modification is necessary to reflect the choice of a different location of the cartesian axes. The term 'γ' presented in Equation(7.9) is a constant which determines the rate of decrease of displacements with depth. Despite the fact that 'γ' was first introduced by Vlasov (1966), he did not provide a specific value for that parameter in his text. Vallabhan and Das (1988) proved that this parameter is dependent of the soil and structure mechanical properties and dimensions. They introduced an iterative numerical technique to calculate 'γ' for the case of an elastic beam resting on soil. Many research efforts that consider other types of structures resting on soil have followed Vallabhan and Das' attempt. Straughan (1990) provided

a similar numerical technique for calculating 'γ' for the case of an elastic plate resting on soil.

Since the scope of this research is limited to the introduction of a new analysis of buried flexible pipes, deriving a specific value of 'γ' is not considered. However, because of the limited effect of the pipe existence on the overall soil behavior, it would be justifiable to use the same 'γ' used in a similar problem of soil stratum as if no pipe or soil hole exists.

7.3.3.2 Region II

Similar to Region I, the displacements in the soil mass in Region II can be expressed by

$$w(r,\theta) = W(\theta)\,\phi_2(r) + Y(x)\phi_1(y)\sin\theta \quad \ldots (7.10)$$

$$v(r,\theta) = V(\theta)\,\psi_2(r) + Y(x)\phi_1(y)\cos\theta \quad \ldots (7.11)$$

where $w(r,\theta)$ and $v(r,\theta)$ represent the radial and circumferential displacements within the soil mass in Region II, respectively (Fig. 7.2). Functions $W(\theta)$ and $V(\theta)$ represent the radial and circumferential pipe displacements, respectively. The shape functions $\phi_2(r)$ and $\psi_2(r)$ describe the rate of change of $W(\theta)$ and $V(\theta)$ inside Region II and are assumed to be linear as follows:

$$\phi_2(r) = \frac{r-b}{a-b} \quad \ldots (7.12)$$

$$\psi_2(r) = \frac{r-b}{a-b} \quad \ldots (7.13)$$

7.3.4 Total Potential Energy Function

The proposed solution depends on determining the total potential energy function for the entire system as follows:

$$\Pi = U_{pipe} + U_{soil} - W_p \quad \text{. . (7.14)}$$

where

Π = total potential energy;

U_{pipe} = strain energy of the pipe;

U_{soil} = strain energy of the soil; and,

W_p = work done by the external loads.

The resulting total potential energy of the entire system is a function of the unknown top surface displacement function *Y(x)* and the pipe displacement functions *W(θ)* and *V(θ)*.

7.3.5 Soil Strain Energy

The general form for the strain energy stored in an elastic medium is (Langhaar, 1962)

$$U_{soil} = \frac{1}{2}\int \varepsilon_{ij}\sigma_{ij}dv \quad \text{. . (7.15)}$$

where ε_{ij} are the strain components and σ_{ij} are the corresponding stress components. Imposing the plane strain condition in the solution requires

$$E = \frac{E_s}{1-\nu_s^2}, \qquad \nu = \frac{\nu_s}{1-\nu_s}, \qquad G = \frac{E}{2(1+\nu)} \quad \text{. . (7.16)}$$

where E_s and ν_s are the soil modulus of elasticity and Poission's ratio, respectively. Neglecting the horizontal strain in the soil mass, as argued before, then the strain energy expression of Equation (7.15) reduces to

$$U_{soil} = \frac{1}{2}\int_A [\frac{E}{(1-\nu^2)}\varepsilon_y^2 + G\gamma_{xy}^2]dA \qquad \ldots (7.17)$$

Equation (7.17) is a general expression for the soil strain energy in cartesian coordinates and shall be used to generate the strain energy expression in Region I.

7.3.5.1 Strain Energy in Region I

Substituting with Equation (7.8) into the kinematic relationships for the case of plane strain, the strain components in Region I can be expressed as follows:

$$\varepsilon_y = \frac{\partial y_1(x,y)}{\partial y} = Y(x)\frac{d\phi_1(y)}{dy} \qquad \ldots (7.18)$$

$$\gamma_{xy} = \frac{\partial y_1(x,y)}{\partial x} = \frac{dY(x)}{dx}\phi_1(y) \qquad \ldots (7.19)$$

Substituting Equations (7.18) and (7.19) into Equation (7.17), one obtains the following expression for the strain energy in Region I:

$$U_1 = \frac{1}{2}\int_{h-H}^{h}\int_{-\infty}^{\infty}\left\{\frac{E_1}{1-\nu_1^2}[Y(x)\frac{d\phi_1(y)}{dy}]^2 + G_1[\frac{dY(x)}{dx}\phi_1(y)]^2\right\}dxdy - \frac{E_1}{1-\nu_1^2}I_1 - G_1 I_2 \qquad \ldots (7.20)$$

where

$$I_1 = \int_{-\pi/2}^{\pi/2}\int_{0}^{b}\left[\begin{array}{l}(Y\frac{d\phi_1}{dy}\sin^2\theta + \frac{dY}{dx}\phi_1\sin\theta\cos\theta)^2 \\ + 2\nu_1(Y\frac{d\phi_1}{dy}\sin^2\theta + \frac{dY}{dx}\phi_1\sin\theta\cos\theta) \\ \qquad \times(Y\frac{d\phi_1}{dy}\cos^2\theta - \frac{dY}{dx}\phi_1\sin\theta\cos\theta) \\ + (Y\frac{d\phi_1}{dy}\cos^2\theta - \frac{dY}{dx}\phi_1\sin\theta\cos\theta)^2\end{array}\right] r\,dr\,d\theta \qquad \ldots (7.21)$$

$$I_2 = \int_{-\pi/2}^{\pi/2}\int_{0}^{b}(2Y\frac{d\phi_1}{dy}\sin\theta\cos\theta + \frac{dY}{dx}\phi_1\cos 2\theta)^2\, r\,dr\,d\theta \qquad \ldots (7.22)$$

where E_1, ν_1, and G_1 are the moulus of elasticity, Poission's ratio and shear modulus in Region I, respectively. Simplifying Equation (7.20), then

$$U_1 = \int_{0}^{\infty}\left[\frac{E_1}{1-\nu_1^2}f_1 Y^2(x) + G_1 f_2(\frac{dY(x)}{dx})^2\right]dx - \frac{E_1}{1-\nu_1^2}I_1 - G_1 I_2 \qquad \ldots (7.23)$$

where f_1 and f_2 are constants as follows:

$$f_1 = \int_{h-H}^{h}\left[\frac{d\phi_1(y)}{dy}\right]^2 dy = \frac{\gamma^2}{\sinh^2\gamma H}[\frac{H}{2} + \frac{\sinh\gamma H\cosh\gamma H}{2\gamma}] \qquad \ldots (7.24)$$

$$f_2 = \int_{h-H}^{h}[\phi_1(y)]^2 dy = \frac{1}{\sinh^2\gamma H}[\frac{\sinh\gamma H\cosh\gamma H}{2\gamma} - \frac{H}{2}] \qquad \ldots (7.25)$$

7.3.5.2 Strain Energy in Region II

The general expression for strain energy in elastic medium, Equation (7.15), can be expressed in polar coordinates as follows (Langhaar, 1962):

$$U_{soil} = \frac{1}{2}\int_{A} (\varepsilon_r \sigma_r + \varepsilon_\theta \sigma_\theta + \tau_{r\theta}\gamma_{r\theta})\, r\, dr\, d\theta \qquad \ldots (7.26)$$

Using the constitutive relationships for plane strain in polar coordinates, Equation (7.26) reduces to

$$U_{soil} = \frac{1}{2}\int_{A}\left\{ \frac{E_2}{(1-\nu_2^2)}[\varepsilon_r^2 + 2\nu_2\varepsilon_r\varepsilon_\theta + \varepsilon_\theta^2] + G_2\gamma_{r\theta}^2 \right\} r\, dr\, d\theta \qquad \ldots (7.27)$$

Using Equations (7.10) and (7.11), one obtain the following expressions for the radial and the circumferential strains in Region II as follows:

$$\varepsilon_r = \frac{\partial w(r,\theta)}{\partial r} = W(\theta)\frac{d\phi_2(r)}{dr} + \frac{\partial}{\partial r}[Y(x)\phi_1(y)]\sin\theta \qquad \ldots (7.28)$$

Utilizing the following expansion,

$$\frac{\partial}{\partial r} = \frac{\partial}{\partial x}\frac{\partial x}{\partial r} + \frac{\partial}{\partial y}\frac{\partial y}{\partial r} \quad \text{where: } \frac{\partial x}{\partial r} = \cos\theta \text{ ; and } \frac{\partial y}{\partial r} = \sin\theta \qquad \ldots (7.29)$$

then

$$\varepsilon_r = \left[W(\theta)\frac{d\phi_2(r)}{dr}\right] + \left[Y(x)\frac{d\phi_1(y)}{dy}\sin^2\theta + \frac{dY(x)}{dx}\phi_1(y)\sin\theta\cos\theta\right] \qquad \ldots (7.30)$$

Similarly,

$$\varepsilon_\theta = \frac{1}{r}\left[W(\theta)\phi_2(r) + \frac{dV(\theta)}{d\theta}\psi_2\right] + \left[Y(x)\frac{d\phi_1(y)}{dy}\cos^2\theta - \frac{dY(x)}{dx}\phi_1(y)\sin\theta\cos\theta\right] \qquad \ldots (7.31)$$

and

$$\gamma_{r\theta}=\left[V(\theta)\frac{d\psi_2(r)}{dr}+\frac{1}{r}\left(\frac{dW(\theta)}{d\theta}\phi_2(r)-V(\theta)\psi_2(r)\right)\right] + \left[2Y(x)\frac{d\phi_1(y)}{dy}\sin\theta\cos\theta+\frac{dY(x)}{dx}\phi_1(y)\cos 2\right] \quad \ldots (7.32)$$

Substituting Equations (7.30), (7.31), and (7.32) into the general expression of the strain energy in polar coordinates, Equation (7.27), then the strain energy in Region II can be simplified as follows:

$$U_2 = U_{21} + U_{22} + U_{23} \quad \ldots (7.33)$$

where

$$U_{21}=\frac{1}{2}\int_a^b\int_{-\pi}^{\pi}\left\{\frac{E_2}{(1-\nu_2^2)}\left[\left(W\frac{d\phi_2}{dr}\right)^2+\frac{2\nu_2}{r}\left(W\frac{d\phi_2}{dr}\right)\left(W\phi_2+\frac{dV}{d\theta}\psi_2\right) + \frac{1}{r^2}\left(W\phi_2+\psi_2\frac{dV}{d\theta}\right)^2\right]+G_2\left(\frac{\phi_2}{r}\frac{dW}{d\theta}+V\frac{d\psi_2}{dr}-\frac{\psi_2}{r}V\right)^2\right\} \quad \ldots (7.34)$$

Introducing the following constants,

$$k_1 = \int_a^b (\frac{d\phi_2}{dr})^2 r\,dr \qquad t_1 = \int_a^b (\frac{d\psi_2}{dr})^2 r\,dr \qquad s_1 = \int_a^b \frac{d\phi_2}{dr}\psi_2\,dr$$

$$k_2 = \int_a^b \phi_2 \frac{d\phi_2}{dr}\,dr \qquad t_2 = \int_a^b \psi_2 \frac{d\psi_2}{dr}\,dr \qquad s_2 = \int_a^b \phi_2 \frac{d\psi_2}{dr}\,dr$$

$$k_3 = \int_a^b \frac{\phi_2^2}{r}\,dr \qquad t_3 = \int_a^b \frac{\psi_2^2}{r}\,dr \qquad s_3 = \int_a^b \frac{\phi_2\psi_2}{r}\,dr$$

$$j_1 = \int_{-\frac{\pi}{2}}^{\frac{\pi}{2}} W^2 d\theta \qquad j_2 = \int_{-\frac{\pi}{2}}^{\frac{\pi}{2}} W\frac{dV}{d\theta}d\theta \qquad j_3 = \int_{-\frac{\pi}{2}}^{\frac{\pi}{2}} (\frac{dV}{d\theta})^2 d\theta \qquad \text{. . (7.35)}$$

$$j_4 = \int_{-\frac{\pi}{2}}^{\frac{\pi}{2}} V^2 d\theta \qquad j_5 = \int_{-\frac{\pi}{2}}^{\frac{\pi}{2}} \frac{dW}{d\theta}V d\theta \qquad j_6 = \int_{-\frac{\pi}{2}}^{\frac{\pi}{2}} (\frac{dW}{d\theta})^2 d\theta$$

$$j_7 = \int_{-\frac{\pi}{2}}^{\frac{\pi}{2}} (W + \frac{d^2W}{d\theta^2})^2 d\theta$$

Equation (7.34) reduces to

$$U_{21} = \frac{E_2}{(1-\nu_2^2)}[(k_1 + 2\nu_2 k_2 + k_3)j_1 + 2(s_3 + \nu_2 s_1)j_2 + t_3 j_3] + G_2[(t_1 - 2t_2 + t_3)j_4 + 2(s_2 - s_3)j_5 + k_3 j_6] \qquad \text{. . (7.36)}$$

and the term U_{22} would be

$$U_{22}=\int_a^b\int_{-\frac{\pi}{2}}^{\frac{\pi}{2}}\{\frac{E_2}{1-\nu_2^2}[(2W\frac{d\phi_2}{dr})(Y\frac{d\phi_1}{dy}\sin^2\theta+\frac{dY}{dx}\phi_1\sin\theta\cos\theta)$$

$$+2\nu_2(W\frac{d\phi_2}{dr})(Y\frac{d\phi_1}{dy}\cos^2\theta-\frac{dY}{dx}\phi_1\sin\theta\cos\theta)$$

$$+\frac{2\nu_2}{r}(W\phi_2+\frac{dV}{d\theta}\psi_2)(Y\frac{d\phi_1}{dy}\sin^2\theta+\frac{dY}{dx}\phi_1\sin\theta\cos\theta) \qquad \ldots (7.37)$$

$$+\frac{2}{r}(W\phi_2+\frac{dV}{d\theta}\psi_2)(Y\frac{d\phi_1}{dy}\cos^2\theta-\frac{dY}{dx}\phi_1\sin\theta\cos\theta)]$$

$$+2G_2[(V\frac{d\psi_2}{dr}+\frac{dW}{d\theta}\frac{\phi_2}{r}-\frac{V}{r}\psi_2)$$

$$\times(2Y\frac{d\phi_1}{dy}\sin\theta\cos\theta+\frac{dY}{dx}\phi_1\cos2\theta)]\}rdrd\theta$$

Simplifying, then

$$U_{22}=\frac{E_2}{1-\nu_2^2}(I_3+I_4)+G_2(I_5+I_6) \qquad \ldots (7.38)$$

where

$$I_3=\int_a^b\int_{-\frac{\pi}{2}}^{\frac{\pi}{2}}\Big[(2W\frac{d\phi_2}{dr})(Y\frac{d\phi_1}{dy}\sin^2\theta+\frac{dY}{dx}\phi_1\sin\theta\cos\theta)$$

$$+2\nu_2(W\frac{d\phi_2}{dr})(Y\frac{d\phi_1}{dy}\cos^2\theta-\frac{dY}{dx}\phi_1\sin\theta\cos\theta) \qquad \ldots (7.39)$$

$$+\frac{2\nu_2}{r}(W\phi_2)(Y\frac{d\phi_1}{dy}\sin^2\theta+\frac{dY}{dx}\phi_1\sin\theta\cos\theta)$$

$$+\frac{2}{r}(W\phi_2)(Y\frac{d\phi_1}{dy}\cos^2\theta-\frac{dY}{dx}\phi_1\sin\theta\cos\theta)]\Big]rdrd\theta$$

$$I_4 = \int_a^b \int_{-\frac{\pi}{2}}^{\frac{\pi}{2}} \left[\frac{2\nu_2}{r}\left(\frac{dV}{d\theta}\psi_2\right)\left(Y\frac{d\phi_1}{dy}\sin^2\theta + \frac{dY}{dx}\phi_1 \sin\theta\cos\theta\right) + \frac{2}{r}\left(\frac{dV}{d\theta}\psi_2\right)\left(Y\frac{d\phi_1}{dy}\cos^2\theta - \frac{dY}{dx}\phi_1 \sin\theta\cos\theta\right)\right] r\,dr\,d\theta \quad \ldots (7.40)$$

$$I_5 = \int_a^b \int_{-\frac{\pi}{2}}^{\frac{\pi}{2}} \left[\frac{2}{r}\left(\frac{dW}{d\theta}\phi_2\right)\left(2Y\frac{d\phi_1}{dy}\sin\theta\cos\theta + \frac{dY}{dx}\phi_1\cos 2\theta\right)\right] r\,dr\,d\theta \quad \ldots (7.41)$$

$$I_6 = \int_a^b \int_{-\frac{\pi}{2}}^{\frac{\pi}{2}} \left[2\left(V\frac{d\psi_2}{dr} - \frac{V\psi_2}{r}\right)\left(2Y\frac{d\phi_1}{dy}\sin\theta\cos\theta + \frac{dY}{dx}\phi_1\cos 2\theta\right)\right] r \quad \ldots (7.42)$$

The term U_{23} is

$$\begin{aligned} U_{23} = \int_a^b \int_{-\frac{\pi}{2}}^{\frac{\pi}{2}} \Bigg\{ & \frac{E_2}{1-\nu_2^2}\left[\left(Y\frac{d\phi_1}{dy}\sin^2\theta + \frac{dY}{dx}\phi_1\sin\theta\cos\theta\right)^2\right. \\ & + 2\nu_2\left(Y\frac{d\phi_1}{dy}\sin^2\theta + \frac{dY}{dx}\phi_1\sin\theta\cos\theta\right) \\ & \times \left(Y\frac{d\phi_1}{dy}\cos^2\theta - \frac{dY}{dx}\phi_1\sin\theta\cos\theta\right) \\ & \left. + \left(Y\frac{d\phi_1}{dy}\cos^2\theta - \frac{dY}{dx}\phi_1\sin\theta\cos\theta\right)^2\right] \\ & + 2G_2\left[\left(2Y\frac{d\phi_1}{dy}\sin\theta\cos\theta + \frac{dY}{dx}\phi_1\cos 2\theta\right)^2\right] \Bigg\} r\,dr\,d\theta \end{aligned} \quad \ldots (7.43)$$

Simplifying Equation (7.43), then

$$U_{23} = \frac{E_2}{1-\nu_2^2} I_7 + G_2 I_8 \qquad \text{. . (7.44)}$$

where

$$I_7 = \int_a^b \int_{-\frac{\pi}{2}}^{\frac{\pi}{2}} \Big\{ (Y\frac{d\phi_1}{dy}\sin^2\theta + \frac{dY}{dx}\phi_1 \sin\theta\cos\theta)^2$$
$$+2\nu_2 (Y\frac{d\phi_1}{dy}\sin^2\theta + \frac{dY}{dx}\phi_1 \sin\theta\cos\theta) \qquad \text{. . (7.45)}$$
$$\times (Y\frac{d\phi_1}{dy}\cos^2\theta - \frac{dY}{dx}\phi_1 \sin\theta\cos\theta)$$
$$+(Y\frac{d\phi_1}{dy}\cos^2\theta - \frac{dY}{dx}\phi_1 \sin\theta\cos\theta)^2 \Big\} r\,dr\,d\theta$$

and

$$I_8 = \int_a^b \int_{-\frac{\pi}{2}}^{\frac{\pi}{2}} (2Y\frac{d\phi_1}{dy}\sin\theta\cos\theta + \frac{dY}{dx}\phi_1 \cos 2\theta)^2 \, r\,dr\,d\theta \qquad \text{. . (7.46)}$$

7.3.6 Pipe Strain Energy

Strain energy stored in a two-dimensional elastic body in terms of the polar coordinates is given in Equation (7.27). For the case of thin pipes, it is assumed that the stresses normal to the mid-plane 'σ_r' are very small compared with other stress components. The same is also true for the shear stresses '$\tau_{r\theta}$.' Neglecting σ_r and $\tau_{r\theta}$ in Equation (7.27) leads to

$$U_{pipe} = \frac{1}{2}\int_A \varepsilon_\theta \sigma_\theta \, a\,dr\,d\theta \qquad \text{. . (7.47)}$$

Using the following expression for strains in a thin cylinder shell (Flügge 1973, and Kerr and Soifer 1969),

$$\varepsilon_\theta = \hat{\varepsilon}_\theta + \rho\,\hat{\kappa}_\theta \qquad \ldots (7.48)$$

where

$\hat{\varepsilon}_\theta$ = mid-surface circumferential strain;

$\hat{\kappa}_\theta$ = change in curvature of mid-surface in the circumferential direction;

ρ = radial distance measured from mid-surface up to the point under consideration.

By neglecting the nonlinear terms, the mid-surface strain and change of curvature components can be presented in terms of the pipe mid-surface displacements as follows:

$$\hat{\varepsilon}_\theta = \frac{1}{a}\left(\frac{\partial \hat{v}}{\partial \theta} + \hat{w}\right) \qquad \ldots (7.49)$$

$$\hat{\kappa}_\theta = -\frac{1}{a^2}\left(\hat{w} + \frac{\partial^2 \hat{w}}{\partial \theta^2}\right) \qquad \ldots (7.50)$$

where $\hat{w}$ and $\hat{v}$ represent the radial and circumferential pipe displacements, respectively. Substituting Equations (7.48), (7.49), and (7.50) into Equation (7.47),

$$U_{pipe} = \frac{E_p}{2(1-\nu_p^2)} \int_0^{2\pi} \int_{\frac{-t}{2}}^{\frac{t}{2}} (\hat{\varepsilon}_\theta^{\,2} + \rho^2 \hat{\kappa}_\theta^{\,2})\, a\,dr\,d\theta \qquad \ldots (7.51)$$

Performing the integration over the thickness of the pipe wall,

$$U_{pipe} = \frac{D}{a^3} \int_{-\frac{\pi}{2}}^{\frac{\pi}{2}} \left\{ \frac{12a^2}{t^2} \left(\frac{\partial \hat{v}}{\partial \theta} + \hat{w}\right)^2 + \left(\hat{w} + \frac{\partial^2 \hat{w}}{\partial \theta^2}\right)^2 \right\} d\theta \qquad \ldots (7.52)$$

where

D = flexural rigidity = $E_p t^3/\{12(1-\nu_p^2)\}$;

ν_p = pipe Poisson's ratio;

E_p = pipe modulus of elasticity;

t = pipe wall thickness; and,

a = pipe mean radius.

The pipe mid-surface displacements are

$$\hat{w}(a,\theta) = W(\theta) + Y(\bar{x})\,\phi_1(\bar{y})\sin\theta \quad \ldots (7.53)$$

$$\hat{v}(a,\theta) = V(\theta) + Y(\bar{x})\,\phi_1(\bar{y})\cos\theta \quad \ldots (7.54)$$

where $\bar{x}$, $\bar{y}$ are the coordinates of the pipe mid-surface. Substituting Equations (7.53) and (7.54) into the general expression of pipe strain energy, Equation (7.52), then

$$\begin{aligned} U_{pipe} = \int_{-\frac{\pi}{2}}^{\frac{\pi}{2}} \Bigg\{ & \frac{12D}{at^2}\left[W + \frac{dV}{d\theta} + aY(\bar{x})\frac{d\phi_1(\bar{y})}{d\bar{y}}\cos^2\theta - a\frac{dY(\bar{x})}{d\bar{x}}\phi_1(\bar{x})\sin\theta\cos\theta \right] \\ & + \frac{D}{a^3}\Bigg[W + \frac{d^2W}{d\theta^2} + a(2\cos^2\theta - \sin^2\theta)Y(\bar{x})\frac{d\phi_1(\bar{y})}{d\bar{y}} \\ & - 3a\sin\theta\cos\theta\frac{dY(\bar{x})}{d\bar{x}}\phi_1(\bar{y}) + a^2Y(\bar{x})\frac{d^2\phi_1(\bar{y})}{d\bar{y}^2}\sin\theta\cos^2\theta \\ & - 2a^2\frac{dY(\bar{x})}{d\theta}\frac{d\phi_1(\bar{y})}{d\bar{y}}\sin^2\theta\cos\theta + a^2\frac{d^2Y(\bar{x})}{d\theta^2}\phi_1(\bar{y})\sin^3\theta \Bigg] \Bigg\} d\theta \end{aligned} \quad \ldots (7.55)$$

Simplifying, then

$$U_{pipe} = \frac{12D}{at^2}[I_9 + I_{10} + I_{11} + j_1 + 2j_2 + j_3] + \frac{D}{a^3}[I_{12} + I_{13} + j_7] \quad \ldots (7.56)$$

where

$$I_9 = \int_{-\frac{\pi}{2}}^{\frac{\pi}{2}} \left[a\,Y(\bar{x}) \frac{d\phi_1(\bar{y})}{d\bar{y}} \cos^2\theta - a \frac{dY(\bar{x})}{d\bar{x}} \phi_1(\bar{x}) \sin\theta\cos\theta \right]^2 d\theta \qquad \ldots (7.57)$$

$$I_{10} = \int_{-\frac{\pi}{2}}^{\frac{\pi}{2}} 2W \left[a\,Y(\bar{x}) \frac{d\phi_1(\bar{y})}{d\bar{y}} \cos^2\theta - a \frac{dY(\bar{x})}{d\bar{x}} \phi_1(\bar{x}) \sin\theta\cos\theta \right] d\theta \qquad \ldots (7.58)$$

$$I_{11} = \int_{-\frac{\pi}{2}}^{\frac{\pi}{2}} 2 \frac{dV}{d\theta} \left[a\,Y(\bar{x}) \frac{d\phi_1(\bar{y})}{d\bar{y}} \cos^2\theta - a \frac{dY(\bar{x})}{d\bar{x}} \phi_1(\bar{x}) \sin\theta\cos\theta \right] d\theta \qquad \ldots (7.59)$$

$$\begin{aligned} I_{12} = \int_{-\frac{\pi}{2}}^{\frac{\pi}{2}} \Bigg[& a^2 Y(\bar{x}) \frac{d^2\phi_1(\bar{y})}{d\bar{y}^2} \sin\theta\cos^2\theta - 2a^2 \frac{dY(\bar{x})}{d\theta} \frac{d\phi_1(\bar{y})}{d\bar{y}} \sin^2\theta\cos\theta \\ & + a^2 \frac{d^2Y(\bar{x})}{d\theta^2} \phi_1(\bar{y}) \sin^3\theta + aY(\bar{x}) \frac{d\phi_1(\bar{y})}{d\bar{y}} (2\cos^2\theta - \sin^2\theta) \\ & - 3a \frac{dY(\bar{x})}{\bar{x}} \phi_1(\bar{y}) \sin\theta\cos\theta \Bigg]^2 d\theta \end{aligned} \qquad \ldots (7.60)$$

$$\begin{aligned} I_{13} = \int_{-\frac{\pi}{2}}^{\frac{\pi}{2}} 2\left(W + \frac{d^2W}{d\theta^2}\right) \Bigg[& a^2 Y(\bar{x}) \frac{d^2\phi_1(\bar{y})}{d\bar{y}^2} \sin\theta\cos^2\theta - 2a^2 \frac{dY(\bar{x})}{d\theta} \frac{d\phi_1(\bar{y})}{d\bar{y}} \sin^2\theta\cos\theta \\ & + a^2 \frac{d^2Y(\bar{x})}{d\theta^2} \phi_1(\bar{y}) \sin^3\theta + aY(\bar{x}) \frac{d\phi_1(\bar{y})}{d\bar{y}} (2\cos^2\theta - \sin^2\theta) \\ & - 3a \frac{dY(\bar{x})}{d\bar{x}} \phi_1(\bar{y}) \sin\theta\cos\theta \Bigg] d\theta \end{aligned} \qquad \ldots (7.61)$$

7.3.7 Solution

Equations (7.23), (7.33), and (7.56) represent the strain energy stored due to the deformation in Region I, Region II, and the pipe, respectively. These expressions are written in terms of the unknown displacement functions $Y(x)$, $W(\theta)$, and $V(\theta)$. Employing the Rayleigh-Ritz principle, a reasonable yet practical solution for the problem can be reached by assuming the following displacement functions:

$$Y(x) = C_1 e^{-\alpha x} \qquad \ldots (7.62)$$

where

$$\alpha = \sqrt{\frac{2f_1}{(1-\nu_1)f_2}} \qquad \ldots (7.63)$$

also,

$$W(\theta) = C_2 \cos 2\theta \qquad \ldots (7.64)$$

$$V(\theta) = C_3(\sin 2\theta + \cos 2\theta) \qquad \ldots (7.65)$$

where C_1, C_2, and C_3 are constants to be determined. The assumed displacement function for the top surface displacement, Equation (7.62), is the same solution presented by Vlasov (1966) for the case of a soil stratum loaded with a concentrated load on the surface. Substituting Equations (7.62), (7.64), and (7.65) in the presented expressions for strain energies, then

$$U_1 = C_1^2 \left[\frac{E_1}{1-\nu_1^2}\left(\frac{f_1}{2\alpha} - i_1\right) + G_1\left(\frac{\alpha f_2}{2} - i_2\right)\right] \qquad \ldots (7.66)$$

$$U_{21} = [\frac{E_2 j_1}{(1-\nu_2^2)}(k_1 + 2\nu_2 k_2 + k_3) + j_6 G_2 k_3]\ C_2^2 + [\frac{2E_2 j_2}{(1-\nu_2^2)}(s_3 + \nu_2 s_1) + 2j_5 G_2 (s_2 - s_3)]\ C_2 C_3 + [\frac{E_2 j_3}{(1-\nu_2^2)} t_3 + G_2 j_4 (t_1 - 2t_2 + t_3)]\ C_3^2 \quad \ldots (7.67)$$

$$U_{22} = \frac{E_2}{1-\nu_2^2}(i_3 C_1 C_2 + i_4 C_1 C_3) + G_2 (i_5 C_1 C_2 + i_6 C_1 C_3) \quad \ldots (7.68)$$

$$U_{23} = [\frac{E_2}{1-\nu_2^2} i_7 + G_2 i_8]\ C_1^2 \quad \ldots (7.69)$$

$$U_{plate} = \frac{12D}{at^2}[i_9 C_1^2 + i_{10} C_1 C_2 + i_{11} C_1 C_3 + j_1 C_2^2 + j_3 C_3^2 + 2j_2 C_2 C_3] + \frac{D}{a^3}[i_{12} C_1^2 + i_{13} C_1 C_2 + j_7 C_2^2] \quad \ldots (7.70)$$

where $i_{1,2,3,...}$ are the integrations $I_{1,2,3,...}$ after substituting the assumed displacement functions and factoring out the constants C_1, C_2, and C_3.

7.3.8 External Work Done

The general expression for the work done by external loads and soil weight is

$$W_p = -PC_1 - \int_{h-H}^{h} \int_{-\infty}^{\infty} \gamma_g Y(x)\, \phi_1(h)\, dx\, dy \quad \ldots (7.71)$$

where P is the surface concentrated load (Fig. 7.2), and γ_g is the soil specific weight. Substituting Equations (7.9), and (7.62) and performing the integration, then

$$W_p = -C_1 [P + \frac{2\gamma_g}{\alpha \gamma \sinh \gamma H}(\cosh \gamma H - 1)] \quad \ldots (7.72)$$

The total potential energy of the whole system in terms of its regional strain energies can be expressed as follows:

$$\Pi = U_1 + (U_{21} + U_{22} + U_{23}) + U_{pipe} - W_p \quad \ldots (7.73)$$

The above equation is a function of the unknown constants C_1, C_2, and C_3. A set of three algebraic equations is obtained by the partial differentiation of Equation (7.73) with respect to the unknown constants; then

$$[A]\ \{C\} = \{P\} \quad \ldots (7.74)$$

where [A] is a 3x3 matrix and {C} and {P} are the unknown constants and the load vectors, respectively. The coefficients of matrix [A] are given in the following page. The unknown constants and the load vectors are as follows:

$$\{C\} = \begin{Bmatrix} C_1 \\ C_2 \\ C_3 \end{Bmatrix};\ and\ \{P\} = \begin{Bmatrix} -\left[P + \dfrac{2\gamma_g}{\alpha\gamma \sinh\gamma H}(\cosh\gamma H - 1)\right] \\ 0 \\ 0 \end{Bmatrix} \quad \ldots (7.75)$$

$$A_{11} = 2[\frac{E_1}{1-\nu_1^2}(\frac{f_1}{2\alpha} - i_1) + G_1(\frac{\alpha f_2}{2} - i_2)] + 2[\frac{E_2}{1-\nu_2^2} i_7 + G_2 i_8] + 2[\frac{12D}{at^2} i_9 + \frac{D}{a^3} i_{12}]$$

$$A_{12} = [\frac{E_2}{1-\nu_2^2} i_3 + G_2 i_5] + [\frac{12D}{at^2} i_{10} + \frac{D}{a^3} i_{13}]$$

$$A_{13} = [\frac{E_2}{1-\nu_2^2} i_4 + G_2 i_6] + [\frac{12D}{at^2} i_{11}]$$

$$A_{21} = A_{12}$$

$$A_{22} = 2[\frac{E_2 j_1}{(1-\nu_2^2)}(k_1 + 2\nu_2 k_2 + k_3) + j_6 G_2 k_3] + 2[\frac{12 j_1 D}{at^2} + \frac{j_7 D}{a^3}]$$

$$A_{23} = [\frac{2E_2 j_2}{1-\nu_2^2}(s_3 + \nu_2 s_1) + 2 j_5 G_2 (s_2 - s_3)] + [\frac{24 j_2 D}{at^2}]$$

$$A_{31} = A_{13}$$

$$A_{32} = A_{23}$$

$$A_{33} = 2[\frac{E_2 j_3}{1-\nu_2^2} t_3 + j_4 G_2 (t_1 - 2t_2 + t_3) + \frac{12 j_3 D}{at^2}]$$

7.4 Results

A computer program was written in MathCad code (Appendix B) to evaluate the solution of buried flexible pipes based on the above equations. The program was then used to solve for a problem of a buried pipe and loaded with a surface concentrated load. The solution is compared with a finite element solution for the same problem. The finite element solution was conducted using CANDE-89 program (CANDE-89 User Manual, 1989).

The following parameters are used in the example

E_s (Region I)	= 2000 psi;	ν_s (Region I)	= 0.35
E_s (Region II)	= 2000 psi;	ν_s (Region II)	= 0.35
P	= 2000 lb/inch;	γ_g	= 0.064 lb/in3
h	= 60 inch;	H	= 120 inch
γH	= 2;	t	= 0.5 inch
a	= 12 inch;	b	= 2a
E_p	= 350,000 psi;	ν_p	= 0.3

Figures (7.3) to (7.6) show the results for the pipe radial and circumferential displacements, bending moments, and thrust force in the pipe wall. Three solutions for the same example are presented: the proposed solution, the finite element solution, and the solution proposed by Burns and Richard (1964). Attention should be drawn to the sign convention used in these figures, where a positive sign indicates outward radial

displacement, counterclockwise circumferential displacement, tension thrust force, and positive bending moment which creates tension in the inner pipe surface.

Results show that the proposed solution and the FE solution are in good agreement for the case of radial displacement (Fig. 7.3). The proposed solution gives almost 92% of the FE result at the point of maximum radial displacement. Figure (7.4) shows that the proposed solution underestimates pipe circumferential displacement when it is compared with the FE solution. At the point of maximum circumferential displacement, it is found that the proposed solution gives only 72% of the FE results. In both cases of radial and circumferential displacements, the solution proposed by Burns and Richard (1964) seems to be incomparable with the results of the FE solution or the proposed solution. It should be noted that the solution proposed by Burns and Richard does not address the rigid displacement of the pipe.

The results also show that there is some discrepancy of the bending moment results between the proposed solution and the FE solution (Fig. 7.5). This tends to be true especially around the pipe crown. However, the difference in the maximum bending moment in both cases is in the acceptable range. It is found that the proposed solution gives almost 73% of the maximum bending moment resulted from the FE solution.

Figure (7.6) shows an agreement between the proposed solution and the FE solution regarding the thrust force sign around the pipe circumference. The proposed solution seems to overestimate the thrust force when it is compared with the FE

solution. However, this increase in the estimated thrust force is conservative for pipe design.

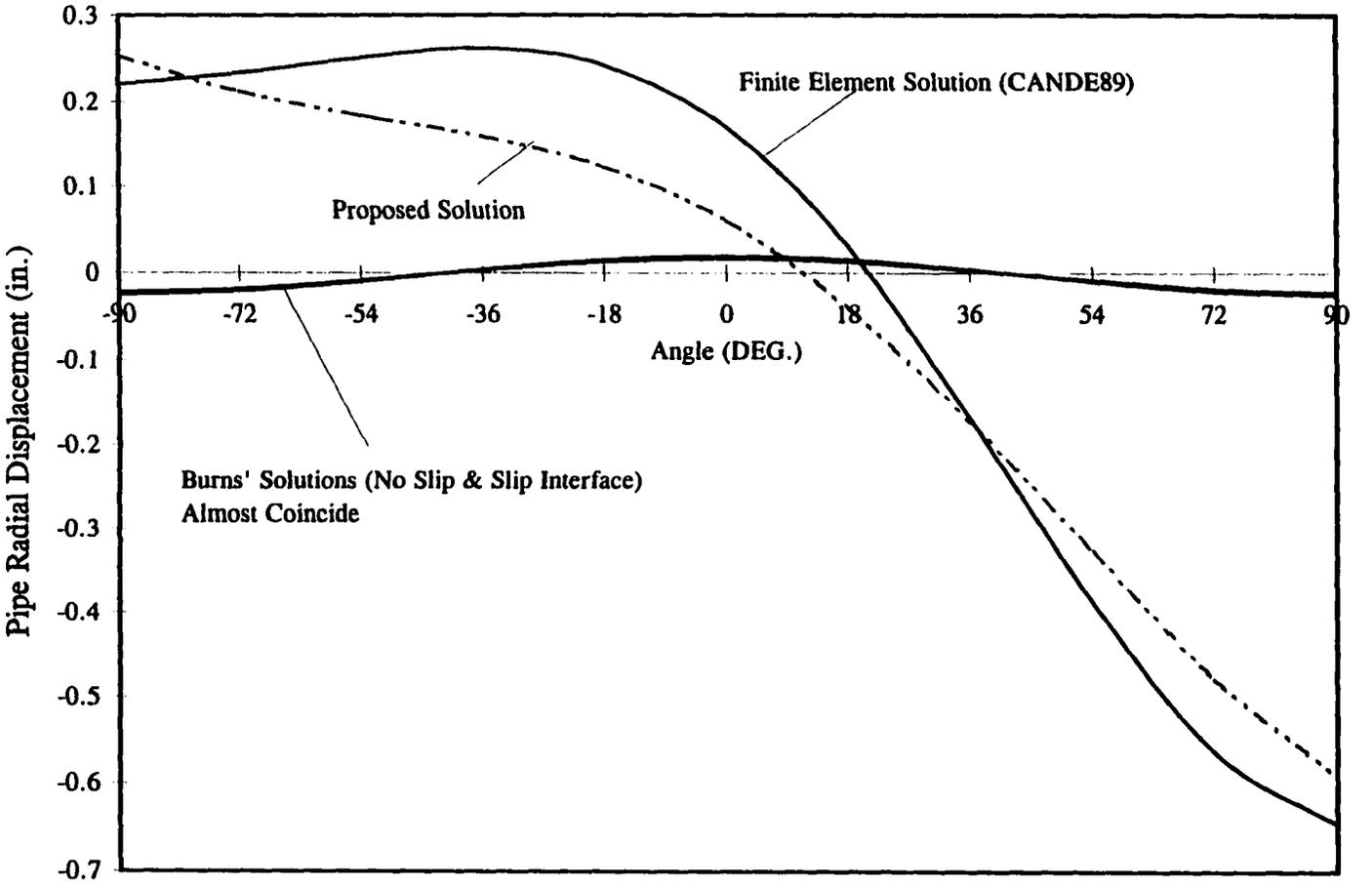

Fig. 7.3 Pipe Radial Displacement

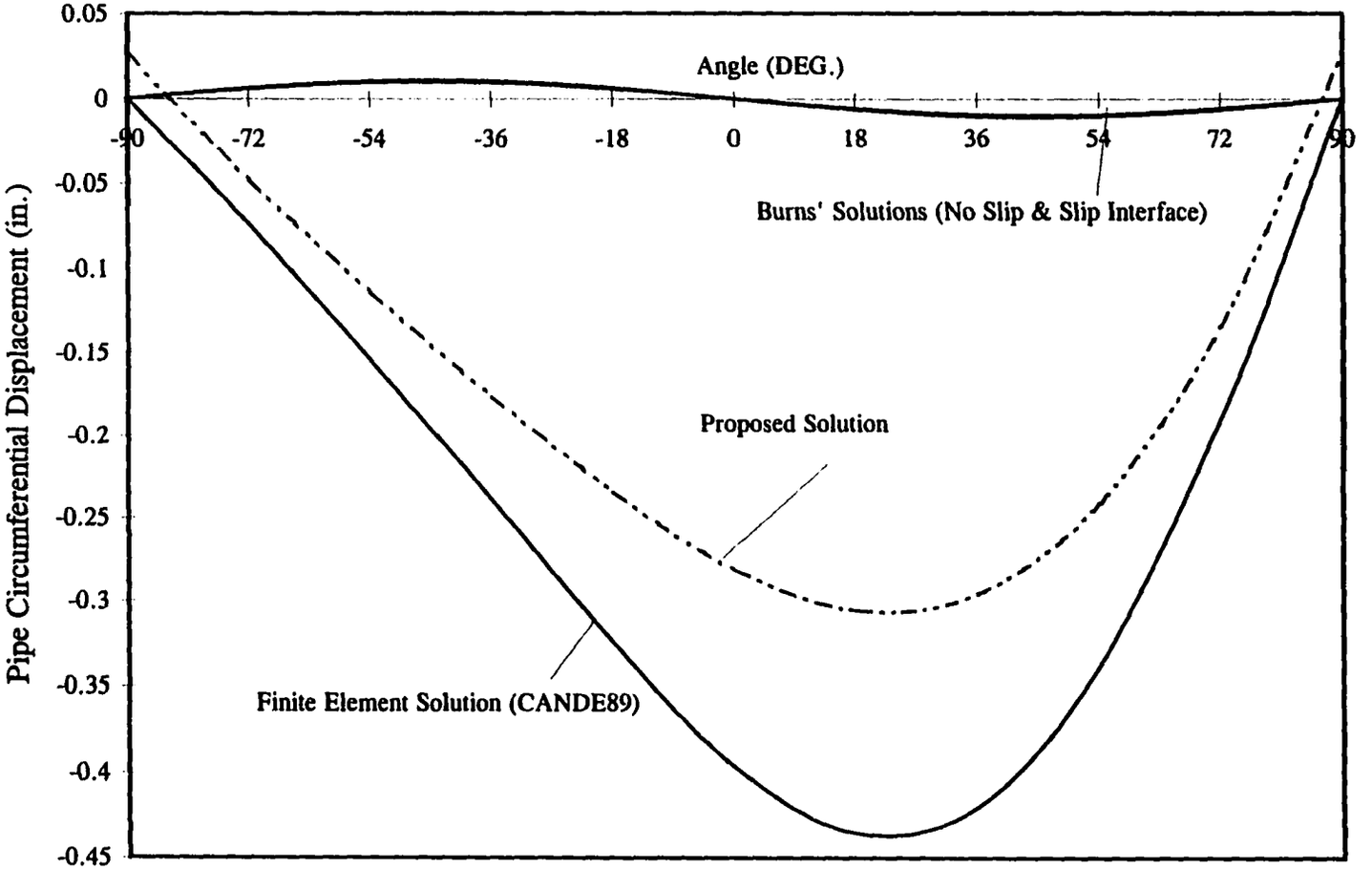

Fig. 7.4 Pipe Circumferential Displacement

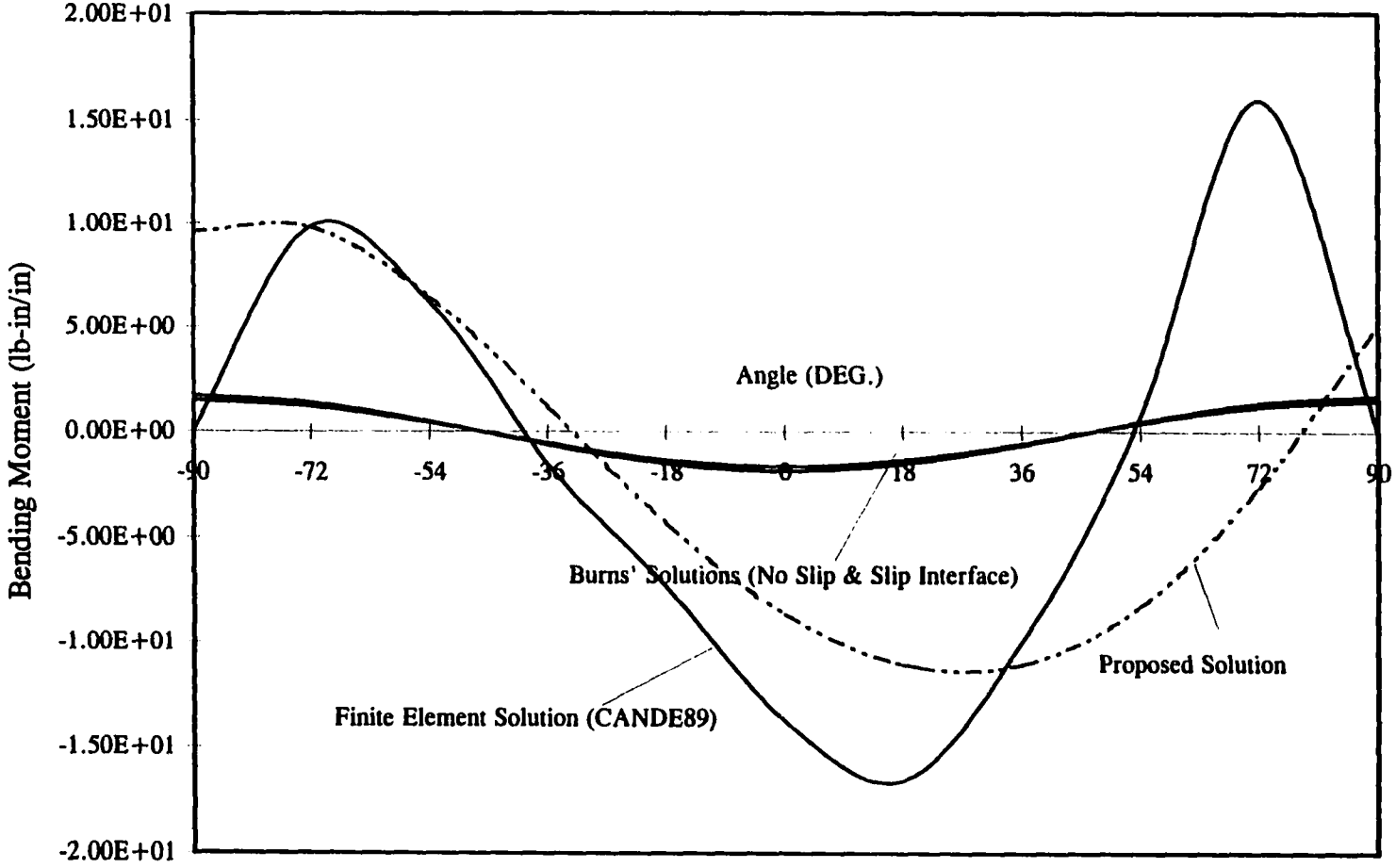

Fig 7.5 Bending Moment in Pipe Wall

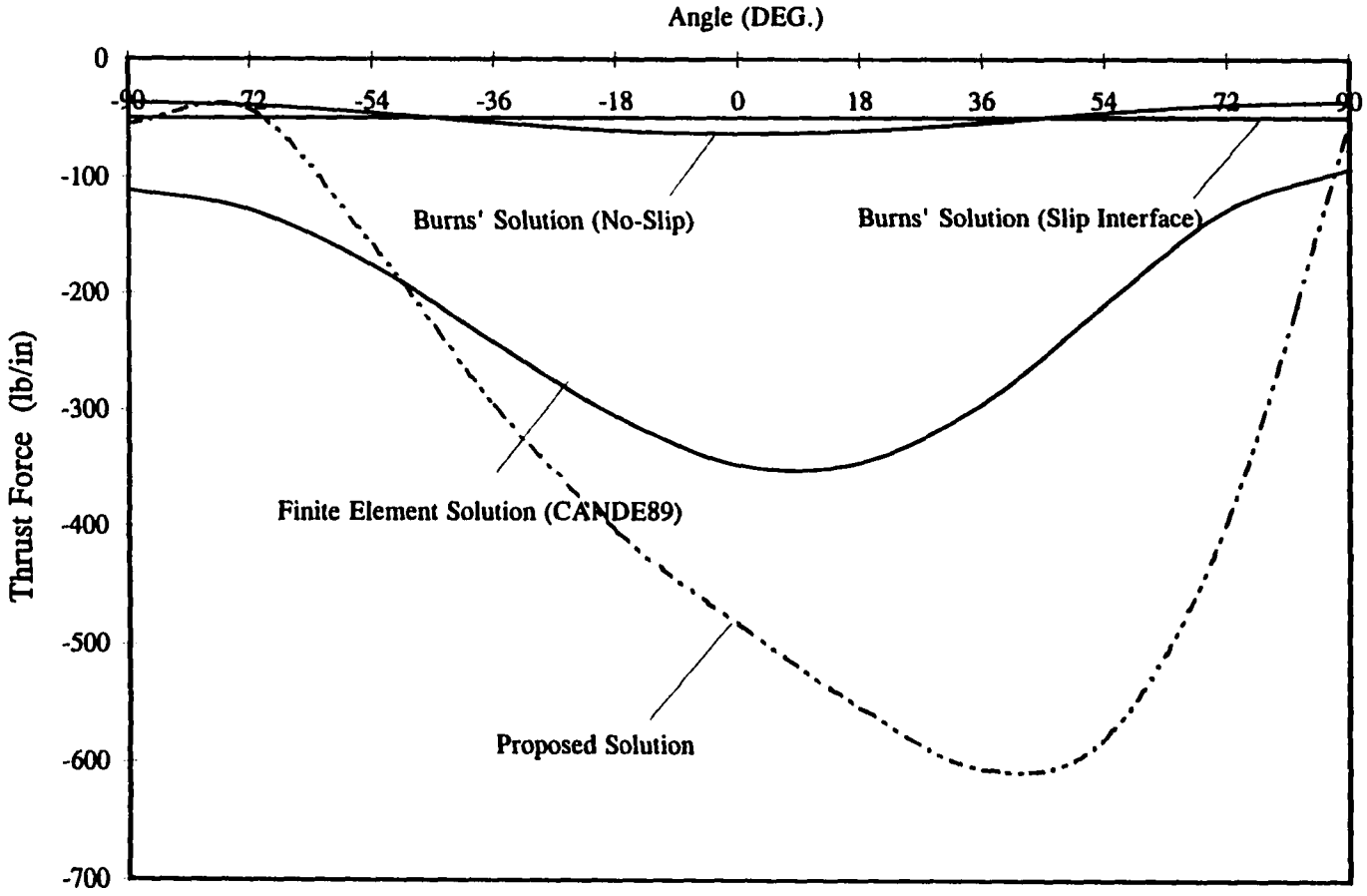

Fig. 7.6 Thrust Force in Pipe Wall

CHAPTER 8

CONCLUSIONS AND RECOMMENDATIONS FOR FURTHER RESEARCH (PART II)

8.1 Conclusions

The soil model proposed by Vlasov and Leont'ev (1966) for solving soil-structure interaction problems is expanded to model the behavior of buried flexible pipes. The new method is capable of predicting the behavior of flexible pipes buried at a depth of one pipe diameter or more. In his solution of a single-layer soil model, Vlasov introduced the idea of shape functions to represent the rate of decay of soil displacement. In this research, a second shape function is introduced to describe the rate of change of the displacements in the soil mass surrounding the buried pipe. This shape function can be selected to reflect the behavior of the soil mass disturbed by the pipe installation or because of the host pipe leaking.

The presented solution utilizes the energy principles of mechanics to solve for the static of buried pipes. The resulting total potential energy function of the whole system is calculated, and the well-known Raleigh-Ritz principle is used to solve for the pipe displacements and internal forces. A comparison study between the proposed solution, the finite element solution, and Burns and Richard's solution for one example

of buried pipe was conducted. The results of the comparison study show that there is a good agreement between the proposed solution and the finite element solution.

Applying Vlasov's soil model through this research in the solution of buried flexible pipe problems has proved that it has the following advantages over the conventional solutions:

1. It has a better presentation of the boundary conditions.
2. It employs the energy methods which open the door for the application of many useful approximate techniques designed especially for the application of the energy methods such as the Rayleigh-Ritz method. Also, the solution could be expanded to study the stability problem of buried pipes.

In addition, this model has the following potentials to solve the soil-pipe problems:

1. The flexibility in addressing different site and construction conditions.
2. The solution could be done for any type of loads.

8.2 Future Work

The method of static analysis of buried flexible pipes presented here provides researchers with a versatile model for describing the behavior of the soil mass surrounding the buried pipe. Certain assumptions and limitations were imposed in order to present the analysis in a simple and understandable format. Future research work should expand the solution beyond the imposed limitations and validate it using either numerical or experimental results. Some topics which could be pursued in future research are:

1. Conduct field and laboratory experimental work to observe the behavior of the soil mass surrounding the pipe under different pipe installation methods in order to justify the use of different shape functions and to compare the new method of analysis with field and laboratory results.
2. Expand the analysis for other types of surface loads.
3. Investigate the effect of the viscoelastic behavior of soils and pipes on the long-term behavior of pipe-soil systems.
4. Expand the new approach to study the stability behavior of buried flexible pipes.
5. Modify existing public domain programs such as CANDE (Katona 1976) to accommodate the new approach or develop a new software package, whichever is more feasible.
6. Develop design guidelines, charts, and tables which can be utilized by the pipe design engineer in most design works without the reliance on exhaustive FE analysis or complex formulation.
7. Develop an expert system for the design of flexible pipes capable of capturing the accumulated experience and wisdom of contractors, engineers, designers, and manufacturers in the field. Analysis and design software can be tied to this expert system software to facilitate the design/analysis process.

APPENDIX A

MATERIAL CHARACTERIZATION

TEST RESULTS

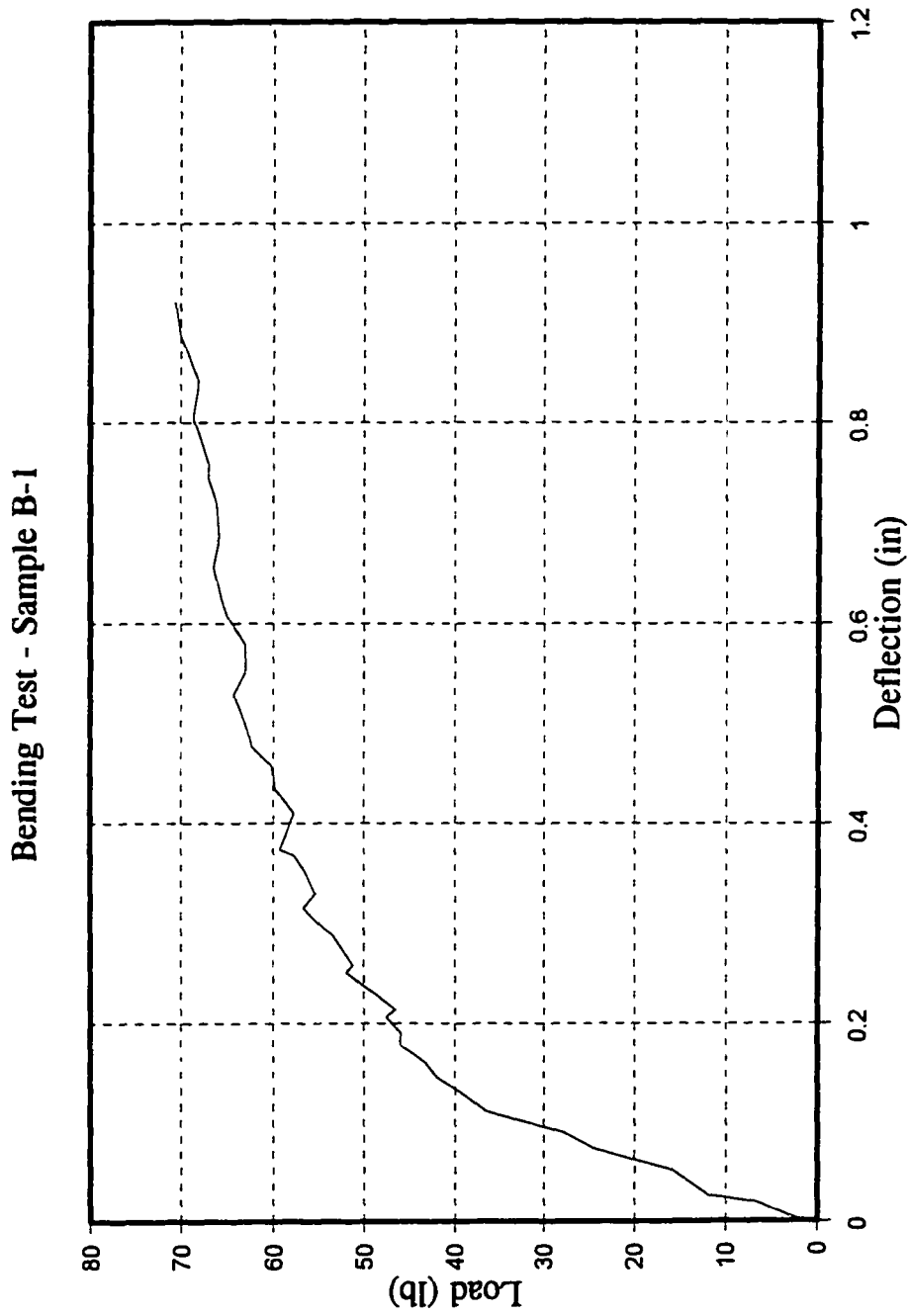

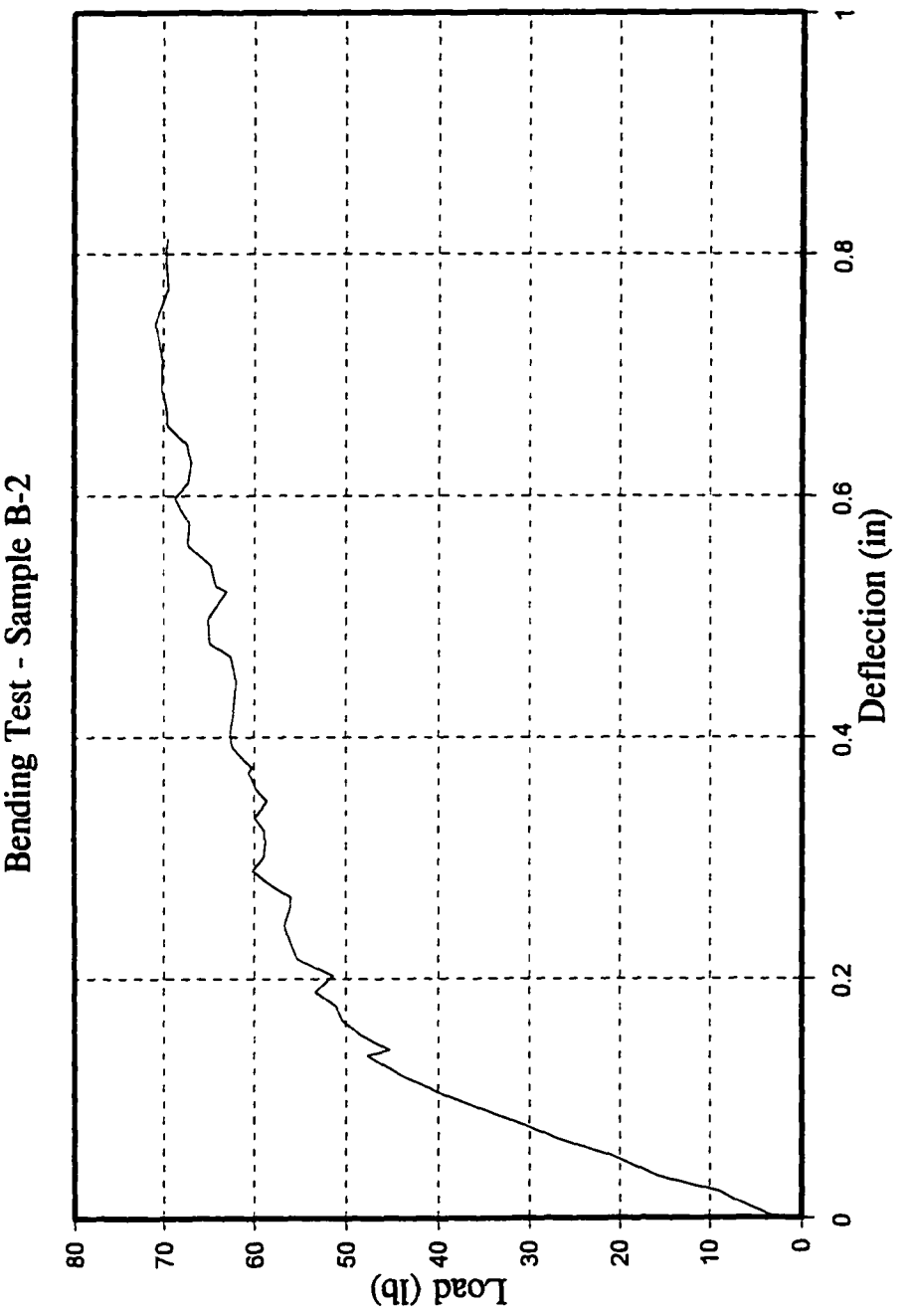

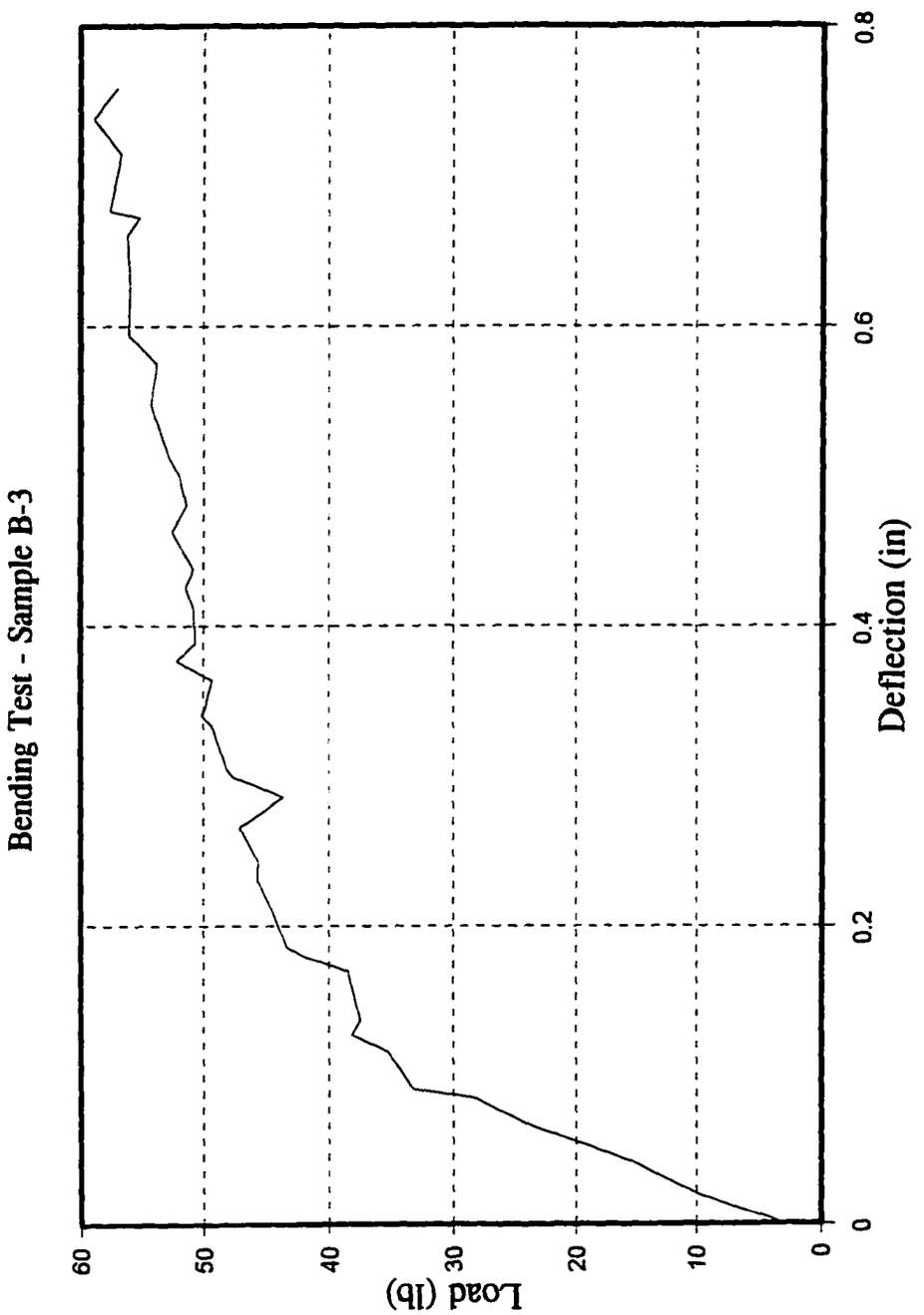

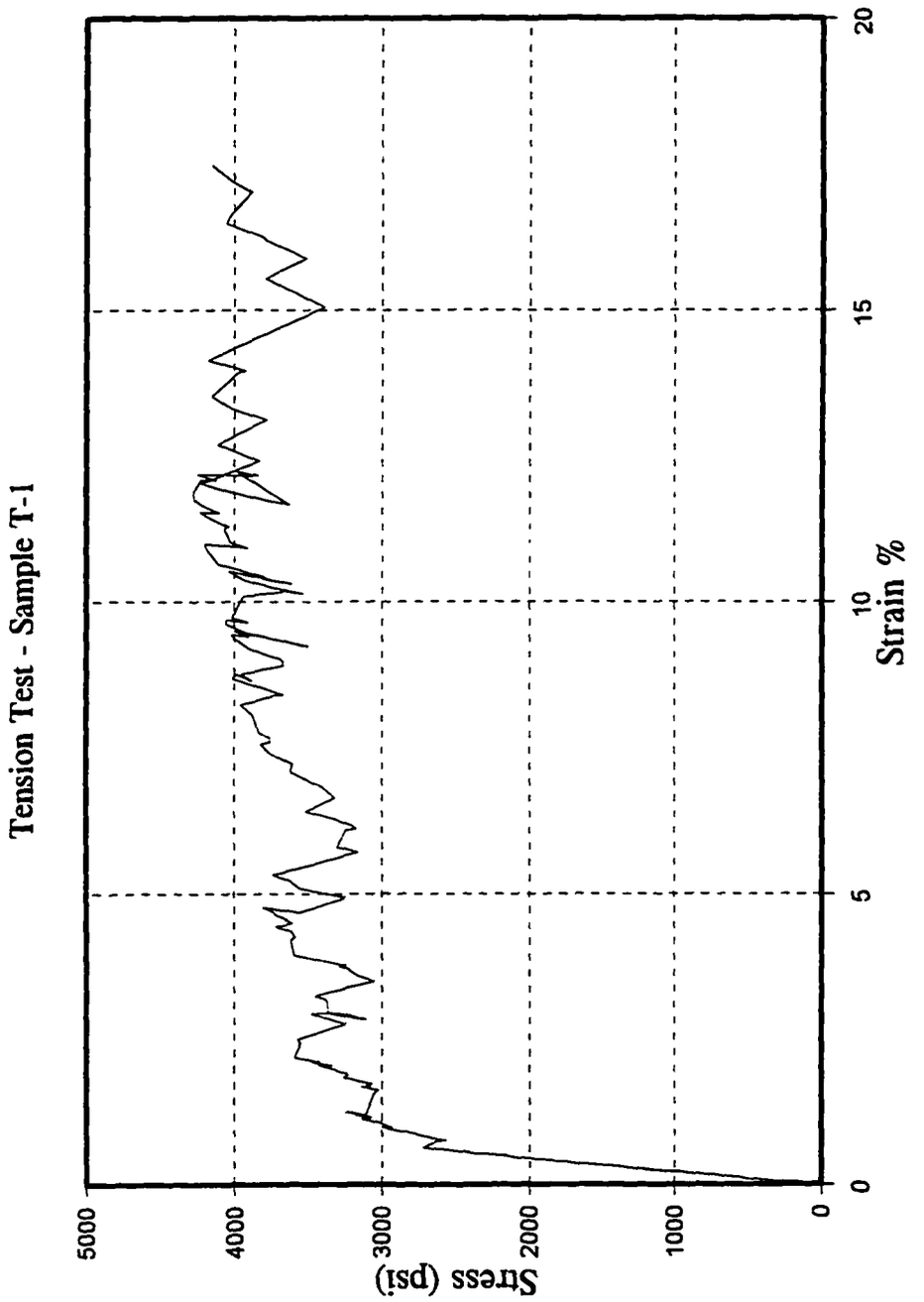

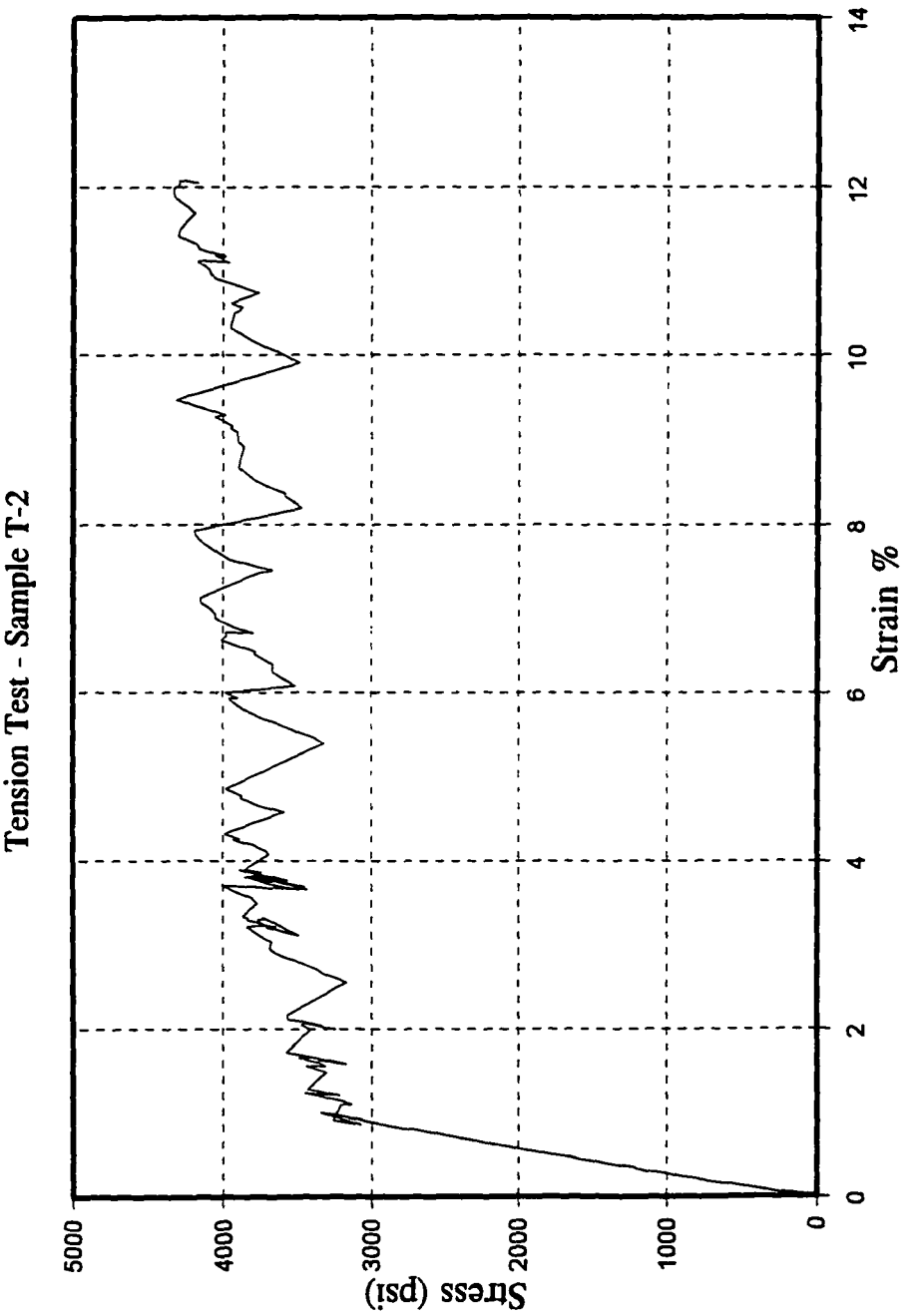

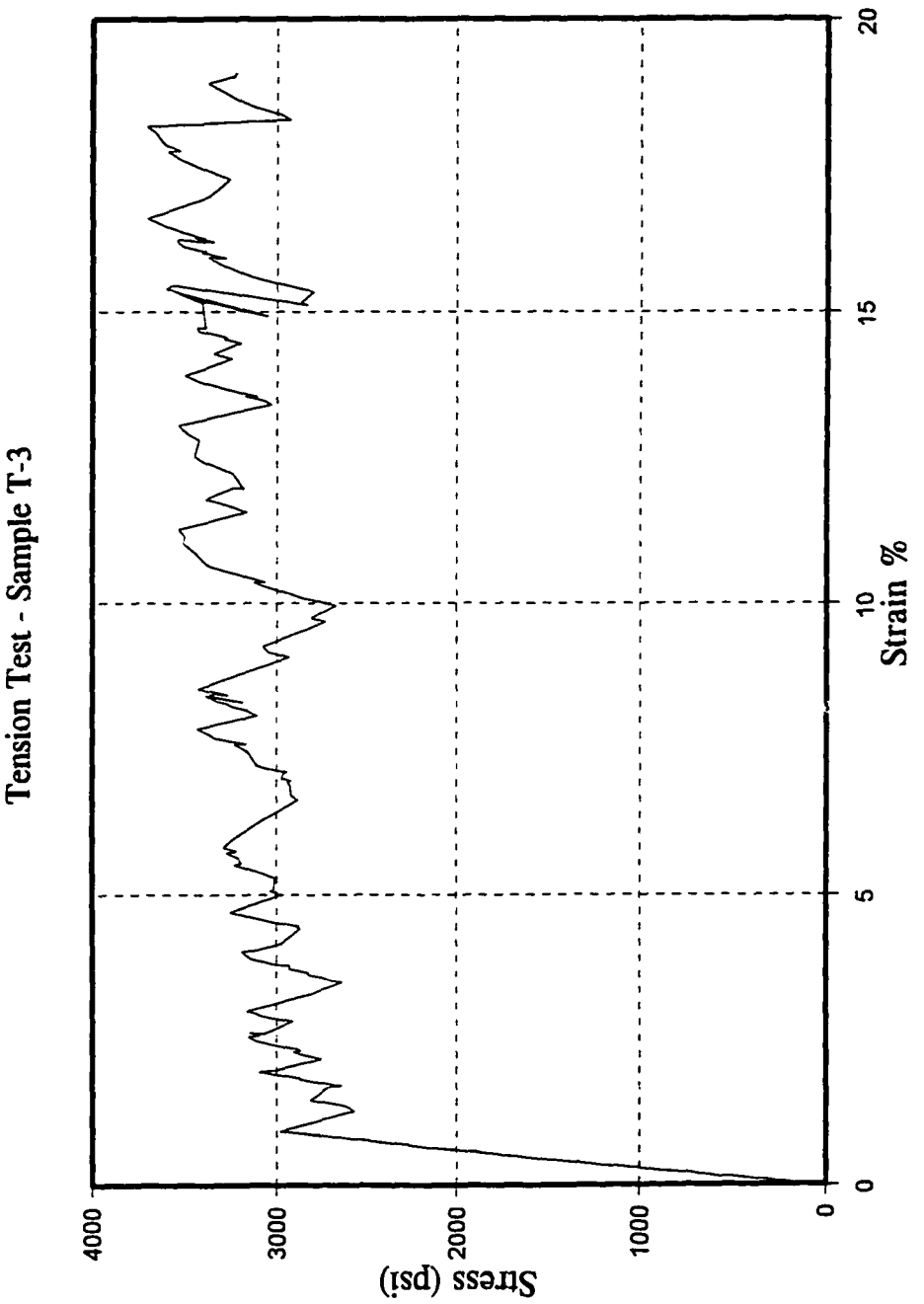

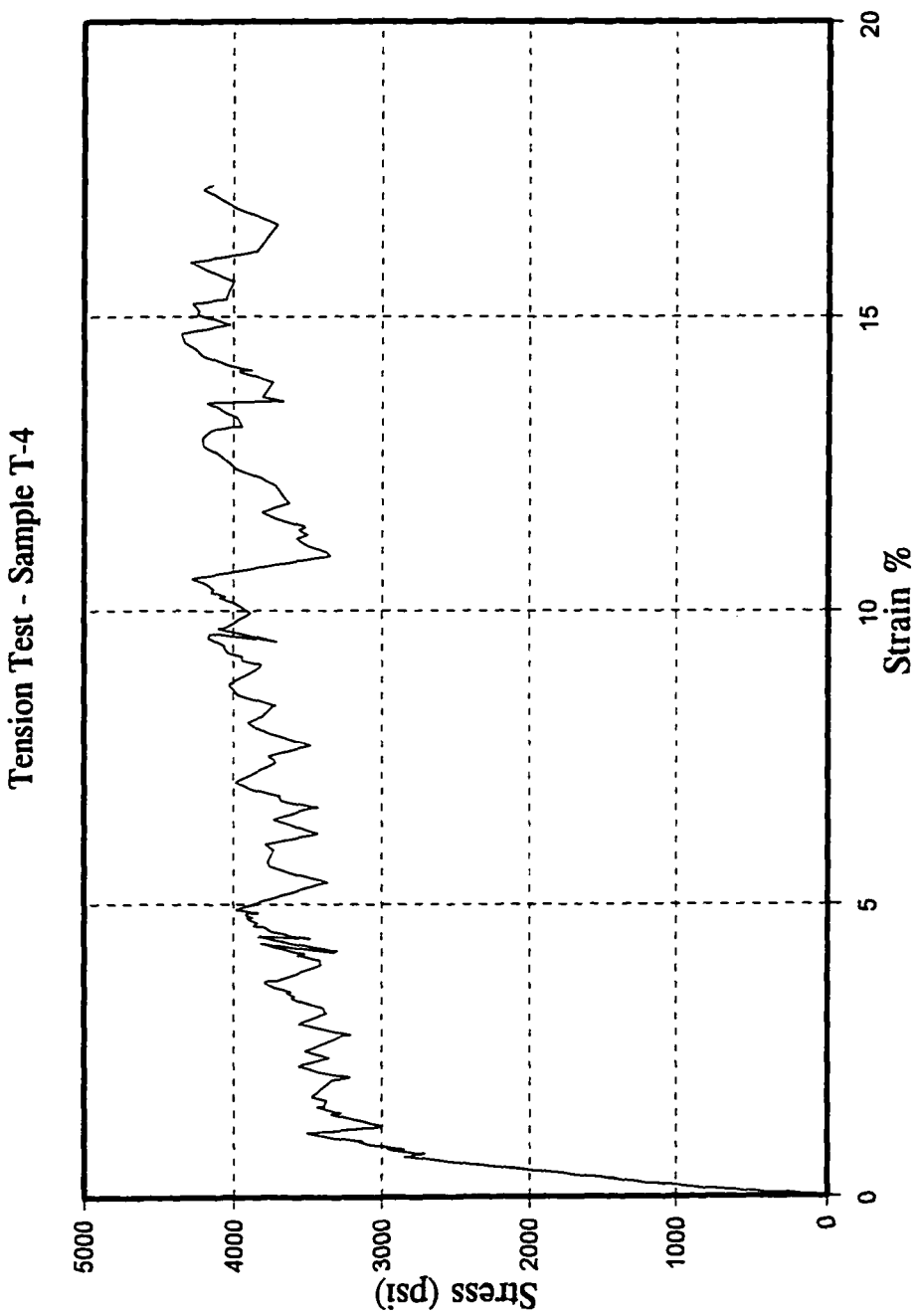

APPENDIX B

MATHCAD PROGRAM

Soil Properties

Region I

$vs1 = 0.35$ **Soil Poisson's Ratio in Region I**

$Es1 = 2000$ **psi** **Soil Modulus of Elasticity in Region I**

$$v1 = \frac{vs1}{(1 - vs1)}$$

$$E1 = \frac{Es1}{(1 - vs1^2)} \quad \textbf{psi}$$

$$G1 = \frac{E1}{2\cdot(1 - v1)} \quad \textbf{psi}$$

$\gamma g = 0.064$ **lb/in^3** **Soil Self Weight**

$\gamma H = 2$

$H = 120$ **inches** **Depth of Bed Rock**

$$\gamma = \frac{\gamma H}{H} \qquad \gamma = 0.01667$$ **Shape Function Relaxation Factor**

$$f1 = \frac{\gamma^2}{\sinh(\gamma H)^2}\cdot\left(\frac{H}{2} - \frac{\sinh(\gamma H)\cdot\cosh(\gamma H)}{2\cdot\gamma}\right)$$

$$f2 = \frac{1}{\sinh(\gamma H)^2}\cdot\left(\frac{\sinh(\gamma H)\cdot\cosh(\gamma H)}{2\cdot\gamma} - \frac{H}{2}\right)$$

$$\alpha = \sqrt{\frac{2\cdot f1}{(1 - v1)\cdot f2}} \qquad \alpha = 0.04021$$

Region II

$vs2 = 0.35$ **Soil Poisson's Ratio in Region II**

$Es2 = 2000$ **psi** **Soil Modulus of Elasticity in Region II**

$$v2 = \frac{vs2}{(1 - vs2)}$$

$$E2 = \frac{Es2}{(1 - vs2^2)} \quad \textbf{psi}$$

$$G2 = \frac{E2}{2\cdot(1 - v2)} \quad \textbf{psi}$$

Pipe Properties

$a = 12$ **inches** **Pipe Mean Radius**

$b = 3\cdot a$ **inches** **Imaginary Soil Cylinder Radius**

$t = \frac{1}{2}$ **inches** **Pipe Wall Thickness**

$vp = 0.3$ **Pipe Poisson's Ratio**

$Ep = 350000$ **psi** **Pipe Modulus of Elasticity**

$$D = \frac{Ep\cdot t^3}{12\cdot(1 - vp^2)}$$ **Pipe Flexural Rigidity**

$h = 60$ **inches** **Pipe Burial Depth**

Assumed Functions and Their Derivatives

$$Y(r,\theta) = e^{(-\alpha \cdot r \cdot \cos(\theta))}$$

$$\phi 1(r,\theta) = \frac{\sinh(\gamma \cdot (H - h + r \cdot \sin(\theta)))}{\sinh(\gamma \cdot H)}$$

$$Y'(r,\theta) = -\alpha \cdot Y(r,\theta)$$

$$\phi 1'(r,\theta) = \frac{\gamma \cdot \cosh(\gamma \cdot (H - h + r \cdot \sin(\theta)))}{\sinh(\gamma \cdot H)}$$

$$W(\theta) = \cos(2 \cdot \theta)$$

$$W'(\theta) = -2 \cdot \sin(2 \cdot \theta)$$

$$W''(\theta) = -4 \cdot \cos(2 \cdot \theta)$$

$$V(\theta) = (\sin(2 \cdot \theta) - \cos(2 \cdot \theta))$$

$$V'(\theta) = 2 \cdot (\cos(2 \cdot \theta) - \sin(2 \cdot \theta))$$

$$V''(\theta) = -4 \cdot (\sin(2 \cdot \theta) - \cos(2 \cdot \theta))$$

$$\phi 2(r) = \frac{r - b}{(a - b)}$$

$$\phi 2'(r) = \frac{1}{(a - b)}$$

$$\psi 2(r) = \frac{r - b}{(a - b)}$$

$$\psi 2'(r) = \frac{1}{(a - b)}$$

Integrations

$$I1 = \int_0^b \int_{-\frac{\pi}{2}}^{\frac{\pi}{2}} r \cdot \left[\left(Y(r,\theta)\cdot\phi1'(r,\theta)\cdot\sin(\theta)^2 - Y'(r,\theta)\cdot\phi1(r,\theta)\cdot\sin(\theta)\cdot\cos(\theta)\right)^2 \ldots \right. \\ + 2\cdot\nu1\cdot\left(Y(r,\theta)\cdot\phi1'(r,\theta)\cdot\sin(\theta)^2 - Y'(r,\theta)\cdot\phi1(r,\theta)\cdot\sin(\theta)\cdot\cos(\theta)\right) \ldots \\ + \left(Y(r,\theta)\cdot\phi1'(r,\theta)\cdot\cos(\theta)^2 - Y'(r,\theta)\cdot\phi1(r,\theta)\cdot\sin(\theta)\cdot\cos(\theta)\right) \ldots \\ \left. + \left(Y(r,\theta)\cdot\phi1'(r,\theta)\cdot\cos(\theta)^2 - Y'(r,\theta)\cdot\phi1(r,\theta)\cdot\sin(\theta)\cdot\cos(\theta)\right)^2 \right] d\theta\, dr$$

$$I2 = \int_0^b \int_{-\frac{\pi}{2}}^{\frac{\pi}{2}} r\cdot\left(2\cdot Y(r,\theta)\cdot\phi1'(r,\theta)\cdot\sin(\theta)\cdot\cos(\theta) - Y'(r,\theta)\cdot\phi1(r,\theta)\cdot\cos(2\cdot\theta)\right)^2 d\theta\, dr$$

$$I3 = \int_a^b \int_{-\frac{\pi}{2}}^{\frac{\pi}{2}} r\cdot\left[\left(2\cdot W(\theta)\cdot\phi2'(r)\right)\cdot\left(Y(r,\theta)\cdot\phi1'(r,\theta)\cdot\sin(\theta)^2 - Y'(r,\theta)\cdot\phi1(r,\theta)\cdot\sin(\theta)\cdot\cos(\theta)\right) \ldots \right. \\ + \left(2\cdot\nu2\cdot W(\theta)\cdot\phi2'(r)\right)\cdot\left(Y(r,\theta)\cdot\phi1'(r,\theta)\cdot\cos(\theta)^2 - Y'(r,\theta)\cdot\phi1(r,\theta)\cdot\sin(\theta)\cdot\cos(\theta)\right) \ldots \\ \left(2\cdot\frac{\nu2}{r}\cdot W(\theta)\cdot\phi2(r)\right)\cdot\left(Y(r,\theta)\cdot\phi1'(r,\theta)\cdot\sin(\theta)^2 - Y'(r,\theta)\cdot\phi1(r,\theta)\cdot\sin(\theta)\cdot\cos(\theta)\right) \ldots \\ \left. + \left(\frac{2}{r}\cdot W(\theta)\cdot\phi2(r)\right)\cdot\left(Y(r,\theta)\cdot\phi1'(r,\theta)\cdot\cos(\theta)^2 - Y'(r,\theta)\cdot\phi1(r,\theta)\cdot\sin(\theta)\cdot\cos(\theta)\right) \right] d\theta\, dr$$

$$I4 = \int_a^b \int_{-\frac{\pi}{2}}^{\frac{\pi}{2}} r\cdot\left[\left(2\cdot\frac{\nu2}{r}\cdot V'(\theta)\cdot\psi2(r)\right)\cdot\left(Y(r,\theta)\cdot\phi1'(r,\theta)\cdot\sin(\theta)^2 - Y'(r,\theta)\cdot\phi1(r,\theta)\cdot\sin(\theta)\cdot\cos(\theta)\right) \ldots \right. \\ \left. + \left(\frac{2}{r}\cdot V'(\theta)\cdot\psi2(r)\right)\cdot\left(Y(r,\theta)\cdot\phi1'(r,\theta)\cdot\cos(\theta)^2 - Y'(r,\theta)\cdot\phi1(r,\theta)\cdot\sin(\theta)\cdot\cos(\theta)\right) \right] d\theta\, dr$$

$$I5 = \int_a^b \int_{-\frac{\pi}{2}}^{\frac{\pi}{2}} r \cdot \left(\frac{2}{r} \cdot W'(\theta) \cdot \phi 2(r)\right) \cdot (2 \cdot Y(r,\theta) \cdot \phi 1'(r,\theta) \cdot \sin(\theta) \cdot \cos(\theta) - Y'(r,\theta) \cdot \phi 1(r,\theta) \cdot \cos(2 \cdot \theta)) \, d\theta \, dr$$

$$I6 = \int_a^b \int_{-\frac{\pi}{2}}^{\frac{\pi}{2}} r \cdot \left[2 \cdot V(\theta) \cdot \left(\psi 2'(r) - \frac{\psi 2(r)}{r}\right)\right] \cdot \left[\begin{array}{l}(2 \cdot Y(r,\theta) \cdot \phi 1'(r,\theta) \cdot \sin(\theta) \cdot \cos(\theta)) \ldots \\ + Y'(r,\theta) \cdot \phi 1(r,\theta) \cdot \cos(2 \cdot \theta)\end{array}\right] d\theta \, dr$$

$$I7 = \int_a^b \int_{-\frac{\pi}{2}}^{\frac{\pi}{2}} r \cdot \begin{array}{l}\left(Y(r,\theta) \cdot \phi 1'(r,\theta) \cdot \sin(\theta)^2 - Y'(r,\theta) \cdot \phi 1(r,\theta) \cdot \sin(\theta) \cdot \cos(\theta)\right)^2 \ldots \\ + 2 \cdot \nu 2 \cdot \left(Y(r,\theta) \cdot \phi 1'(r,\theta) \cdot \sin(\theta)^2 - Y'(r,\theta) \cdot \phi 1(r,\theta) \cdot \sin(\theta) \cdot \cos(\theta)\right) \ldots \ldots \\ \left(Y(r,\theta) \cdot \phi 1'(r,\theta) \cdot \cos(\theta)^2 - Y'(r,\theta) \cdot \phi 1(r,\theta) \cdot \sin(\theta) \cdot \cos(\theta)\right) \\ + \left(Y(r,\theta) \cdot \phi 1'(r,\theta) \cdot \cos(\theta)^2 - Y'(r,\theta) \cdot \phi 1(r,\theta) \cdot \sin(\theta) \cdot \cos(\theta)\right)^2\end{array} d\theta \, dr$$

$$I8 = \int_a^b \int_{-\frac{\pi}{2}}^{\frac{\pi}{2}} r \cdot (2 \cdot Y(r,\theta) \cdot \phi 1'(r,\theta) \cdot \sin(\theta) \cdot \cos(\theta) - Y'(r,\theta) \cdot \phi 1(r,\theta) \cdot \cos(2 \cdot \theta))^2 \, d\theta \, dr$$

Other Integrations in terms of Solution Constants

$$j1 = \int_{-\frac{\pi}{2}}^{\frac{\pi}{2}} W(\theta)^2 \, d\theta \qquad j2 = \int_{-\frac{\pi}{2}}^{\frac{\pi}{2}} W(\theta) \cdot V'(\theta) \, d\theta$$

$$j3 = \int_{-\frac{\pi}{2}}^{\frac{\pi}{2}} V'(\theta)^2 \, d\theta \qquad j4 = \int_{-\frac{\pi}{2}}^{\frac{\pi}{2}} V(\theta)^2 \, d\theta$$

$$j5 = \int_{-\frac{\pi}{2}}^{\frac{\pi}{2}} W'(\theta)\cdot V(\theta)\, d\theta \qquad j6 = \int_{-\frac{\pi}{2}}^{\frac{\pi}{2}} W''(\theta)^2\, d\theta$$

$$j7 = \int_{-\frac{\pi}{2}}^{\frac{\pi}{2}} (W(\theta) - W''(\theta))^2\, d\theta$$

$$Y(\theta) = e^{(-\alpha\cdot a\cdot\cos(\theta))}$$

$$\phi 1(\theta) = \frac{\sinh(\gamma\cdot(H - h + a\cdot\sin(\theta)))}{\sinh(\gamma\cdot H)}$$

$$Y'(\theta) = -\alpha\cdot Y(\theta)$$

$$\phi 1'(\theta) = \frac{\gamma\cdot\cosh(\gamma\cdot(H - h + a\cdot\sin(\theta)))}{\sinh(\gamma\cdot H)}$$

$$Y''(\theta) = \alpha^2\cdot Y(\theta)$$

$$\phi 1''(\theta) = \gamma^2\cdot\phi 1(\theta)$$

$$I9 = \int_{-\frac{\pi}{2}}^{\frac{\pi}{2}} \left[a\cdot\left(Y(\theta)\cdot\phi 1'(\theta)\cdot\cos(\theta)^2 - Y'(\theta)\cdot\phi 1(\theta)\cdot\sin(\theta)\cdot\cos(\theta)\right)\right]^2 d\theta$$

$$I10 = \int_{-\frac{\pi}{2}}^{\frac{\pi}{2}} 2\cdot W(\theta)\cdot\left[a\cdot\left(Y(\theta)\cdot\phi 1'(\theta)\cdot\cos(\theta)^2 - Y'(\theta)\cdot\phi 1(\theta)\cdot\sin(\theta)\cdot\cos(\theta)\right)\right] d\theta$$

$$I11 = \int_{-\frac{\pi}{2}}^{\frac{\pi}{2}} 2\cdot W'(\theta)\cdot\left[a\cdot\left(Y(\theta)\cdot\phi 1'(\theta)\cdot\cos(\theta)^2 - Y'(\theta)\cdot\phi 1(\theta)\cdot\sin(\theta)\cdot\cos(\theta)\right)\right] d\theta$$

$$I12 = \int_{-\frac{\pi}{2}}^{\frac{\pi}{2}} \left[\begin{array}{l}\left(a^2\cdot Y(\theta)\cdot\phi 1''(\theta)\cdot\sin(\theta)\cdot\cos(\theta)^2\right) - \left(2\cdot a^2\cdot Y'(\theta)\cdot\phi 1'(\theta)\cdot\sin(\theta)^2\cdot\cos(\theta)\right) \ldots \\ + \left(a^2\cdot Y''(\theta)\cdot\phi 1(\theta)\cdot\sin(\theta)^3\right) \ldots \\ + a\cdot Y(\theta)\cdot\phi 1'(\theta)\cdot\left(2\cdot\cos(\theta)^2 - \sin(\theta)^2\right) - 3\cdot a\cdot Y'(\theta)\cdot\phi 1(\theta)\cdot\sin(\theta)\cdot\cos(\theta)\end{array}\right]^2 d\theta$$

$$I13 = \int_{-\frac{\pi}{2}}^{\frac{\pi}{2}} 2\cdot\left(W(\theta) - W''(\theta)\right)\cdot\left[\begin{array}{l}a^2\cdot Y(\theta)\cdot\phi 1''(\theta)\cdot\sin(\theta)\cdot\cos(\theta)^2 \ldots \\ +(-2)\cdot a^2\cdot Y'(\theta)\cdot\phi 1'(\theta)\cdot\sin(\theta)^2\cdot\cos(\theta) \ldots \\ +a^2\cdot Y''(\theta)\cdot\phi 1(\theta)\cdot\sin(\theta)^3 \ldots \\ +a\cdot Y(\theta)\cdot\phi 1'(\theta)\cdot\left(2\cdot\cos(\theta)^2 - \sin(\theta)^2\right) \ldots \\ +(-3)\cdot a\cdot Y'(\theta)\cdot\phi 1(\theta)\cdot\sin(\theta)\cdot\cos(\theta)\end{array}\right] d\theta$$

Solution Constants

$$k1 = \int_a^b r\cdot\phi 2''(r)^2\, dr \qquad t1 = \int_a^b r\cdot\psi 2'(r)^2\, dr \qquad s1 = \int_a^b \psi 2(r)\cdot\phi 2'(r)\, dr$$

$$k2 = \int_a^b \phi 2(r)\cdot\phi 2'(r)\, dr \qquad t2 = \int_a^b \psi 2(r)\cdot\psi 2'(r)\, dr \qquad s2 = \int_a^b \phi 2(r)\cdot\psi 2'(r)\, dr$$

$$k3 = \int_a^b \frac{\phi 2(r)^2}{r}\, dr \qquad t3 = \int_a^b \frac{\psi 2(r)^2}{r}\, dr \qquad s3 = \int_a^b \frac{\phi 2(r)\cdot\psi 2(r)}{r}\, dr$$

External Load

P = 2000 **lb** **Top Soil Surface Concentrated Load**

Elements of the Solution Matrix

$$A11 = 2\cdot\left[\frac{E1}{(1-\nu1^2)}\cdot\left(\frac{f1}{2\cdot\alpha}-I1\right)+G1\cdot\left(\frac{\alpha\cdot f2}{2}-I2\right)\right]-2\cdot\left[\frac{E2}{(1-\nu2^2)}\cdot I7-G2\cdot I8\right]-2\cdot\left(\frac{12\cdot D}{a\cdot t^2}\cdot I9-\frac{D}{a^3}\cdot I12\right)$$

$$A12 = \frac{E2}{(1-\nu2^2)}\cdot I3-G2\cdot I5-\frac{12\cdot D}{a\cdot t^2}\cdot I10-\frac{D}{a^3}\cdot I13$$

$$A13 = \frac{E2}{(1-\nu2^2)}\cdot I4-G2\cdot I6-\frac{12\cdot D}{a\cdot t^2}\cdot I11$$

$$A21 = A12$$

$$A22 = 2\cdot\left[\frac{E2\cdot j1}{(1-\nu2^2)}\cdot(k1-2\cdot\nu2\cdot k2-k3)-j6\cdot G2\cdot k3-\frac{12\cdot j1\cdot D}{a\cdot t^2}-\frac{j7\cdot D}{a^3}\right]$$

$$A23 = \left[\frac{2\cdot E2\cdot j2}{(1-\nu2^2)}\cdot(s3-\nu2\cdot s1)-2\cdot j5\cdot G2\cdot(s2-s3)\right]-\frac{24\cdot j2\cdot D}{a\cdot t^2}$$

$$A31 = A13$$

$$A32 = A23$$

$$A33 = 2\cdot\left[\frac{(E2\cdot j3)}{1-\nu2^2}\cdot t3-j4\cdot G2\cdot(t1-2\cdot t2-t3)-12\cdot j3\cdot\frac{D}{a\cdot t^2}\right]$$

Solution for Constants

$$A = \begin{pmatrix} A11 & A12 & A13 \\ A21 & A22 & A23 \\ A31 & A32 & A33 \end{pmatrix}$$

$$L = \begin{bmatrix} -P - \frac{\gamma g \cdot 2}{\alpha} \cdot \frac{1 - \cosh(\gamma \cdot H)}{\gamma \cdot \sinh(\gamma \cdot H)} \\ 0 \\ 0 \end{bmatrix}$$

$$C = A^{-1} \cdot L$$

$$C = \begin{pmatrix} -1.27721 \\ 0.05914 \\ -0.02615 \end{pmatrix}$$

Pipe Displacement and Internal Forces (Bending Moments and Axial Force) Diagrams

1- Pipe Displacements

$$\theta := -\frac{\pi}{2}, -\frac{99 \cdot \pi}{200} .. \frac{\pi}{2}$$

$W1(\theta) := C_1 \cdot W(\theta)$ $V1(\theta) := C_2 \cdot V(\theta)$ $Y1(\theta) := C_0 \cdot Y(\theta)$

$W1'(\theta) := C_1 \cdot W'(\theta)$ $V1'(\theta) := C_2 \cdot V'(\theta)$ $Y1'(\theta) := C_0 \cdot Y'(\theta)$

$W1''(\theta) := C_1 \cdot W''(\theta)$ $V1''(\theta) := C_2 \cdot V''(\theta)$ $Y1''(\theta) := C_0 \cdot Y''(\theta)$

$$w(\theta) = W1(\theta) + Y1(\theta)\cdot\phi1(\theta)\cdot\sin(\theta)$$

$$v(\theta) = V1(\theta) + Y1(\theta)\cdot\phi1(\theta)\cdot\cos(\theta)$$

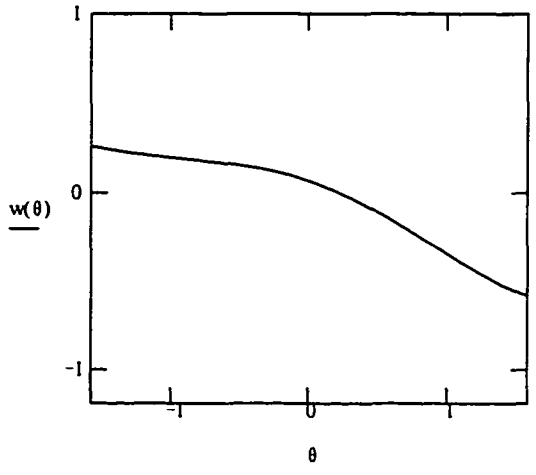

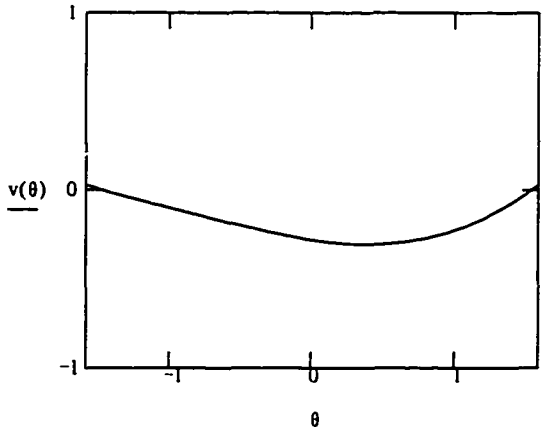

2- Pipe Internal Forces

$$M(\theta) := \left(\frac{-D}{a^2}\right)\cdot\left[W1(\theta) - W1''(\theta) - \begin{bmatrix} a^2\cdot Y1(\theta)\cdot\phi1''(\theta)\cdot\sin(\theta)\cdot\cos(\theta)^2 \ldots \\ +(-2)\cdot a^2\cdot Y1'(\theta)\cdot\phi1'(\theta)\cdot\sin(\theta)^2\cdot\cos(\theta) \ldots \\ +a^2\cdot Y1''(\theta)\cdot\phi1(\theta)\cdot\sin(\theta)^3 \ldots \\ +a\cdot Y1(\theta)\cdot\phi1'(\theta)\cdot\left(2\cdot\cos(\theta)^2 - \sin(\theta)^2\right) \ldots \\ +(-3)\cdot a\cdot Y1'(\theta)\cdot\phi1(\theta)\cdot\sin(\theta)\cdot\cos(\theta) \end{bmatrix}\right]$$

$$N(\theta) := \frac{Ep\cdot t^2}{a\cdot\left(1 - \nu p^2\right)}\cdot\left[V1'(\theta) + a\cdot\left(Y1(\theta)\cdot\phi1'(\theta)\cdot\cos(\theta)^2 - Y1'(\theta)\cdot\phi1(\theta)\cdot\sin(\theta)\cdot\cos(\theta)\right) - W1(\theta)\right]$$

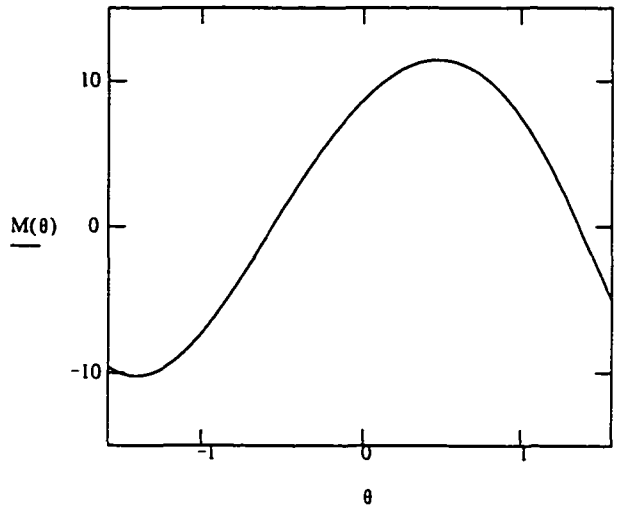

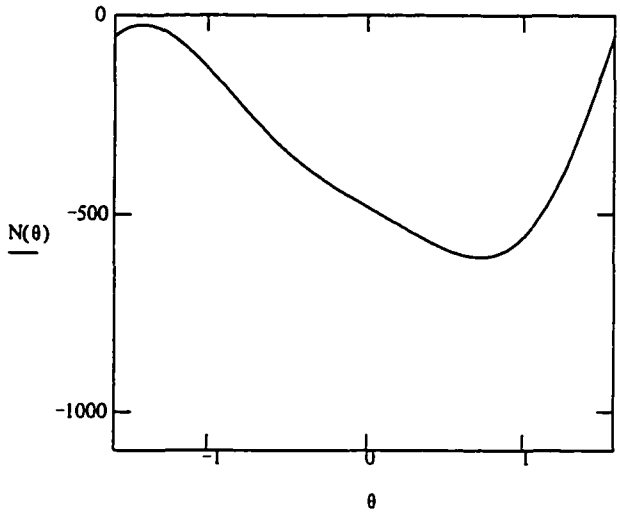

REFERENCES

Aggarwal, S. C., and Cooper, M. J. (1984). "External Pressure Testing of Insituform Linings." *Internal Report* (unpublished), Coventry (Lanchester) Polytechnic.

Amstutz, E. (1969). " Das Einbeulen von Schaeht- und Stollenpanzerungen." *Schweizeriche Bauzeitung*, Vol. 87, 541-549. (English Translation: United States Department of the Interior, Bureau of Reclamation, *Translation No. 825*).

Armenakas, A. E., and Herrmann, G. (1963). "Buckling of Thin Shells Under External Pressure." *J. Engrg. Mech.*, ASCE, 89(EM3), 131-146.

Bodner, S. R. (1958). "On the Conservativeness of Various Distributed Force Systems." *J. Aerone. Sci.*, 25(2), 152-158.

Boresi, A. P. (1955). "A Refinement of the Theory of Buckling of Rings Under Uniform Pressure." *J. Appl. Mech.*, ASME, 22(1), 95-102.

Bresse, M. (1866). *Cours de Méchanique Appliquée*, 2nd. ed., pp. 334.

Bryan, G. H. (1888). "Application of the Energy Test to the Collapse of a Long Pipe Under External Pressure." *Proc. Cambridge Phi. Soc.*, Vol. 6, 287-292.

Burns, J. Q., and Richard R. M. (1964). "Attenuation of Stresses for Buried Cylinders." *Proc. Symp. on Soil-Structure Interaction*, Univ. of Arizona, 378-392.

"CANDE-89; Culvert Analysis and Design Computer Program - User Manual." (1989). *Publication No. FHWA-RD-89-169*, US Dept. of Transportation, Federal Highway Administration.

Cheney, J. A. (1971). "Pressure Buckling of Ring Encased in Cavity." *J. Engrg. Mech.*, ASCE, 97(2), 333-342.

Chicurel, R. (1968). "Shrink Buckling of Thin Circular Rings." *J. Appl. Mech.*, ASME, Vol. 35, 608-610.

"Culvert Load Determination." (1926). *Bulletin 284*, Amer. Rail. Engrg. Assoc.

Duns, C. S., and Butterfield, R. (1971). "Flexible Buried Cylinders; Part III - Buckling Behavior." *Int. J. Rock Mech. Min. Sci.*, Vol. 8, 613-627.

El-Bayoumy, L. (1972). "Buckling of a Circular Elastic Ring Confined to a Uniformly Contracting Circular Boundary." *J. Appl. Mech.*, ASME, Vol. 39, 758-766.

Fairbairn, W. (1858). "On the Resistance of Tubes to Collapse." *Phil. Trans. Royal Soc.*, Vol. 148, London, 389-413.

Flügge, W. (1960). *Stresses in Shells*. Springer-Verlag, Berlin.

Forrestal, M. J., and Herrmann, G. (1965). "Buckling of a Long Cylindrical Shell Surrounded By an Elastic Medium." *Int. J. Solids and Structures*, Vol. 1, 247-309.

Galili, N., and Shmulevich, I. (1981). "A Refined Elastic Model for Soil-Pipe Interaction." *Proc. Int. Conf. on Underground Plastic Pipe*, ASCE, New Orleans, LA, 213-226.

Galili, N., Shmulevich, I., Bar-Shlomo, S., and Foux, A. (1978). "Soil-Pipe Interaction, Stage I and II, Final Report." *Publication No. 291*, Agricul. Engrg. Dept., Technion City, Haifa, Israel.

Glock, D. (1977). "Post-Critical Behavior of a Rigidly Encased Circular Pipe Subject to External Water Pressure and Temperature Rise." *Der Stahlbau*, 46(7), 212-217, (in German).

Guice, L. K., Straughan, W. T., Norris, C. R., and Bennett, R. D. (1994). "Long-Term Structural Behavior of Pipeline Rehabilitation Systems." *Technical Report No 302*, Trenchless Technology Center, Louisiana Tech University, Ruston, LA.

Höeg, K. (1968). "Stresses Against Underground Structural Cylinders." *J. Soil Mech. Found.*, ASCE, 94(SM4), 833-858.

Howard, A. K. (1981). "The USBR Equation for Predicting Flexible Pipe Deflection." *Proc. Int. conf. on Underground Plastic Pipe*, ASCE, New Orleans, LA, 37-55.

Katona, M. G. (1993). "On the Analysis of Buried Conduits - Past, Present and Future." *Proc. Second Conf. Structural Performance of Pipes*, Columbus, OH, 1-5.

Katona, M. G. (1976). "CANDE : A Modern Approach for the Structural Design of Buried Pipe Culvert." *Report No FHWA-RD-77-5 FHWA*, U.S. Dept. of Transportation.

Kerr, A. D. (1964). "Elastic and Viscoelastic Foundation Model." *J. Appl. Mech.*, ASME, 31(3), 491-498.

Kerr, A. D., and Soifer, M. T. (1969). "The Linearization of the Prebuckling State and Its Effect on the Determined Instability Loads." *J. Appl. Mech.*, 36(4), Trans. ASME, Vol 91, Series E, 775-783.

Kurt, C. E., and Mark, K.Y. (1981). "Collapse of Non-Circular Supported Thermoplastic Pipelines." *Proc. Int. Conf. on Underground Plastic Pipe*, ASCE, New Orleans, LA, 360-372.

Langhaar, H. L. (1962) *Energy methods in Applied Mechanics,* John-Wiley, p. 49.

Li, J. Y. (1994). "Design Criterion Analysis for Cured-In-Place Pipe," MS thesis, Dept. of Civil Engrg., Louisiana Tech Univ., Ruston, LA.

Li, J. Y., and Guice, L. K. (1995). "Buckling of Encased Elliptic Thin Ring." *J. Engrg. Mech.*, ASCE, 121(12), 1325-1329.

Linger, D. A. (1972). "Historical Development of the Soil-Structure Interaction Problem." *High. Res. Rec., No. 413, Soil-structure Interaction : A Symposium*, HRB, Washington D.C., 5-11.

Lo, K. H., Chang, B. T. A., Zhang, Q., and Wright, W. J. (1993). "Collapse Resistance of Cured-In-Place Pipes." *Proc. North Amer. No-Dig 93*, NASTT, San Jose, CA.

Lo, K. H., Bogdanoff, J. L., Goldberg, J. E., and Crawford, R. F. (1962). "A Buckling Problem of a Circular Ring." *Proc. 4th U.S. National Cong. Appl. Mech.*, ASME, 559-562.

Luscher, U. (1966). "Buckling of Soil-Surrounded Tubes." *J. Soil Mech. Found.*, ASCE, 92(SM6), 211-228.

Luscher, U., and Höeg, K. (1964). "The Beneficial Action of the Surrounding Soil on the Load Bearing Capacity of Buried Tubes." *Proc. Symp. Soil-Structure Interaction*, Univ. of Arizona, 393-402.

Marston, A., and Anderson, A. O. (1913). "The Theory of Loads on Pipes in Ditches and Test of Cement and Clay Drain Tile and Sewer Pipe." *Bulletin 31*, Iowa Engrg. Exp. Station, Ames, Iowa.

McDonald, J. R., and White, K. R. (1973). "Effect of Out-of-Roundness on the Elastic Instability of Thin Circular Cylindrical Shells." *Proc. 1971 Symp. Int. Assoc. Shell Structures, Pacific Symp., Part I,* University Press of Hawaii, 442-456.

Meyerhof, G. G., and Baikie, L. D. (1963). "Strength of Steel Culvert Sheets Bearing Against Compacted Sand Backfill." *High. Res. Record 30*, HRB, 1-19.

Moore, I. D., and Booker, J. R. (1985). "Simplified Theory for the Behavior of Buried Flexible Cylinders Under the Influence of Uniform Hoop Compression." *Int. J. Solids and Structures*, 21(9), 929-941.

Moore, I. D., and Booker, J. R. (1985). "Simplified Theory for the Behavior of Buried Flexible Cylinders Under the Influence of Non-Uniform Hoop Compression." *Int. J. Solids and Structures*, 21(9), 943-956.

Moser, A. P. (1990). *Buried Pipe Design*, McGraw Hill, Inc.

Novozhilov, V.V. (1959). *The Theory of Thin Shells*, P. Nourdhoff Ltd., Groningen, The Netherlands.

Novozhilov, V. V. (1953) *Foundation of the Nonlinear Theory of Elasticity*, Graylock Press, Rochester, Chapter 5, p. 43.

Romano, F., and Kempner, J. (1962). "Stresses in Short Non-Circular Cylindrical Shells Under Lateral Pressure." *J. Appl. Mech.*, ASME, 669-674.

Saunders, H. E., and Windenburg, D. F. (1931). "Strength of Thin Cylindrical Shells Under External Pressure." Trans. ASME (Appl. Mech.), *Paper APM-53-17b*, Vol. 53.

Selig, E. T., McVay, M. C., and Chang, C. S. (1982). "Finite Element Modeling of Buried Concrete Pipe Installations." *Tran. Res. Records 878*, TRB, 17-23.

Shams, I. H., and Dym, C. L. (1985) *Energy and Finite Element Methods in Structural Mechanics,* Hemisphere Publishing Corp., New York, NY, Chapter 1, p.48.

Shmulevich, I. (1980). "An Experimental Investigation of the Interaction between Pipes and Soil," D.Sc. Thesis, Technion, Israel Institute of Technology.

Slocum, S.E. (1909). "The Collapse of Tubes under External Pressure." Engineering, Jan. 8, 35-37.

Soong, T.C., and Choi, I. (1985). "Buckling of an Elastic Elliptical Ring Inside a Rigid Boundary." *J. Appl. Mech.*, ASME, 52(3), 523-528.

Spangler, M. G. (1941). "The Structural Design of Flexible Pipes Culverts." *Bulletin 153*, Iowa Engrg. Exp. Station, Ames, Iowa.

Spangler, M. G., and Handy, R. L. (1973). *Soil Engineering*, 3rd, Harper and Row, Edu. Publishers Inc., New York, N.Y., Chapters 26 and 27.

"Standard Practice for Rehabilitation of Existing Pipelines and Conduits by the Inversion and Curing of a Resin-Impregnated Tube." (1993). *F1216-93*, ASTM, Philadelphia, PA.

"Standard Test Methods for Flexural Properties of Unreinforced and Reinforced Plastics and Electrical Insulating Materials." (1989). D798-89, ASTM, Philadelphia, PA.

"Standard Test Method for Tensile Properties of Plastics." (1989). D638-89, ASTM, Philadelphia, PA.

Straughan, W.T. (1990). "Analysis of Plates on Elastic Foundations," Dissertation presented to Texas Tech Univ., Lubbock, Texas, in partial fulfillment of the requirements for the degree doctor of philosophy.

Timoshenko, S.P., and Gere, J.M. (1961). *Theory of Elastic Stability*, 2nd ed., McGraw-Hill, New York, 204-221.

Ugural, A. C. (1981). *Stresses in Plates and Shells*, McGraw-Hill, New York, N.Y.

Vallabhan, C. V. G., and Das, Y. C. (1988). "A Parametric Study of Beams on Elastic Foundations." *J. Engrg. Mech.*, ASCE, 114(12), 2072-2092.

Vlasov, V. Z., and Leont'ev, N. N. (1966). *Beams, Plate and Shells on Elastic Foundations*, Gosudarstvennoe Izdatel'stvo Fizikp Matematicheskoi Literatury, Moskva. Translated from Russian, Israel Program of Scientific Translation, Jerusalem.

Watkins, R. K. (1964). "Structural Design Trends in Buried Flexible Conduits." *Proc. Symp. on Soil-Structure Interaction*, Univ. of Arizona, 378-392.

Watkins, R. K., and Spangler, M. G. (1958). "Some Characteristics of the Modulus of the Passive Resistance of the Soil - A Study in Similitude." *High. Res. Proc.*, Vol. 37, HRB, 576-583.

White, H. C., and Layer, J. P. (1960). "The Corrugated Metal Conduit as a Compressed Ring." *High. Res. Proc.*, Vol. 39, HRB, 389-397.

Windenburg, D. F., and Trilling, C. (1934). "Collapse by Instability of Thin Cylindrical Shells Under External Pressure." Trans. ASME (Appl. Mech.), *APM-56-20*, Vol. 56, 819-825.

Winkler, E. (1867). "Die Lehre Von der Elasticitaet and Festigkeit." Prag, Dominicus.

Zagustin, E. A., and Herrmann, G. (1967). "Stability of an Elastic Ring in a Rigid Cavity." *J. Appl. Mech.*, 34(2), Trans., ASME, Series E, Vol. 89, 263-270.